

**UNCLASSIFIED**

---

**AD 295 088**

*Reproduced  
by the*

**ARMED SERVICES TECHNICAL INFORMATION AGENCY  
ARLINGTON HALL STATION  
ARLINGTON 12, VIRGINIA**



---

**UNCLASSIFIED**

NOTICE: When government or other drawings, specifications or other data are used for any purpose other than in connection with a definitely related government procurement operation, the U. S. Government thereby incurs no responsibility, nor any obligation whatsoever; and the fact that the Government may have formulated, furnished, or in any way supplied the said drawings, specifications, or other data is not to be regarded by implication or otherwise as in any manner licensing the holder or any other person or corporation, or conveying any rights or permission to manufacture, use or sell any patented invention that may in any way be related thereto.

63-2-3

295 088

**U. S. A R M Y**  
**TRANSPORTATION RESEARCH COMMAND**  
**FORT EUSTIS, VIRGINIA**

CATALOGED BY ASTIA

AS AD No.

29508

TCREC TECHNICAL REPORT 62-46

**INVESTIGATION OF CONTROLLED FLOW PHENOMENA**  
**FOR AIR CUSHION VEHICLES**

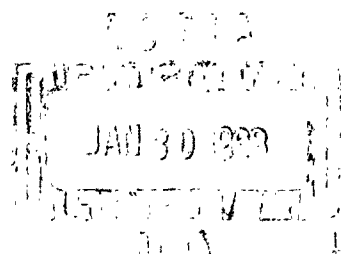
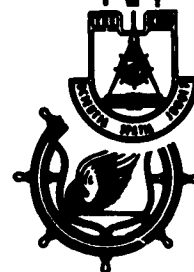
Task 9R99-01-005-05

Contract DA 44-177-TC-744

November 1962

**prepared by:**

**BELL HELICOPTER COMPANY**  
**Fort Worth, Texas**



#### DISCLAIMER NOTICE

When Government drawings, specifications, or other data are used for any purpose other than in connection with a definitely related Government procurement operation, the United States Government thereby incurs no responsibility nor any obligation whatsoever; and the fact that the Government may have formulated, furnished, or in any way supplied the said drawings, specifications, or other data is not to be regarded by implication or otherwise as in any manner licensing the holder or any other person or corporation, or conveying any rights or permission, to manufacture, use, or sell any patented invention that may in any way be related thereto.

#### ASTIA AVAILABILITY NOTICE

Qualified requesters may obtain copies of this report from

Armed Services Technical Information Agency  
Arlington Hall Station  
Arlington 12, Virginia

This report has been released to the Office of Technical Services, U. S. Department of Commerce, Washington 25, D. C., for sale to the general public.

The information contained herein will not be used for advertising purposes.

The findings and recommendations contained in this report are those of the contractor and do not necessarily reflect the views of the U. S. Army Mobility Command, the U. S. Army Materiel Command, or the Department of the Army.

Contract DA 44-177-TC-744

November 1962

INVESTIGATION OF CONTROLLED FLOW PHENOMENA  
FOR AIR CUSHION VEHICLES

Bell Helicopter Report 532-099-001

TCREC Technical Report 62-46

Task 9R99-01-005-05

Prepared by



for

U. S. ARMY TRANSPORTATION RESEARCH COMMAND

Fort Eustis, Virginia


HEADQUARTERS  
U. S. ARMY TRANSPORTATION RESEARCH COMMAND  
Fort Eustis, Virginia

The inherent simplicity of the plenum configuration GEM is outweighed by its low efficiency and poor stability characteristics at practical operating heights. The application of controlled flow techniques to provide efficiency and stability approaching that of the annular jet while retaining the simplicity of the plenum configuration appeared to offer significant advantages.


This report summarizes an experimental program which compares the performance of several typical controlled flow models with annular jet and plenum counterparts.

The results of the study indicate that performance and stability equivalent and in some instances superior to that of the annular jet can be attained without the use of a base plate or internal ducting.

FOR THE COMMANDER:

  
KENNETH B. ABEL  
Capt, TC  
Adjutant

APPROVED BY:

  
WILLIAM E. SICKLES  
Leader  
Ground Effect Research Group

## FOREWORD

This report summarizes the results of an analytical and experimental model investigation of controlled flow techniques applied to air cushion vehicles. The program was conducted by Bell Helicopter Company of Fort Worth, Texas, under U. S. Army Transportation Research Command contract (Reference 1), during the period from July 1961 to June 1962.

The program was carried out under the technical cognizance of Mr. W. E. Sickles of TRECOM. The Principal Investigator at the onset of the program was Mr. Kenneth G. Wernicke, and Mr. Rodney K. Wernicke was Project Engineer for the entire program. Later, Mr. R. Wernicke assumed the responsibilities of Principal Investigator and led both analytical and experimental investigations on to their conclusion. Other Bell Helicopter personnel associated with the program include Messrs. S. M. Hamzeh, F. Krystinik, J. DeTore and R. Lynn.

## CONTENTS

	<u>Page</u>
FOREWORD . . . . .	iii
LIST OF ILLUSTRATIONS . . . . .	ix
LIST OF TABLES . . . . .	xiii
LIST OF SYMBOLS . . . . .	xv
I. SUMMARY . . . . .	1
II. CONCLUSIONS AND RECOMMENDATIONS . . . . .	3
A. CONCLUSIONS . . . . .	3
B. RECOMMENDATIONS . . . . .	4
III. INTRODUCTION . . . . .	5
IV. APPROACH . . . . .	7
A. GENERAL . . . . .	7
B. IMPROVING THE HOVERING EFFICIENCY OF THE CONTROLLED FLOW CONCEPT . . . . .	7
1. Convex Bend . . . . .	7
2. Concave Bend . . . . .	8
C. CRITERIA . . . . .	10
1. Primary Criterion (Hovering Performance) . . . . .	10
2. Secondary Criteria (Stability, Controllability and Propulsion) . . . . .	12
V. DESCRIPTION OF MODELS . . . . .	13
A. GENERAL . . . . .	13
B. INTERNAL FLOW MODELS . . . . .	13
1. Basic Configurations . . . . .	13
2. Model Modifications . . . . .	16
a. Summary of Modifications . . . . .	16
b. Circular Model . . . . .	18
c. Square Model . . . . .	20
d. Single Fan, Oval Model . . . . .	24
e. Tandem Fan, Oval Model . . . . .	30



C. EXTERNAL FLOW MODEL . . . . .	34
VI. DESCRIPTION OF EXPERIMENTAL EQUIPMENT AND PROCEDURES . .	37
A. GENERAL . . . . .	37
B. LARGE CIRCULAR AND SQUARE MODEL TESTING . . . . .	37
C. SMALL MODEL TESTING . . . . .	37
VII. RESULTS . . . . .	41
A. GENERAL . . . . .	41
B. HOVERING PERFORMANCE . . . . .	41
1. Jet Exit Arrangements . . . . .	41
a. Skirt Length . . . . .	42
b. Jet Inclination Angle . . . . .	45
2. Internal Distribution Systems . . . . .	45
a. Circular Planform Configurations . . . . .	45
b. Square Planform Configurations . . . . .	50
c. Single Fan Oval Planform Configurations . . . . .	50
d. Tandem Fan Oval Planform Configurations . . . . .	60
3. External Flow System . . . . .	62
C. STATIC STABILITY . . . . .	69
1. Static Stability Results . . . . .	70
a. Basic Configurations . . . . .	70
b. Controlled Flow with Additional Inner Side Jets . . . . .	73
c. Controlled Flow with Additional Outer Jet . . . . .	73
d. Controlled Flow with an Athwartship Fence . . . . .	78
2. Performance Penalty with Stability Augmenting Devices . . . . .	78
D. CONTROL . . . . .	83
1. Lateral Control System . . . . .	83
a. Trim Control . . . . .	85
b. Lateral Thrust and Roll Attitude . . . . .	85
2. Heading Control System . . . . .	85
E. PROPULSION . . . . .	89

VIII. EVALUATION . . . . .	93
A. DISCUSSION AND COMPARISON OF THE CONTROLLED FLOW CONCEPT; HOVERING PERFORMANCE CRITERION . . . . .	93
1. Devices for Achieving Controlled Flow . . . . .	93
2. Performance Comparison . . . . .	94
3. Application of Controlled Flow Techniques to Peripheral Jet Configurations with Base Plates . . . . .	96
4. Application of Controlled Flow Techniques to External Flow of Air Cushion Vehicles . . . . .	96
5. Recommendations . . . . .	97
B. DISCUSSION AND COMPARISON OF THE CONTROLLED FLOW CONCEPT; STABILITY, CONTROL AND PROPULSION CRITERIA . . . . .	98
1. Stability, Control and Propulsion Devices; Controlled Flow Configurations . . . . .	98
2. Comparisons . . . . .	98
3. Recommendations . . . . .	99
IX. REFERENCES . . . . .	103
APPENDIX I - ANALYSIS OF THE TWO-DIMENSIONAL POTENTIAL FLOW VELOCITY PROFILES ON CONVEX AND CONCAVE BENDS . . . . .	105
APPENDIX II - INVESTIGATION OF THE EFFECTS OF ARBITRARY CONTOURS ON TWO-DIMENSIONAL LAMINAR BOUNDARY LAYER SEPARATION POINTS . . . . .	111
APPENDIX III - DERIVATION OF THE IDEAL PERFORMANCE PARAMETER EQUATION FOR THE CONCENTRIC PERIPHERAL JET CONFIGURATION . . . . .	119
DISTRIBUTION LIST . . . . .	127

## ILLUSTRATIONS

Figure		Page
1	Peripheral Jet Flow . . . . .	6
2	Early Controlled Flow Model . . . . .	6
3	Two-Dimensional Ideal Controlled Flow . . . . .	9
4	Ideal Hovering Performance . . . . .	11
5a	Circular Model . . . . .	14
5b	Square Model . . . . .	14
6a	Single Fan Oval Model . . . . .	15
6b	Tandem Fan Oval Model . . . . .	15
7	Circular Model Configurations . . . . .	19
8	Square Model Configurations . . . . .	21
9	Photograph and Layout of Square Model Distribution Vanes . . . . .	22
10	Square Model with Contoured Orifice Assembly . .	23
11a	Single Fan Oval Model Configurations 17 and 18 . .	25
11b	Single Fan Oval Model Configurations 19 through 24	26
12	Ten-Inch Diameter Fan Unit . . . . .	27
13	Ten-Inch Diameter Fan Unit . . . . .	28
14	Special Blade Layout . . . . .	29
15a	Tandem Fan Oval Model Configurations 25 through 27	31
15b	Tandem Fan Oval Model Configurations 28 through 30	32
16	Tandem Fan Oval Model Flow Splitter Assembly . .	33
17	Propulsion Port Installation in Configuration No. 30	33
18	External Flow Model . . . . .	35
19	Test Equipment for Large Models . . . . .	39

Figure		Page
20	Small Model Test Stand . . . . .	40
21	Effects of Skirt Length on Performance, $\theta = 0^\circ$ . .	43
22	Effects of Skirt Length on Performance, $\theta = 45^\circ$ . .	44
23	Effects of Jet Inclination on Performance . . .	46
24	Circular Model Performance, Optimum Skirt Length, $\theta = 0^\circ$ . . . . .	48
25	Circular Model Performance, Optimum Skirt Length, $\theta = 45^\circ$ . . . . .	49
26	Square Model Performance, $\theta = 45^\circ$ . . . . .	51
27	Square Model Performance, Controlled Flow Applied to Base Plate Configuration, $\theta = 45^\circ$ . . . . .	52
28	Single Fan Oval Model Performance, $\theta = 45^\circ$ . . .	54
29	Ten-Inch Diameter Fan Performance . . . . .	56
30	Ten-Inch Diameter Ducted Fan Performance . . . .	57
31	Single Fan Oval Model Performance, Special and Conventional Blades, $\theta = 45^\circ$ . . . . .	58
32	Single Fan Oval Model Performance, Controlled Flow Configuration with Base Plate Added, $\theta = 45^\circ$ . . .	59
33	Tandem Fan Oval Model Performance, Controlled Flow Configurations, $\theta = 60^\circ$ . . . . .	61
34	Twin Fan Turning Vane System . . . . .	62
35	Tandem Fan Oval Model Performance, Controlled Flow and Conventional Configurations, $\theta = 60^\circ$ . . . .	63
36	Ideal External Flow Schematic . . . . .	64
37	Theoretical Base Pressure to Jet Total Pressure Ratios . . . . .	65
38	External Flow Model Augmentation, $\theta = 0^\circ$ . . . .	67
39	External Flow Model, Jet Total Pressure to Fan Total Pressure Ratios . . . . .	67
40	External Flow Model Performance, $\theta = 0^\circ$ . . . .	68

Figure		Page
41	Tandem Fan Oval Model, Static Lateral Stability, Basic Configurations . . . . .	71
42	Tandem Fan Oval Model, Static Longitudinal Stability, Basic Configurations . . . . .	72
43	Tandem Fan Oval Model, Static Lateral Stability, Controlled Flow Configuration with Concentric Side Jets . . . . .	74
44	Tandem Fan Oval Model, Static Longitudinal Stability, Controlled Flow Configuration with Concentric Side Jets . . . . .	75
45	Tandem Fan Oval Model, Static Lateral Stability, Controlled Flow Configuration with Concentric Outer Jet . . . . .	76
46	Tandem Fan Oval Model, Static Longitudinal Stability, Controlled Flow Configuration with Concentric Outer Jet . . . . .	77
47	Tandem Fan Oval Model, Static Longitudinal Stability, Controlled Flow Configuration with Athwartship Fence	79
48	Tandem Fan Oval Model Performance, Basic Configura- tions and Stabilized Configurations . . . . .	80
49	Tandem Fan Oval Model, Variation in Mean Hover Height with Roll . . . . .	81
50	Tandem Fan Oval Model, Variation in Mean Hover Height with Pitch . . . . .	82
51	Tandem Fan Oval Model Performance, Ideal and Experi- mental Comparison for Single and Concentric Jet (Controlled Flow) Configurations . . . . .	84
52	Tandem Fan Oval Model Trim Control, Control Capa- bility . . . . .	86
53	Tandem Fan Oval Model Trim Control, Effect on Hover Height . . . . .	86
54	Tandem Fan Oval Model Lateral Control, Trim Attitude	87
55	Tandem Fan Oval Model Lateral Control, Lateral Thrust	87
56	Heading Control System . . . . .	88

Figure		Page
57	Tandem Fan Oval Model Propulsion System, Variations in Height with Thrust . . . . .	91
58	Experimental Hovering Performance: Peripheral Jet, Ducted Fan, and <u>External Flow Models</u> . . . . .	100
59	Potential Flow Conditions on Concave and Convex Bends . . . . .	110
60	Coanda Bends Tested in Two-Dimensional Model; Case One, An Airfoil Curve, Case Two, A Cubic Curve . . .	118
61	Concentric Peripheral Jet Flow Schematic . . . . .	120

## TABLES

Table		Page
1	Large and Small Model Configurations. . .	17
2	Circular Model Numerical Data. . . . .	<del>18</del>
3	Square Model Numerical Data. . . . .	20
4	Single Fan Oval Model Numerical Data. . .	24
5	Tandem Fan Oval Model Numerical Data. . .	30
6	Numerical Data for 10" Fan Unit and External Flow Model. . . . .	34
7	Maximum Heading Control Moments for Yaw Vanes Installed in the Tandem Fan Oval Model, Configuration No. 28. . . . .	88
8	Summary of Performance for Selected Models.	101
9	Summary of Stability Characteristic for Conventional and Controlled Flow Tandem Fan Oval Model Configurations. . . . .	101

# SYMBOLS

<u>Symbol</u>		<u>Units</u>
A	Actual augmentation ratio	
A <sub>i</sub>	Ideal augmentation ratio	
b	Base (total cushion) length	ft
c	Circumference of <del>peripheral jet centerline</del>	ft
d	Base diameter	ft
D	Drag	lb
G	Ground effect power factor = $P/P_i$	
h	Altitude or height above ground	ft
h <sub>o</sub>	Initial h before tilting or actuating control	ft
h <sub>m</sub>	Mean altitude or height above ground = height of center of gravity above ground - height of center of gravity above bottom of vehicle; independent of attitude	ft
HP	Horsepower = $P/550$	
L	Lift	lb
L <sub>f</sub>	Fan lift out of ground effect	lb
M	Moment	ft-lb
M'	Ducted fan figure of merit	
M <sub>p</sub>	$L^{3/2}/HP(\sigma'S)^{1/2}$ , (Performance parameter) <sub>actual</sub>	
(M <sub>p</sub> ) <sub>i</sub>	$L^{3/2}/HP(\sigma'S)^{1/2}$ , (Performance parameter) <sub>ideal</sub>	
OGE	Out of ground effect	
p <sub>b</sub>	Base pressure, gauge	lb/ft <sup>2</sup>
p <sub>o</sub>	Static pressure at outside edge of jet, gauge	lb/ft <sup>2</sup>
p <sub>tf</sub>	Fan total pressure, gauge	lb/ft <sup>2</sup>
p <sub>tj</sub>	Jet total pressure, gauge	lb/ft <sup>2</sup>



P	Power, power of air cushion vehicle	ft-lb/sec
S	Cushion area including jet area	ft <sup>2</sup>
S <sub>b</sub>	Effective base area	ft <sup>2</sup>
S <sub>f</sub>	Fan exit area	ft <sup>2</sup>
S <sub>j</sub>	Jet area at nozzle exit	ft <sup>2</sup>
t <sub>e</sub>	Jet thickness at nozzle exit	inches
w	Base (total cushion) width	ft
x	Skirt extension length	inches
$\eta$	Over-all efficiency of air cushion vehicle lifting system	
$\theta$	Jet inclination angle, measured from vertical, positive inward	
$\rho$	Density of air	lb-sec <sup>2</sup> /ft <sup>4</sup>
$\sigma'$	Density of air/density of air standard day	

## I. SUMMARY

Presented in this report are the findings of an investigation of controlled flow phenomena for air cushion vehicles. Controlled flow is defined as the flow pattern which exists when a peripheral jet is established without the use of internal ducting or a base plate. Objectives of the program were: (a) achieving efficient, practical approximations to ideal controlled flow, (b) evaluating the merits of controlled flow configurations in the hovering flight regime by comparing their performance and stability with conventional plenum and peripheral jet designs, and (c) determining the characteristics of integrated stabilization, propulsion, and control systems in a controlled flow configuration.

A discussion of early model experiments which led to the controlled flow concept is given early in the report and the operational potential of successfully applying these techniques to low-silhouette vehicles is presented. An understanding of the basic problem of attaining controlled flow on realistically proportioned models is facilitated by a discussion of the mechanics involved in the ideal controlled flow situation. Several experimental approaches for achieving practical approximations to the ideal case are discussed and the supporting theoretical work is presented.

For determining the performance merits of controlled flow model configurations, the performance criterion is shown to be primarily a comparison of the ground effect augmentation ratio,  $G$ , rather than that of over-all efficiency, per se. The theoretical expressions of ideal hovering performance for single and concentric peripheral jet configurations are derived and presented. Forward flight characteristics are recognized as important in such an evaluation; however, these were beyond the scope of this program.

The several combinations of jet exit arrangements and internal arrangements of four basic planform models (circular, square, single fan oval and tandem fan oval) resulted in 30 internal model configurations. These model arrangements are catalogued with accompanying illustrations and schematics showing key dimensions and other explanatory information. A dimensioned schematic and photograph of an external flow model is also shown. The test procedures and equipment used in the experimental program are discussed.

The results of the experimental program are presented essentially in chronological order, which is also the sequence of planform variation during the experiments. Hovering performance results are presented for the several versions of the circular, square, single fan oval and tandem fan oval models, in that order, and concludes with two versions of the external flow model. Thereafter, results are given for various arrangements of the tandem fan oval model only, which was used for investigations

of stability, controllability and propulsion characteristics in hovering flight.

It was found that, for the controlled flow configuration as with the others, improving the stability characteristics by altering the basic flow system involves a significant performance loss. Therefore, the evaluation of the controlled flow concept was conducted in two ways; by considering relative hovering performance only, and by considering stability characteristics as well as hovering performance.

A significant conclusion of this investigation is that performance equal to or better than conventional peripheral jets can be achieved without the use of a base plate or internal ducting by using controlled flow techniques. Further, techniques were found to provide positive static stability characteristics for the controlled flow configuration which represent improvements over the characteristics of conventional peripheral jet configurations. At and above an  $h/d$  of .1, the external flow model tested exhibited performance comparable to the conventional annular jet. Considering the external flow vehicle as an accessory to existing hovering vehicles is suggested as a potentially useful application of this device.

## II. CONCLUSIONS AND RECOMMENDATIONS

### A. CONCLUSIONS

Based on the results of this investigation, the conclusions are as follows:

- The fully ducted annular jet shows slightly better performance than the partially ducted annular jet configuration. This indicates that losses due to skin friction are not as great as those associated with the partially ducted version with unconfined internal flow. The difference in performance is small and the partially ducted configuration is much simpler in construction.
- The partially ducted annular jet is only slightly better in performance than the controlled flow version using a flat deflector plate below the fan. The latter is certainly a further simplification of the internal structure and results in little performance penalty.
- Controlled flow versions using a deflector plate were equal to or better than all versions of the peripheral jet configuration with base plate when compared with the same planform. This indicates that the simpler controlled flow internal arrangement is more desirable than the "practical" peripheral jet configuration.
- The circular planform configurations, in general, had the best performance, followed by the oval planform configuration with two fans. The latter represents a more practical arrangement for full-scale vehicles and the performance penalty is slight.
- Too deep a plenum cavity above the base plate in a conventional peripheral jet design can noticeably reduce the over-all efficiency. Control flow techniques may then be applied to improve vehicle hovering performance.
- At heights above values of  $h/d$  of .1, the test results indicate higher performance for the external flow configuration than obtained with the fully ducted annular jet. Below this value of height, the flow begins to separate from the external surface and efficiency drops off. With more effective techniques applied to prevent separation of the flow from the vehicle surface, efficiencies which are competitive with the standard annular jet configurations could be obtained in the lower height, higher base loading range.
- When stabilized, the controlled flow configurations as tested during this investigation lose their performance advantages over the base plate peripheral jet configuration. However, the stability characteristics are superior and they still retain terrain clearance advantages which may prove useful to the air cushion vehicle designer.

## B. RECOMMENDATIONS

1. On the basis of hovering performance, it is recommended that controlled flow internal arrangements be considered when:

- a base plate is not mandatory (for flotation, etc.) on a peripheral jet air cushion vehicle. The advantages to be gained would be reduced terrain interference with the vehicle bottom and performance equivalent to or better than a peripheral jet configuration with a base plate.
- a deep internal plenum cavity is formed between the fan exit and the base plate in a conventional peripheral jet configuration. The principal advantage in such a case will be to improve the internal flow profile within the plenum, thereby improving the over-all efficiency. A "deep" plenum is considered to be one in which the upper surface of the base plate is at least between .25 and .30 fan diameters below the ceiling of the cavity.
- simplicity of internal construction is desired. Only the plenum configuration, with relatively poor performance, is simpler. The fully ducted peripheral jet can be expected to have better performance but at the expense of complicated internal ducting.

2. It is recommended that stabilization techniques involving a concentric jet arrangement be applied to controlled flow configurations. Although this approach represented a significant cost in hovering power requirements in this investigation, a noticeable improvement in stability characteristics over those of the conventional peripheral jet configuration was obtained.

3. It is also recommended that when controlled flow techniques are applied, further optimization of stability characteristics and performance be accomplished through experimentation with scale models of the vehicle under consideration.

4. It is recommended that further consideration be given to some form of external flow configuration since it has potential application when considered as an accessory to an existing lift vehicle. Its ideal performance is the same as the conventional peripheral jet, and in this investigation, actual performance exceeded that of the fully ducted annular jet above an  $h/d$  of .1.

### III. INTRODUCTION

The performance of air cushion vehicles built to date indicates that to fulfill a useful area of military operations, a substantial improvement is required in the ability of these vehicles to negotiate rough terrain.

To date, the peripheral jet configuration has been considered as the most efficient version of the air cushion vehicle from an operating height standpoint. On the other hand, this configuration generally employs a base plate which tends to interfere with rough terrain. From an operational standpoint, a portion of the gain in mean operating heights is offset by the increased susceptibility of the vehicle to ground contact.

A technique considered by some investigators to improve terrain clearance is the flexible skirt (Reference 2), which effectively increases the height between the terrain and the solid vehicle structure without increasing the air curtain gap.

Still another approach to providing improved rough terrain capability for the air cushion vehicle is the controlled flow concept.

A controlled flow configuration is physically similar to the simple plenum configuration except that the flow is made to follow the inner surfaces of the vehicle cavity and exits as a peripheral jet (Figure 1). The performance advantage of the peripheral jet configuration is thereby retained with the simplicity of the plenum configuration. An early experiment showed that a simple circular plenum chamber with a 45 degree conical afterbody between the fan exit and the base, Figure 2, would have peripheral flow characteristics (Reference 3). Its efficiency was therefore superior to a pure plenum configuration. It remained to be seen, however, whether the same flow characteristics and good performance could be attained in a low silhouette design which would more nearly represent operational shapes and planforms. The low silhouette version of the controlled flow configuration is the subject of the investigation reported herein. In this case, the flow is required to negotiate a 90 degree bend immediately below the fan.

The main advantages of this configuration include (a) simple construction and (b) no bottom surface to produce vertical forces and accompanying vertical accelerations when operating in rough terrain. The advantages were not questioned in this investigation; however, a general comparison of this configuration with the conventional peripheral jet and plenum configurations was made to determine quantitatively the relative performance of the controlled flow principle applied to low silhouette designs. A favorable comparison was desired as it would indicate that this family of configurations possessed better rough terrain characteristics than existing versions of the air cushion vehicle without compromising performance.

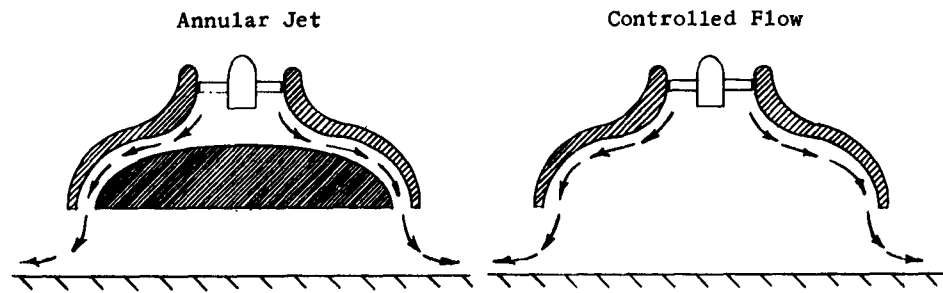


Figure 1. Peripheral Jet Flow

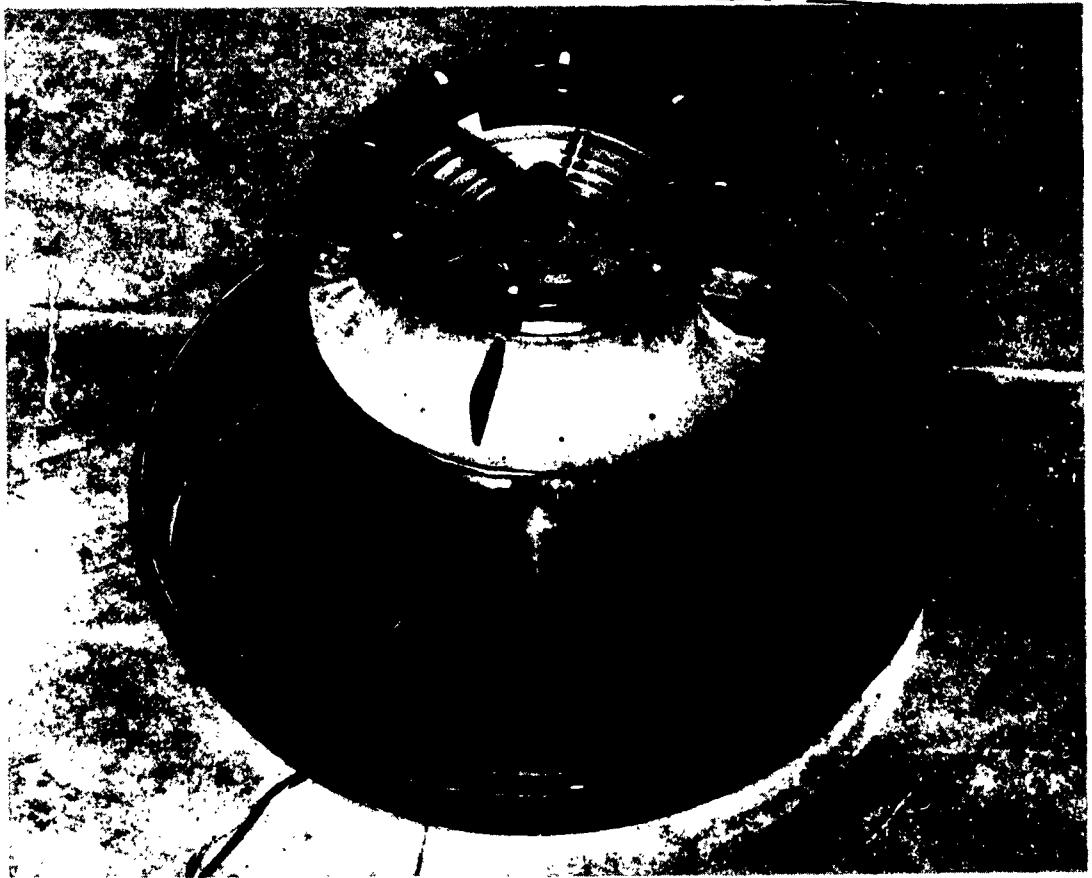


Figure 2. Early Controlled Flow Model

#### IV. APPROACH

##### A. GENERAL

The general approach taken to determine the relative merits of the controlled flow concept was to compare characteristics of models of this configuration with similar models of the peripheral jet and plenum chamber configurations. The over-all comparison involved four basic models having circular, square and oval planforms. The oval planform was tested with one and two lift fans. These combinations were intended to establish general trends of relative hovering efficiency for operational type configurations as well as the more basic planforms. Finally, a specific controlled flow configuration, the oval-shaped model with two lift fans, was used for a more detailed investigation, which also included evaluation of stability, controllability and propulsion characteristics in hovering flight. In addition, the application of controlled flow techniques to a vehicle's external surface (External Flow Vehicle) was investigated with a fifth basic model for the hovering case.

##### B. IMPROVING THE HOVERING EFFICIENCY OF THE CONTROLLED FLOW CONCEPT

The early work on the controlled flow concept, described in Reference 3, involved a conical afterbody which readily attained attached flow along the inside of the afterbody walls. Since, in this current investigation, the flow vein would be required to execute a 90 degree bend as it left the fan unit, it was expected that difficulty would be encountered in keeping the flow attached to the inner walls. This was confirmed early in the experimental program. During the ensuing investigations, various approaches were taken to improve this situation and involved understanding better the flow mechanics involved. A brief discussion of the "ideal" controlled flow processes is presented here to illustrate the nature of the problems associated with the investigation.

Referring to the two-dimensional flow schematic in Figure 3, it can be seen that after being accelerated by a ducted fan (A), the air flows around a convex bend (B), followed by a straight section (C) and a downstream concave bend (D). After completing this bend, the flow is generally downward (E) and ready to leave the vehicle at the jet exit area (F). The inner streamline velocity from fan to exit is theoretically constant in magnitude.

##### 1. Convex Bend

Ideally, the vein undergoes a Coanda flow phenomenon on the first bend. With the exception of the boundary layer, where the viscous forces are considered to be appreciable, the flow at the convex



bend is a potential flow with a velocity distribution as shown at (B) in Figure 3. The build-up and behavior of the boundary layer is significant due to the influence on the losses and instability of the vein. For sufficiently adverse pressure gradients along the wall from (B) to (C), boundary layer separation can cause the vein to separate. Depending on the shape of the contour and the velocity distributions, the vein may remain attached or detach totally or partially, either before or after completing the first bend. The attached vein configuration will be referred to here as one of stable controlled flow. In order to realize, control and sustain a stable flow configuration, an analysis of the Coanda bend was conducted (Appendix I), an analysis of the effect of arbitrary curve shapes on boundary layer separation was conducted (Appendix II), and two- and three-dimensional model experiments were initiated.

An approach used during the program to improve experimentally the free vortex flow at the convex bend involved generating a nonuniform velocity distribution, compatible with the Coanda process, before the flow entered the convex bend. This was done to cause a stronger favorable pressure gradient across the vein which would tend to offset the centrifugal force acting on the entire flow. Two devices for accomplishing this were a special propeller designed for generating the required velocity distribution through the ducted fan and a deflector tab immediately below the spinner.

Another approach used for stabilizing the flow on the convex bend was to confine the vein of air by means of curved and flat deflectors mounted under the fan unit. This was done to insure radial discharge at the bend exit and allowed investigations of the general characteristics of the controlled flow configuration without requiring optimum bend geometry to sustain a free vortex flow. The above mentioned devices for controlling the flow on the convex bend are further described in Section V (Description of Models).

## 2. Concave Bend

After the flow completes the turn at the convex bend, it follows the ceiling of the plenum cavity outward until it reaches the downstream concave bend. Again, the basic flow pattern in the bend is assumed to be a free vortex as shown at Station D in Figure 3. If the radius of the outer wall of the turn is too sharp, separation will occur and a trapped vortex with its accompanying losses will form in the corner. A brief analysis of the free vortex flow geometry at the concave bend is also included in Appendix I. For planforms other than circular, attempts were made to define the flow positively by means of an internal ring arrangement inserted at the concave bend.

This was intended to govern the distribution of air into the concave bend and thereby achieve a uniform distribution around the periphery of the jet exit. Another approach for governing the peripheral

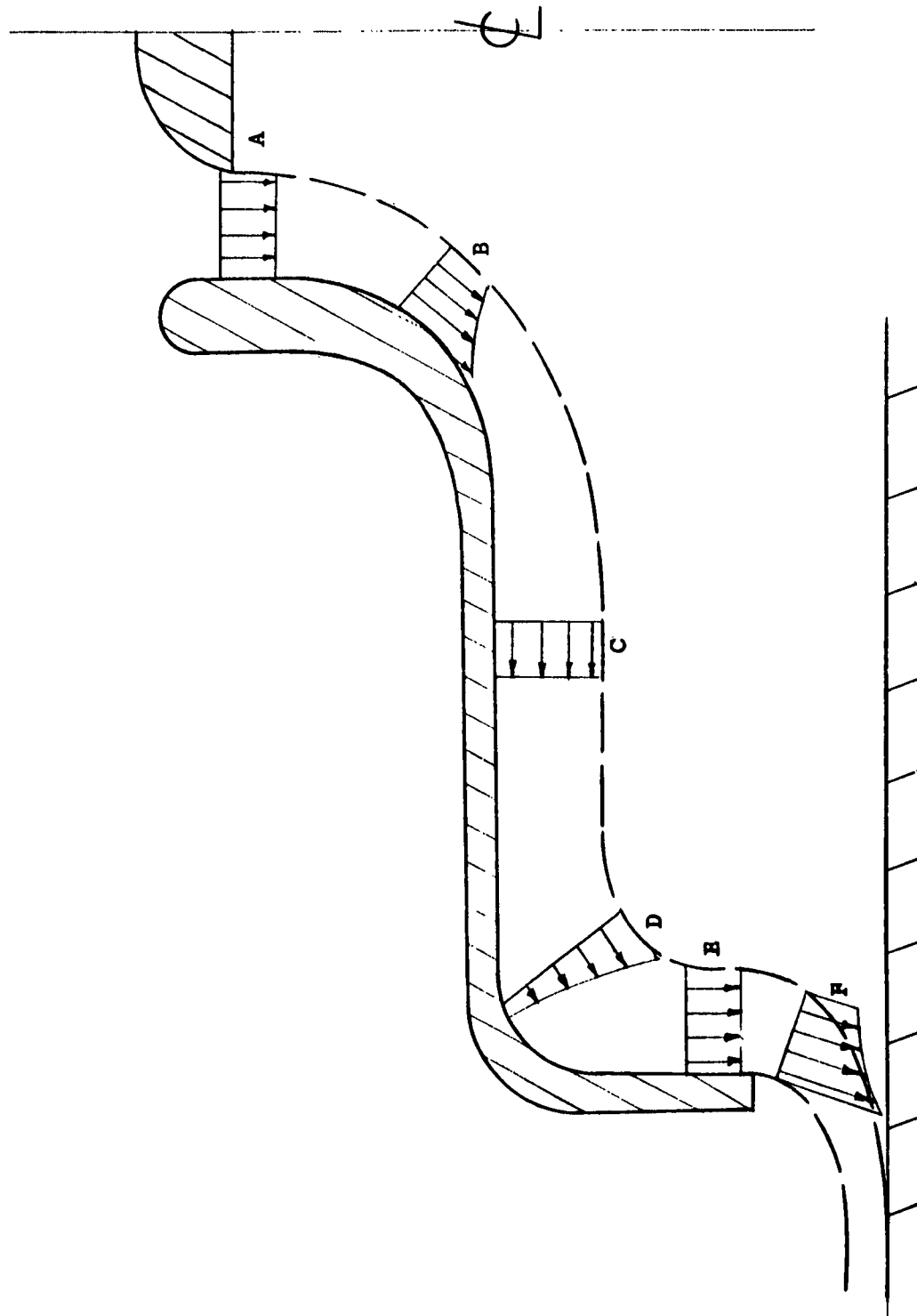


Figure 3. Two Dimensional Ideal Controlled Flow

distribution of air on noncircular planforms included vanes on the plenum ceiling just upstream of the concave bend.

As the flow completes the concave bend it has an ideal velocity distribution similar to that shown at (D) in Figure 3. If the flow entered the jet exit area at this point, the velocity distribution in the vein would be required to make a rapid transition from that shown at (D) to the type shown at (F). It had been noted in previous investigations that extensions of the straight section after the concave bend at (E) had improved over-all efficiencies, apparently by reducing turbulence originating in that area. The approach of using a skirt extension as a means of improving the internal efficiency of all configurations was one of the first attempted during the experimental program. Another question raised early in the program was whether or not inclining the jet inward would induce upstream separation and thereby cause a breakdown of the controlled flow pattern. This item was also explored early in the program.

### C. CRITERIA

#### 1. Primary Criterion (Hovering Performance)

The approach used for comparing the relative hovering performance of the controlled flow concept with the conventional peripheral jet and plenum configurations involved experimentally evaluating the performance parameter,  $M_p$ , at various heights expressed by the height parameter,  $hc/S$ . The ratio of the experimentally determined value of the performance parameter to the theoretically determined ideal value at any height is defined as the over-all efficiency of the system.

The equation for the ideal value of the performance parameter for the peripheral jet, both conventional and controlled flow versions, is

$$(M_p)_i = \frac{L^{3/2}}{HP \sqrt{\sigma} S} = 1100 \sqrt{P_o} \left[ \cos \theta + \frac{1}{2} \left( \frac{S}{hc} \right) \left( \frac{S_f}{S} \right) \left( \cos \theta + \frac{\sin 2\theta}{2} \right) + \left( \frac{S}{hc} \right) \left( \frac{S_b}{S} \right) (1 + \sin \theta) \right]^{3/2} \left[ \frac{\sqrt{(S_f/S)}}{1 + \left( \frac{S}{hc} \right) \left( \frac{S_f}{S} \right) (1 + \sin \theta)} \right]$$

and is derived in this form in Appendix III. (1)

Figure 4 summarizes the variation of the ideal performance with height, as determined by equation (1), for four basic model configurations tested during this investigation.

In addition, ideal values of the performance parameter are included in Figure 4 for the helicopter rotor and ducted fan when operating out of ground effect.

It can be seen that four values of the ideal performance parameter exist, one for each model, at any particular value of  $hc/S$ .

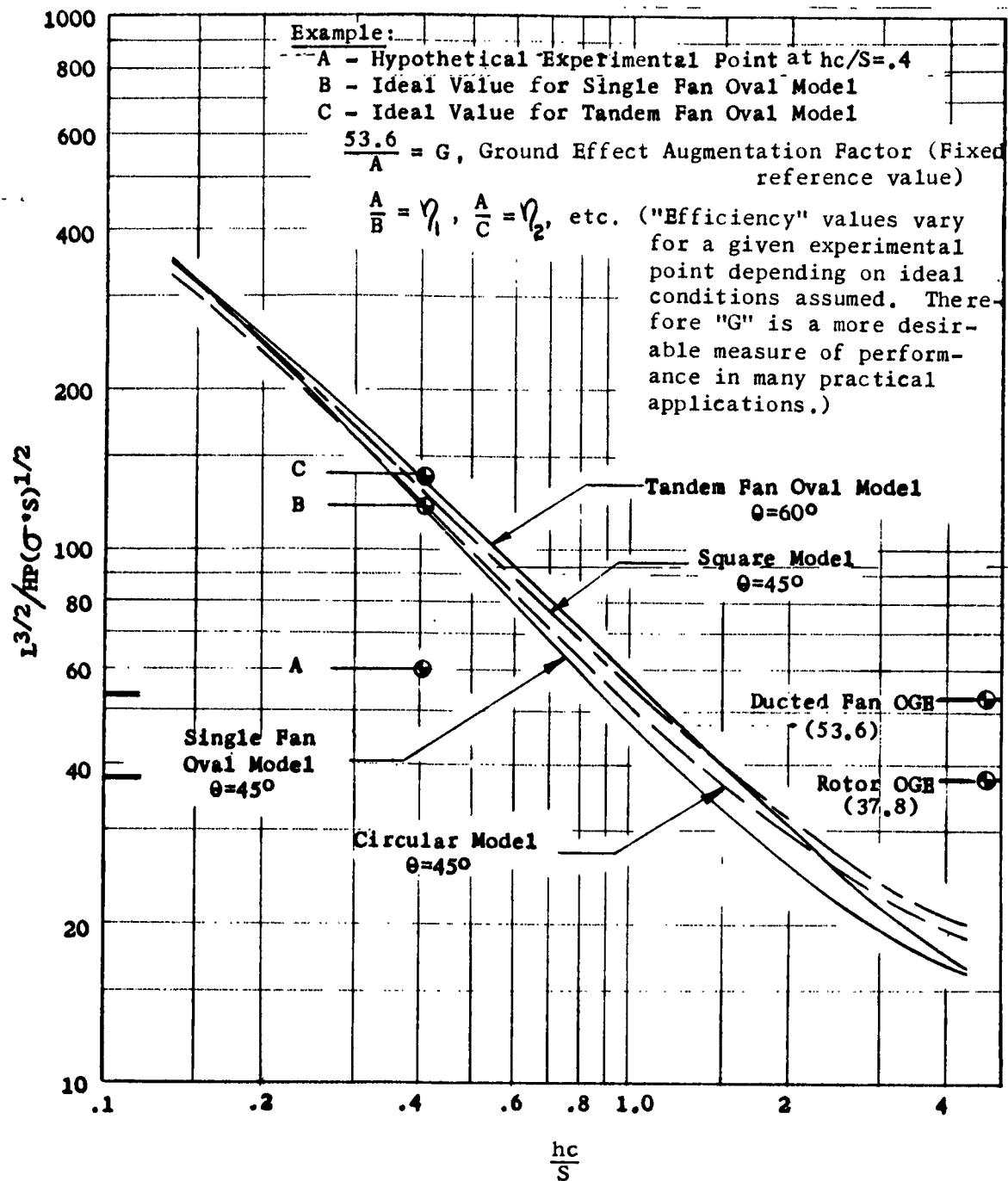


Figure 4. Ideal Hovering Performance

~~This indicates that four different values of over-all efficiency~~  
would result if all models had identical experimentally determined  
values of the performance parameter. From a practical standpoint,  
then, the term "over-all efficiency" loses significance.

Another measure of performance has been adopted (Reference 4) called the ground effect augmentation ratio,  $G$ , and is defined as the ratio of the performance parameter of an ideal ducted rotor operating out of ground effect to that of an air cushion vehicle in ground effect. This term permits a fixed value to be used as a reference when comparing the experimental values of the performance parameter. An example of this is shown in Figure 4.

In most instances, it has been this ratio, rather than over-all efficiencies, per se, which served as the basis of performance comparisons, both for modifications of the controlled flow configuration to improve its performance and for comparisons with the other air cushion vehicle systems. Only in certain instances have over-all efficiencies, based on the appropriate expressions for ideal performance, been stated.

## 2. Secondary Criteria (Stability, Controllability and Propulsion)

Since an evaluation of the controlled flow configuration involves more than simply determining hovering performance, the effects of controlled flow techniques on stability, control and propulsive characteristics were also determined. These, however, were done only for the hovering flight regime since the forward flight regime was beyond the scope of this investigation. The stability, controllability and propulsion evaluation was done with one configuration: the twin fan, oval planform arrangement. The approaches used involved improving, then evaluating, the static stability, control and propulsive characteristics for the configurations being compared and noting the loss, if any, of mean operating height as a function of tilt angle, control application, or propulsive force application.

## V. DESCRIPTION OF MODELS

### A. GENERAL

A total of five basic models were used during this program. Each basic model was subjected to one or more configuration modifications to obtain the required performance or handling qualities information. The first four models were designed for evaluating controlled flow techniques as applied to the internal arrangements of conventional air cushion vehicles, whereas the fifth model was for the purpose of exploring the application of controlled flow techniques to an external flow air cushion vehicle.

### B. INTERNAL FLOW MODELS

#### 1. Basic Configurations

The first four models consisted of two large models powered with an existing contractor-furnished ducted fan unit and two small models using power units constructed during this program. The effective diameters of the large models are approximately 5 feet; the first, with a circular planform, is shown in Figure 5a and the second, with a square planform, is shown in Figure 5b. The two small models had oval planforms and an effective diameter of 2.7 feet; one was powered with a centrally located ducted fan unit and is shown in Figure 6a while the second, shown in Figure 6b, was powered with two fan units in tandem.

It was possible to test plenum, conventional peripheral jet, and controlled flow peripheral jet arrangements by modifying the attachments or internal arrangements of each model. The first three models were used only in hovering performance studies and in developing techniques for improving performance. In addition to determining hovering performance with the tandem fan oval model, stability, controllability, and propulsion system characteristics were also defined.

In the following paragraph, the several modifications tested with each basic configuration are summarized. In subsequent paragraphs, each basic configuration and its modification is described in more detail.



Figure 5A. Circular Model

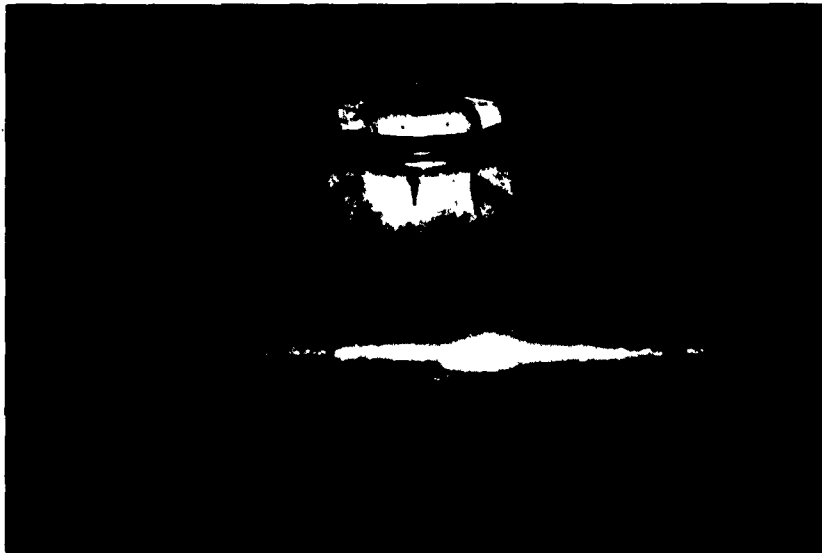


Figure 5B. Square Model



Figure 6A. Single Fan Oval Model

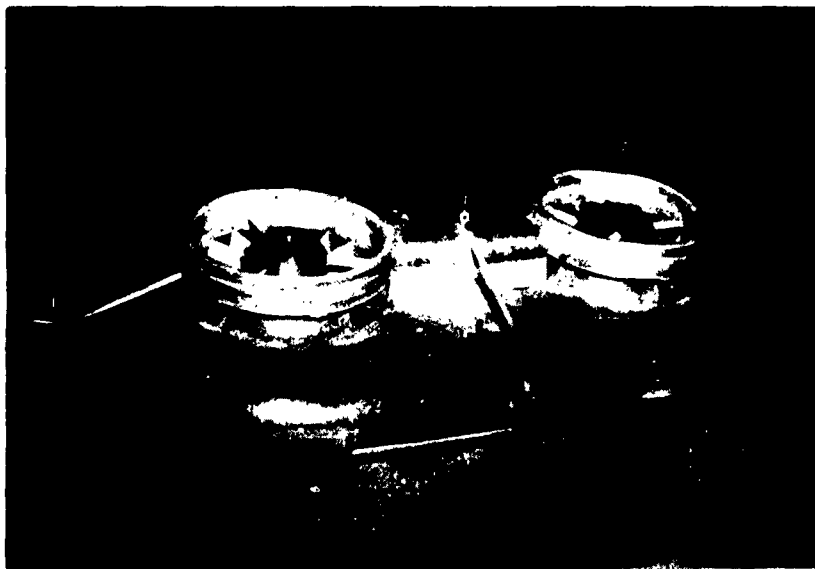


Figure 6B. Tandem Fan Oval Model



## 2. Model Modifications

a. Summary of Modifications - Numerous internal arrangements of each of the four basic models were tested during the course of this investigation. In order to relate the test results with the appropriate version of the model tested, "configuration numbers" have been assigned to each modification. The order is consecutive through all four basic models and is in the approximate chronological order tested. A total of 30 configurations are listed in Table 1.

The table presents the basic configurations with the combination of devices or attachments used to obtain a particular jet exit and/or internal arrangement. In addition, the table presents an index to the figure numbers where schematics of the modifications of each basic configuration may be found.

In the paragraphs following Table 1, each of the basic models and modifications are discussed in more detail. The discussions include schematics showing physical characteristics or dimensions of the basic models and the modification devices. All dimensions are given in inches unless otherwise noted. In addition, tabulated dimensional and nondimensional data are presented for purposes of making performance predictions based on equation (1). For all peripheral jet cases, the jet area is assumed to be equal to the fan area. This was a design criterion with the base plate configurations, and is a close approximation for all controlled flow configurations.

TABLE 1  
LARGE AND SMALL MODEL CONFIGURATIONS

Configuration		Exit Arrangement			Internal Arrangement										Plenum
					Peripheral Jet										
Basic Platform	No.	Jet Incln. (°)	Skirt Length (X)	Conventional Fully Ducted	Base Plate	Spinner Tab	Deflector Plate(s)	Partial Duct	Special Prop	Controlled Flow Full Vanes	Short Fins	Oval Ring Assembly	Contoured Orifice		
Circular See Figure 7	1	0°	Varied	X											
	2	↓	Varied		X										
	3	↓	Fixed												
	4	↓	Varied			X									
	5	↓	Varied					X							
	6	45°	Varied	X											
	7	↓	↓			X									
	8	↓	↓				X								
	9	↓	↓					X							
Square See Figures 8 to 10	10	45°	Fixed		X										
	11	↓	↓			X									
	12	↓	↓				X			X					
	13	↓	↓					X		X					
	14	↓	↓						X	X					
	15	↓	↓		X			X		X					
	16	↓	↓							X		X			
Oval Single Fan See Figures 11 to 14	17	45°	Fixed		X										
	18	↓	↓		X		X								
	19	↓	↓				X								
	20	↓	↓				X			X					
	21	↓	↓				X		X		X				
	22	↓	↓				X					X			
	23	↓	↓				X		X			X			
	24	↓	↓		X		X		X			X			
Oval Tandem Fan See Figures 15 to 17	25	60°	Fixed												
	26	↓	↓		X										
	27	↓	↓				X(2)								
	28	↓	↓				X(1)								
	29	60° to 600°*	↓				X								
	30	0° to 600°*	↓				X								

\* Concentric Jets

b. Circular Model - The circular model in its nine configurations is shown in Figure 7. It was powered with a series-wound, 115-volt, two-horsepower electric motor with a gear-reduced nominal shaft speed of 3400 rpm. This motor was part of a ducted fan lift unit having a fan diameter of 22 inches, supplied by the contractor. The pitch of the rectangular planform, untwisted fan blades was adjustable. A near optimum blade pitch setting of nineteen degrees was used throughout the test program. Further details of this lift unit are presented in Figure 7.

The afterbody of the basic model which was attached to the ducted fan power unit included a transition section and a circular transparent ceiling for the cushion cavity. To the outer rim of the ceiling was attached a cylindrical sheet metal sleeve which could be adjusted vertically for varying skirt length. Another component could be attached to the bottom of the skirt for converting the jet inclination angle from 0 to 45 degrees. All other devices for modifying this basic configuration are shown in Figure 7.

Table 2 below summarizes the dimensional and nondimensional data necessary for predicting ideal model performance.

Table 2

Circular Model Numerical Data

$\theta$ (deg)	S (sq ft)	$S_b$ (sq ft)	$S_f$ (sq ft)	c (ft)	$t_e$ (in)	c/S (1/ft)	$S_b/S$ --	$S_f/S$ --	$S_b/S_f$ --
0	19.65	17.67	1.98	15.3	1.55	.779	.899	.101	8.92
45	18.16	16.76	1.98	14.6	1.55	.804	.923	.109	8.46



c. Square Model - The large square model was tested in Configurations 10 through 15, which are shown in Figure 8. The fan unit used in this model is detailed in Figure 7 of the circular model. Skirt length and jet inclination angle were not variable.

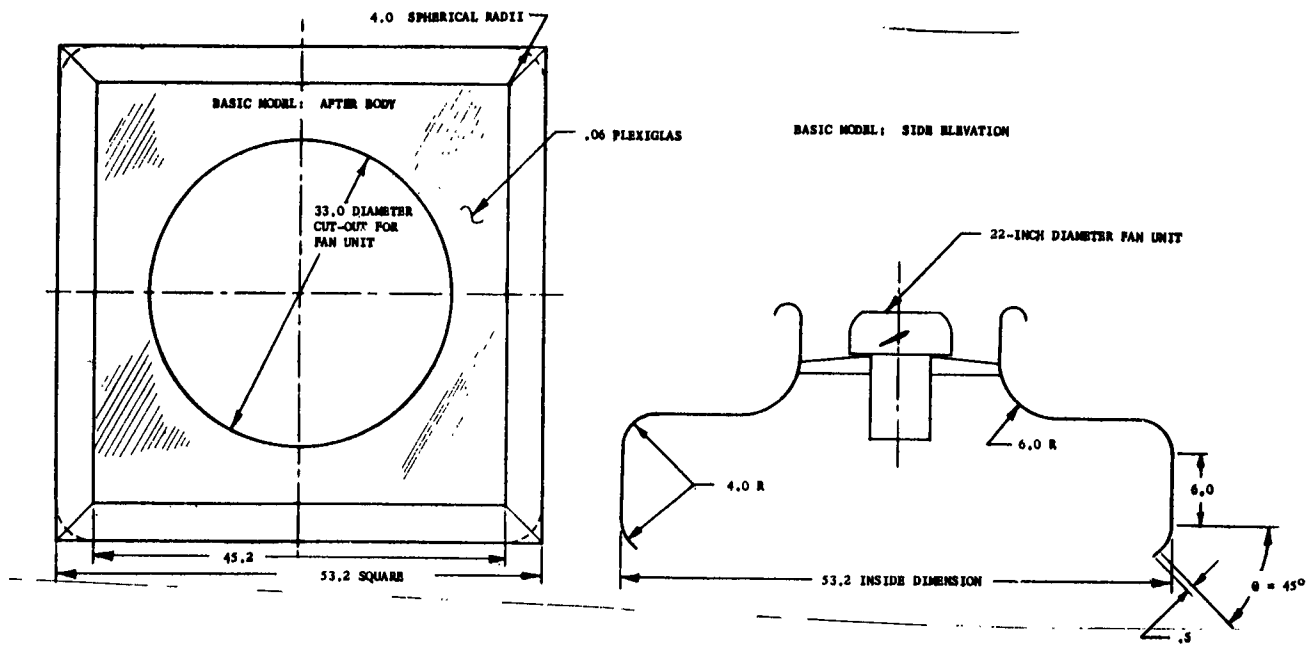
The square model was tested with and without planform distribution vanes. Figure 9 shows the layout of the distribution vanes. These vanes were designed for use with the contoured orifice shown in Figure 10. Control of planform distribution was also effected by the contoured orifice.

Dimensional data necessary for predicting ideal model performance are tabulated below.

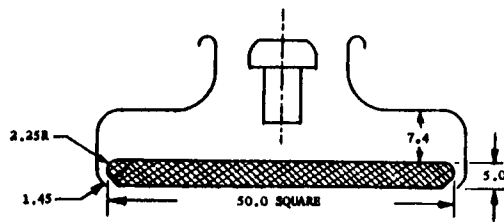
Table 3

Square Model Numerical Data

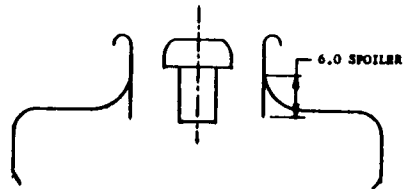
$\theta$ (deg)	S (sq ft)	$S_b$ (sq ft)	$S_f$ (sq ft)	c (ft)	$t_e$ (in)	c/S (1/ft)	$S_b/S$ --	$S_f/S$ --	$S_b/S_f$ --
45	17.50	16.10	1.98	16.0	1.45	.914	.92	.113	8.14



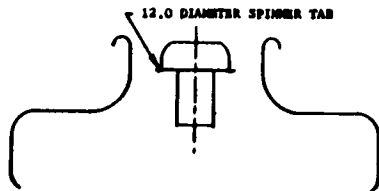
#### FUNDAMENTAL CONFIGURATIONS



BASE PLATE ANNULAR JET  
NO. 10

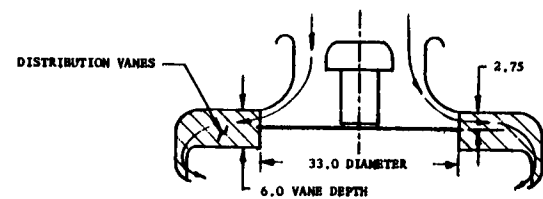


PLENUM  
NO. 11

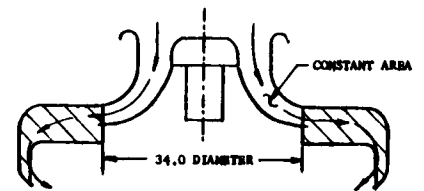


SPINNER TAB  
NO. 12

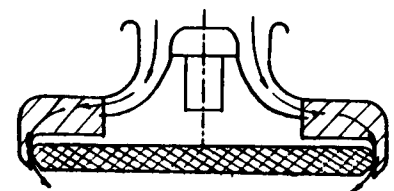
#### CONFIGURATIONS EMPLOYING DISTRIBUTION VANES



DEFLECTOR PLATE  
NO. 13



PARTIAL ANNULAR DUCT  
NO. 14



NO. 15  
(COMBINATION OF CONFIGURATIONS 10 & 14)

Figure 8. Square Model Configurations

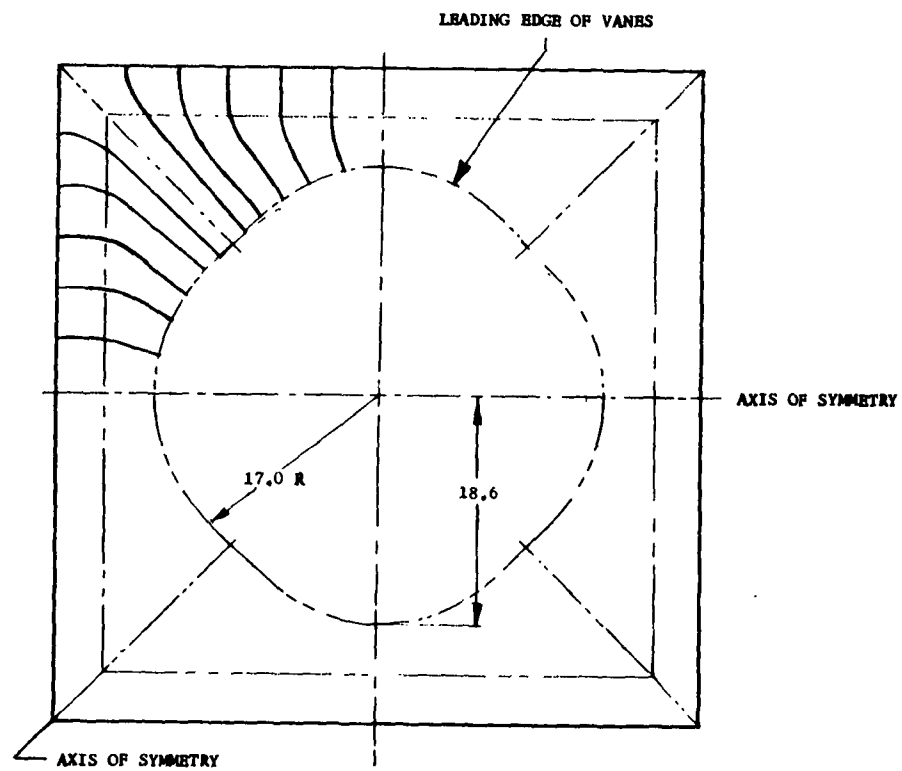
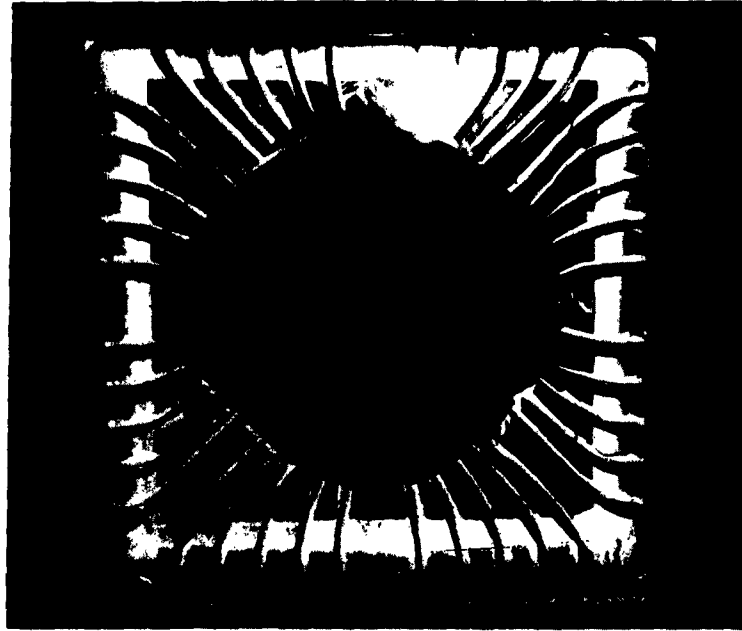


Figure 9. Photograph and Layout of Square Model Distribution Vanes

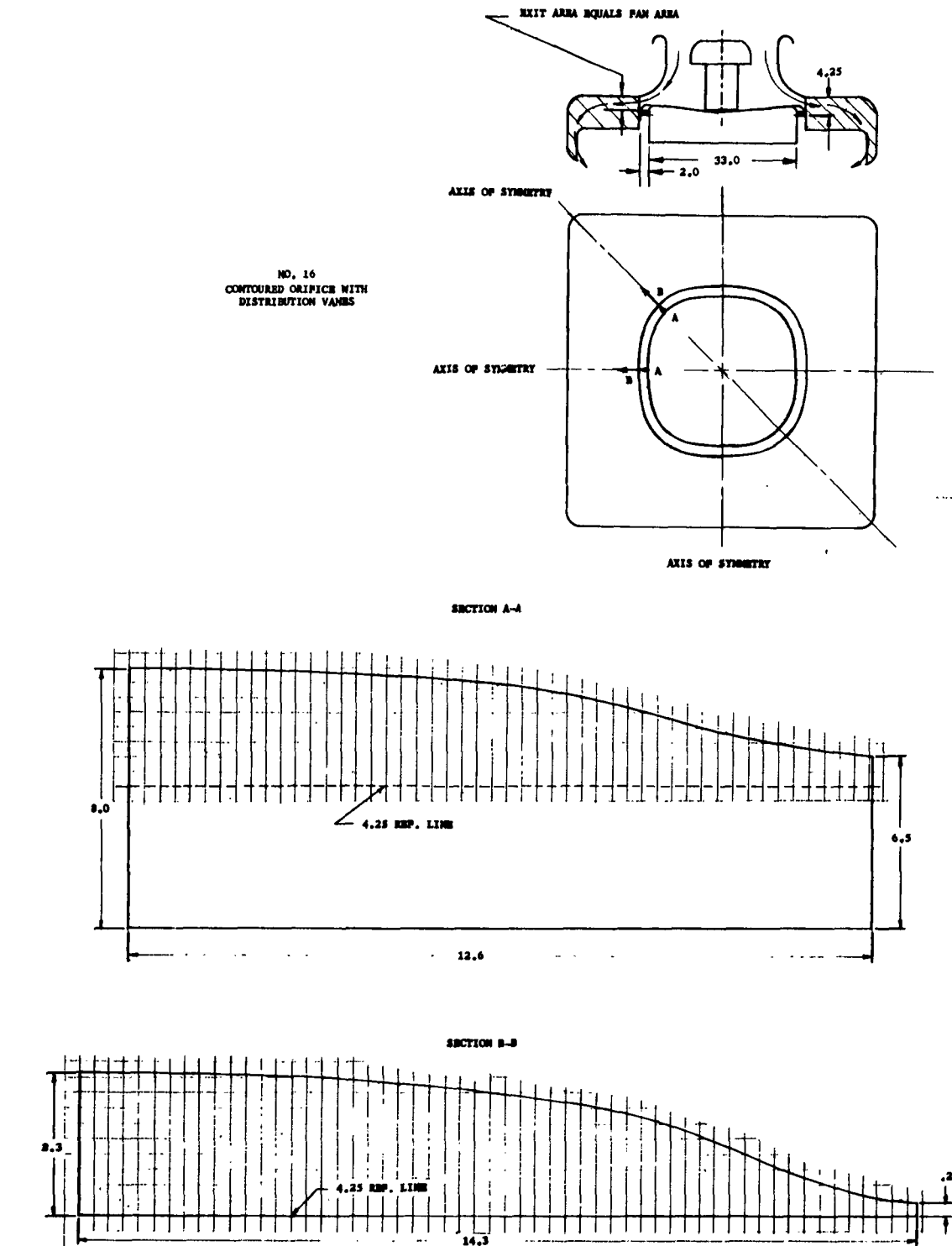


Figure 10. Square Model with Contoured Orifice Assembly



d. Single Fan, Oval Model - The single fan oval model was tested in Configurations 17 through 24. ~~Schematics of Configurations~~ 17 and 18 are shown in Figure 11a, while 19 through 24 are indicated in Figure 11b. The first configuration was that of a base plate peripheral jet. All other configurations incorporated some form of controlled flow. A plenum arrangement was not tested on this model. It should be noted that the deflector plates used as a controlled flow technique in Configurations 18 and 19 are flat, whereas in the subsequent configurations the plates were warped.

The fan unit used in this model is described in Figure 12. Fan pitch was set to obtain a fan speed of approximately 12,000 rpm at the electric motor's rating of 9 amps. Additional information about the standard and special fan blade assemblies used on this model is presented with Figure 13. Details of the special blade are shown in Figure 14.

Presented below are the data necessary for predicting ideal performance of the model.

Table 4

Single Fan Oval Model Numerical Data

$\theta$	S	$S_b$	$S_f$	c	$t_e$	c/S	$S_b/S$	$S_f/S$	$S_b/S_f$
(deg)	(sq ft)	(sq ft)	(sq ft)	(ft)	(in)	(1/ft)	--	--	--
45	5.70	5.41	.41	8.9	.54	1.614	.949	.072	13.2

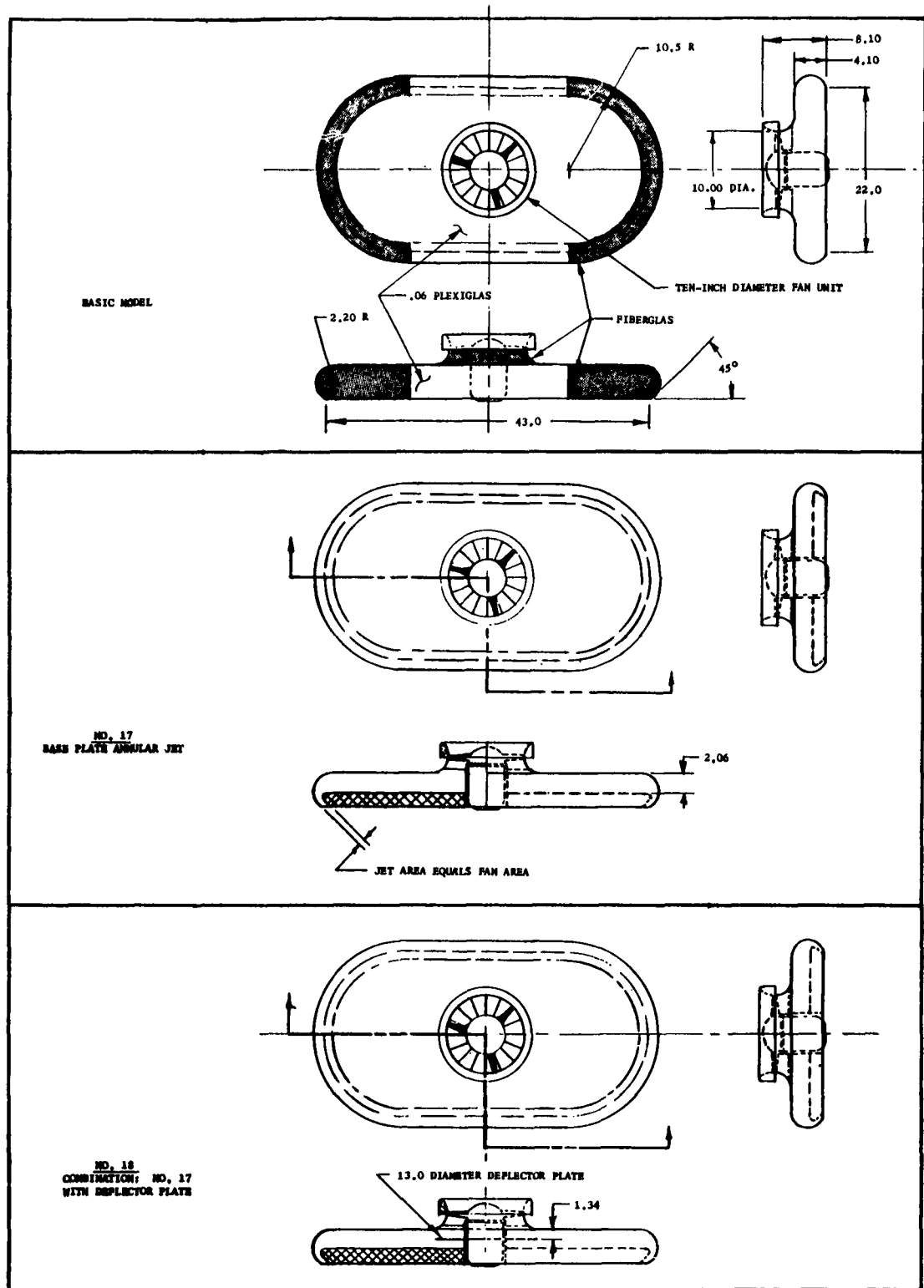


Figure 11a. Single Fan Oval Model Configurations 17 and 18

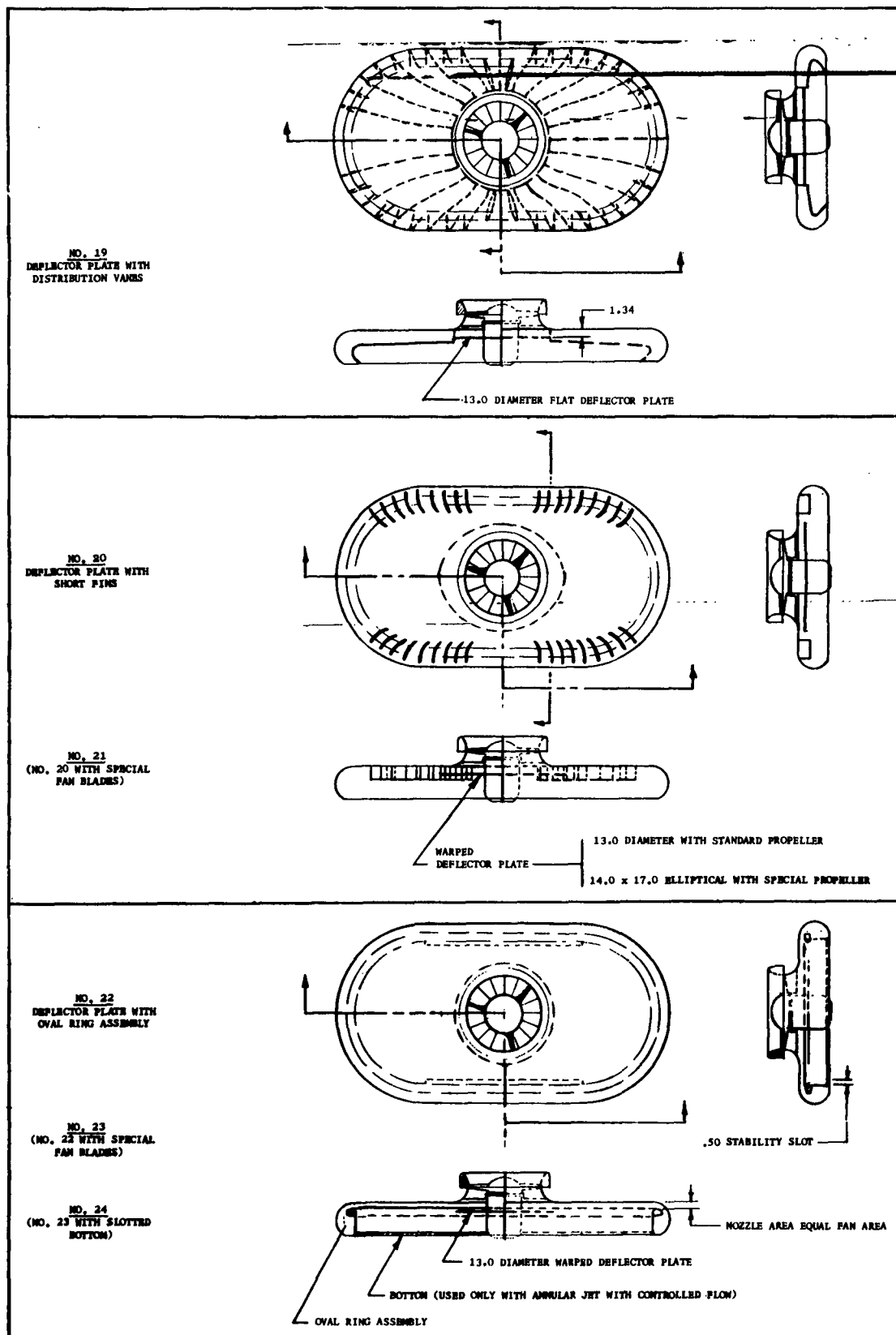


Figure 11h. Single Fan Oval Model Configurations 19 through 24



Two fan blade assemblies were tested in the oval model. Both are shown in the photograph below (Figure 13). The special blades were designed to establish the proper velocity gradient for a Coanda turn immediately downstream of the fan. A layout for these blades is shown in Figure 14. The conventional blades are model airplane propeller blades manufactured by Dynamic Models, Inc., for an eleven-inch automatic pitch propeller. A ten-inch diameter fan resulted from installing the blades in a smaller hub. The airfoil of these blades approximated a R.A.F.-6-F section. At a radius of 3.5 inches, their chord was a maximum of .85 inches. Blade twist was 7 degrees.

Blade pitch measured at 3.75-inch radius was set at 14 degrees for the special blades and 12 degrees for the conventional blades. At the fan motor's rating of 9 amps, both fans turned about 12,000 r.p.m.

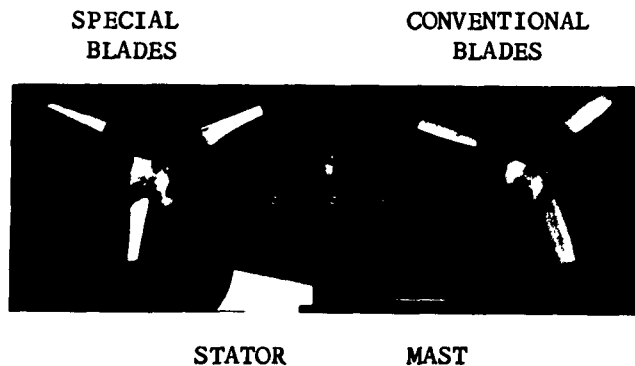
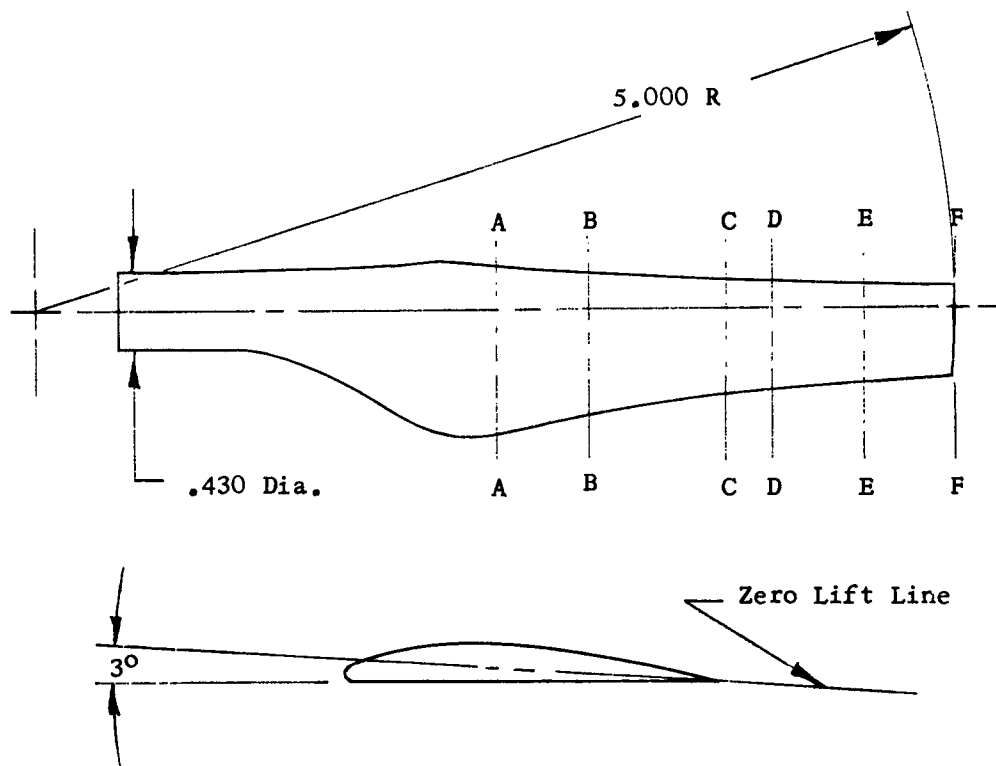


Figure 13. Ten-Inch Diameter Fan Unit



R.A.F-6-F AIRFOIL SECTION

Station	Radius	Chord	Angle to Zero Lift Line	Reference Angle
A-A	2.50	.917	18.7°	1.7°
B-B	3.00	.767	17.6°	0.6°
C-C	3.75	.605	17.0°	0°
D-D	4.00	.570	17.0°	0°
E-E	4.50	.515	17.7°	0.9°
F-F	5.00	.460	18.8°	1.8°

Figure 14. Special Blade Layout

e. Tandem Fan Oval Model - Hovering performance tests were conducted with Configurations 25 through 30 on this model. Static stability of each, with the exception of Configuration 27, was also determined. Figure 15a shows schematics of the model and its modifications for Configurations 25 through 27. The remaining schematics are shown in Figure 15b. Mechanical adjustments on Configurations 29 and 30 allowed alteration of the thickness of the outer jet. Altering the outer jet thickness differentially from side to side was a means of lateral control investigated with these configurations.

A second fan power unit identical to the one used on the single fan oval model was constructed. Both units were used to power this model. To control the flow between the fan exits, a flow splitter was used having the planform shown in Figure 16. Configuration 30 was modified to incorporate a forward propulsion system. This system is shown in Figure 17.

In Table 5 below,  $S$ , the total cushion area, is only 96 per cent of the area shown in Table 4 for the single fan model. A reduction of cushion area resulted from increasing the jet inclination angle from 45 degrees to 60 degrees. (Both models have identical overall planform areas.)

Table 5

Tandem Fan Oval Model Numerical Data

$\theta$ (deg)	$S$ (sq ft)	$S_b$ (sq ft)	$S_f$ (sq ft)	$c$ (ft)	$t_e$ (in)	$c/S$ (1/ft)	$S_b/S$ --	$S_f/S$ --	$S_b/S_f$ --
60	5.47	5.06	.818	8.9	1.12	1.626	.925	.150	6.2

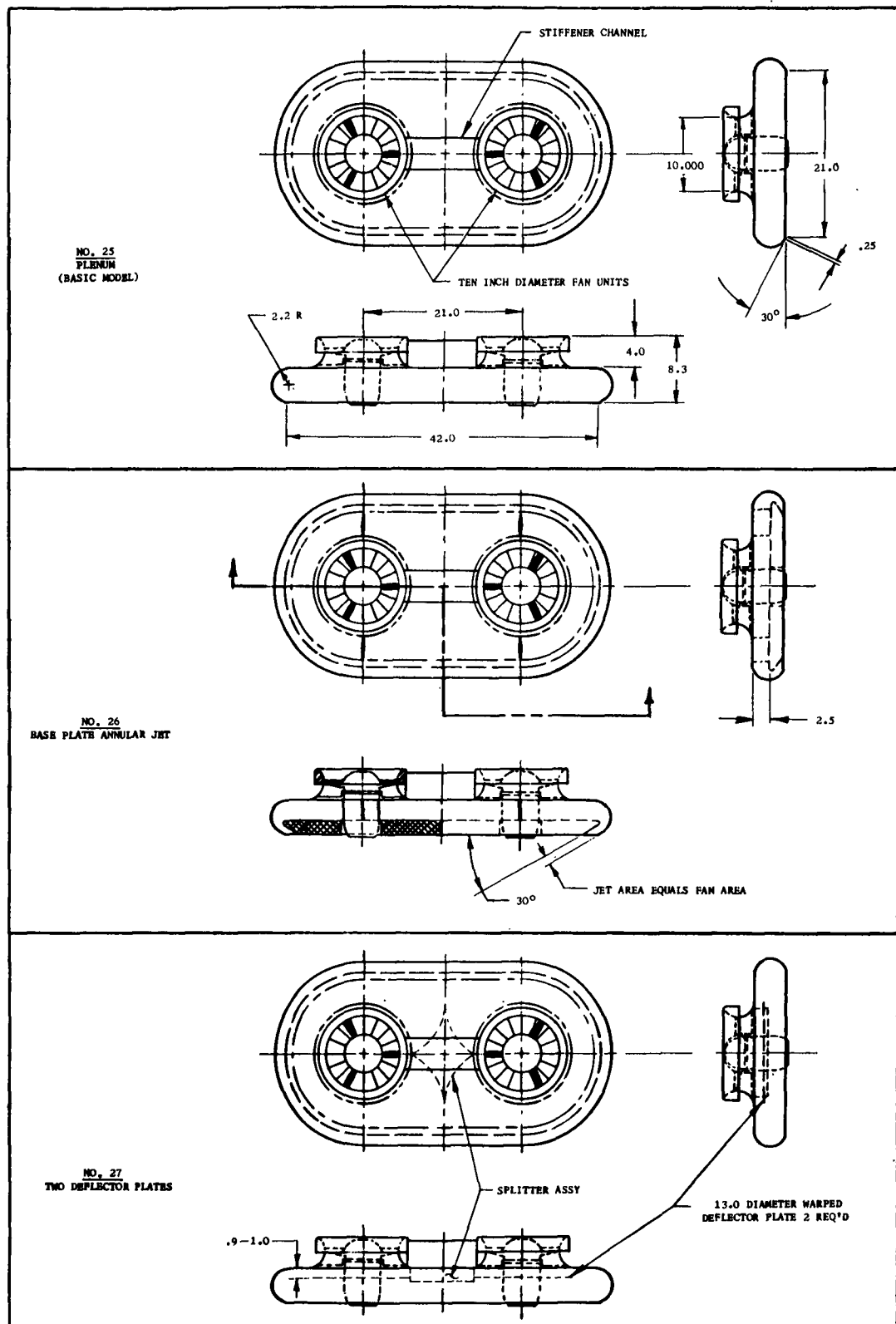


Figure 15a. Tandem Fan Oval Model Configurations 25 through 27



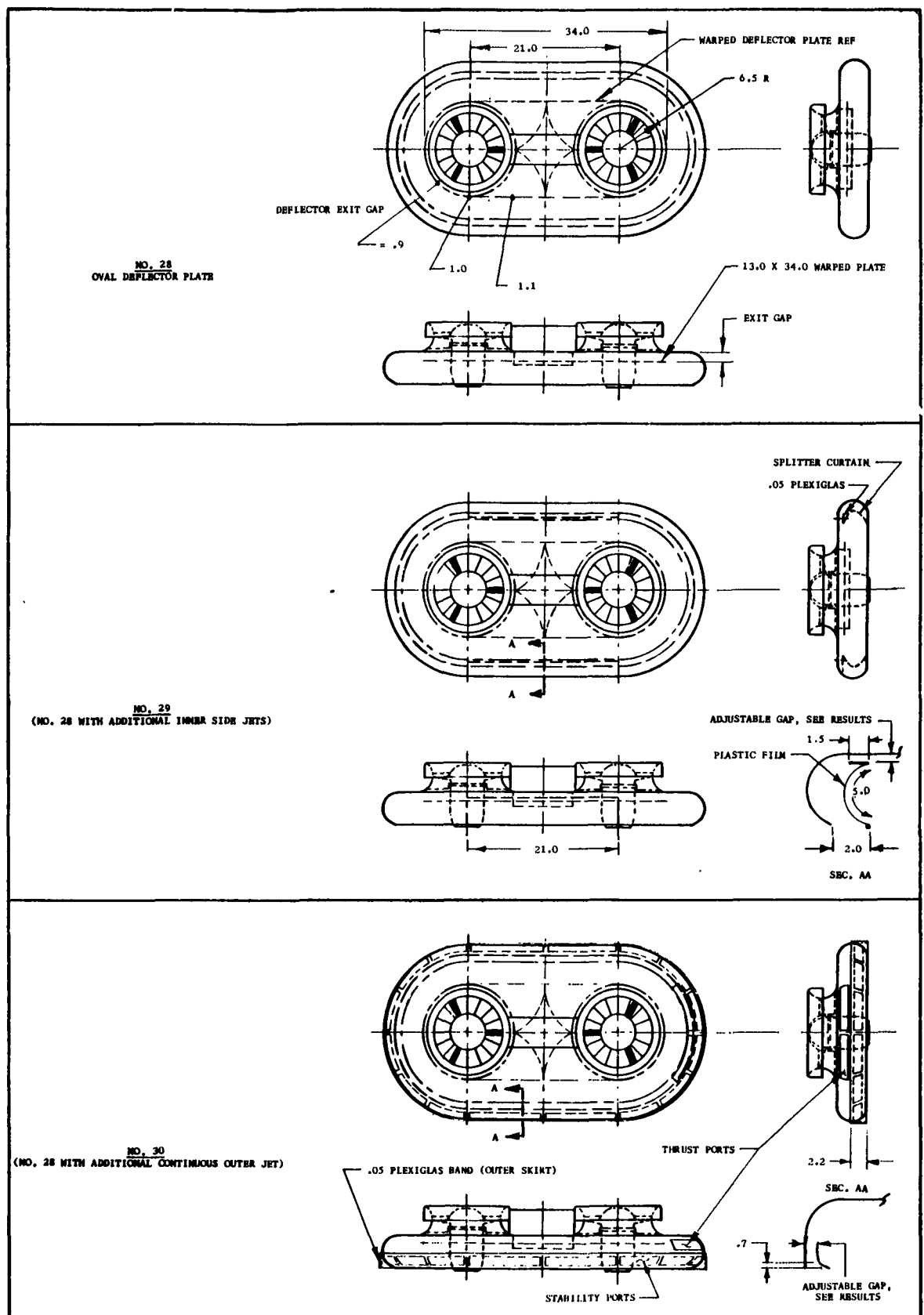


Figure 15b. Tandem Fan Oval Model Configurations 28 through 30

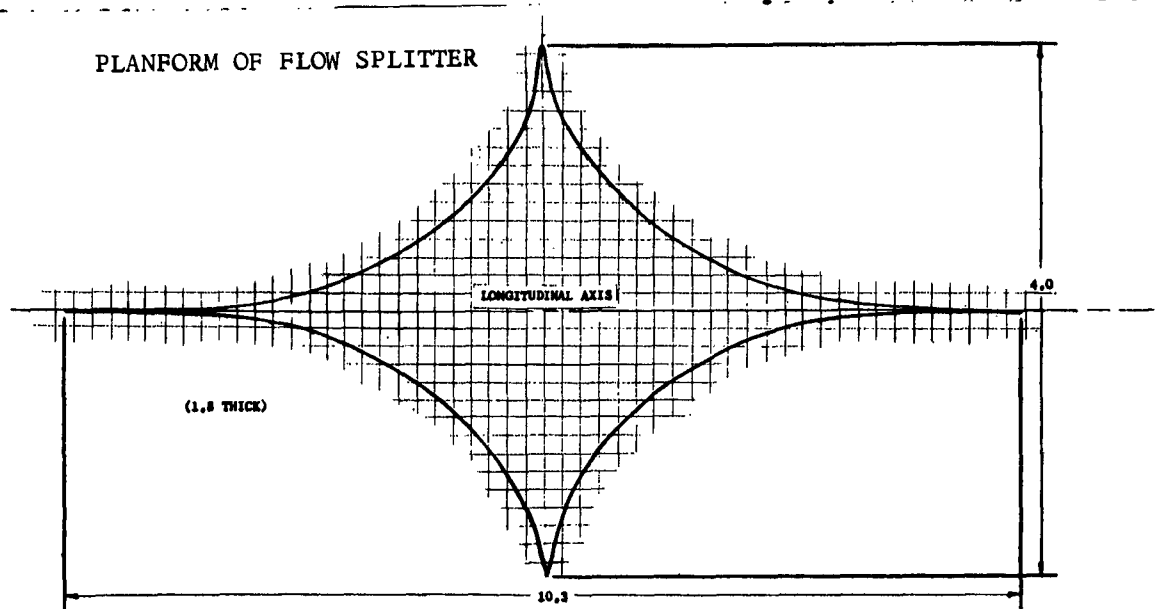


Figure 16. Tandem Fan Oval Model  
Flow Splitter Assembly

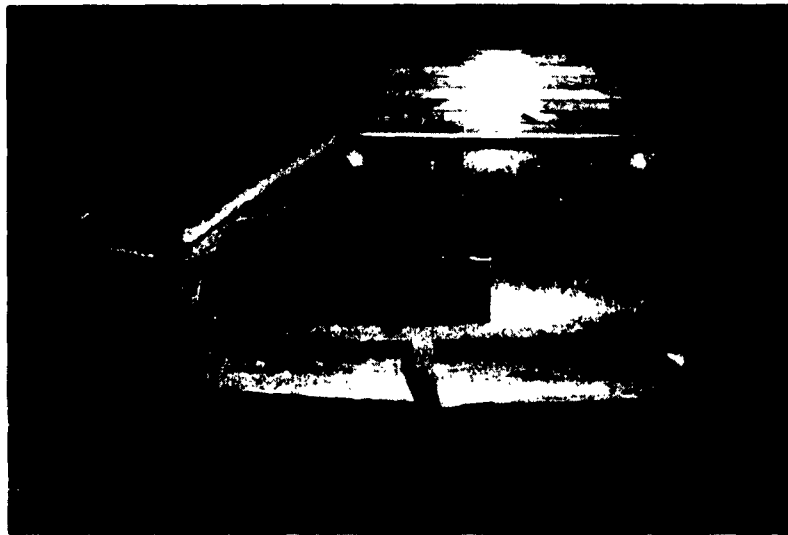


Figure 17. Propulsion Port Installation  
in Configuration No. 30

### C. EXTERNAL FLOW MODEL

The application of controlled flow techniques to an external flow configuration was briefly explored with the model shown in Figure 18. The drawing shows the structural section of the model with a concentric band around the periphery of the base. The photo inset shows the model without the band. This model was tested in both configurations (with and without band).

The power unit was one of the ten-inch diameter ducted fan units used with the oval models. Geometrical data for this model are presented in Table 6 along with similar parameters for the ducted fan power unit.

Table 6

Numerical Data for 10" Fan Unit and External Flow Model

$\theta$ (deg)	S (sq ft)	$S_b$ (sq ft)	$S_f$ (sq ft)	c (ft)	$t_e$ (in)	c/S (1/ft)	$S_b/S$ --	$S_f/S$ --	$S_b/S_f$ --
A. -	.545	.136*	.409	2.62	2.5	4.81	.250	.750	.333
B. 0	1.557	1.148	.409	4.12	1.2	2.58	.738	.263	2.8
* Spinner Area		A. 10" Fan		B. External Flow Model					



PHOTOGRAPH OF MODEL WITHOUT BAND

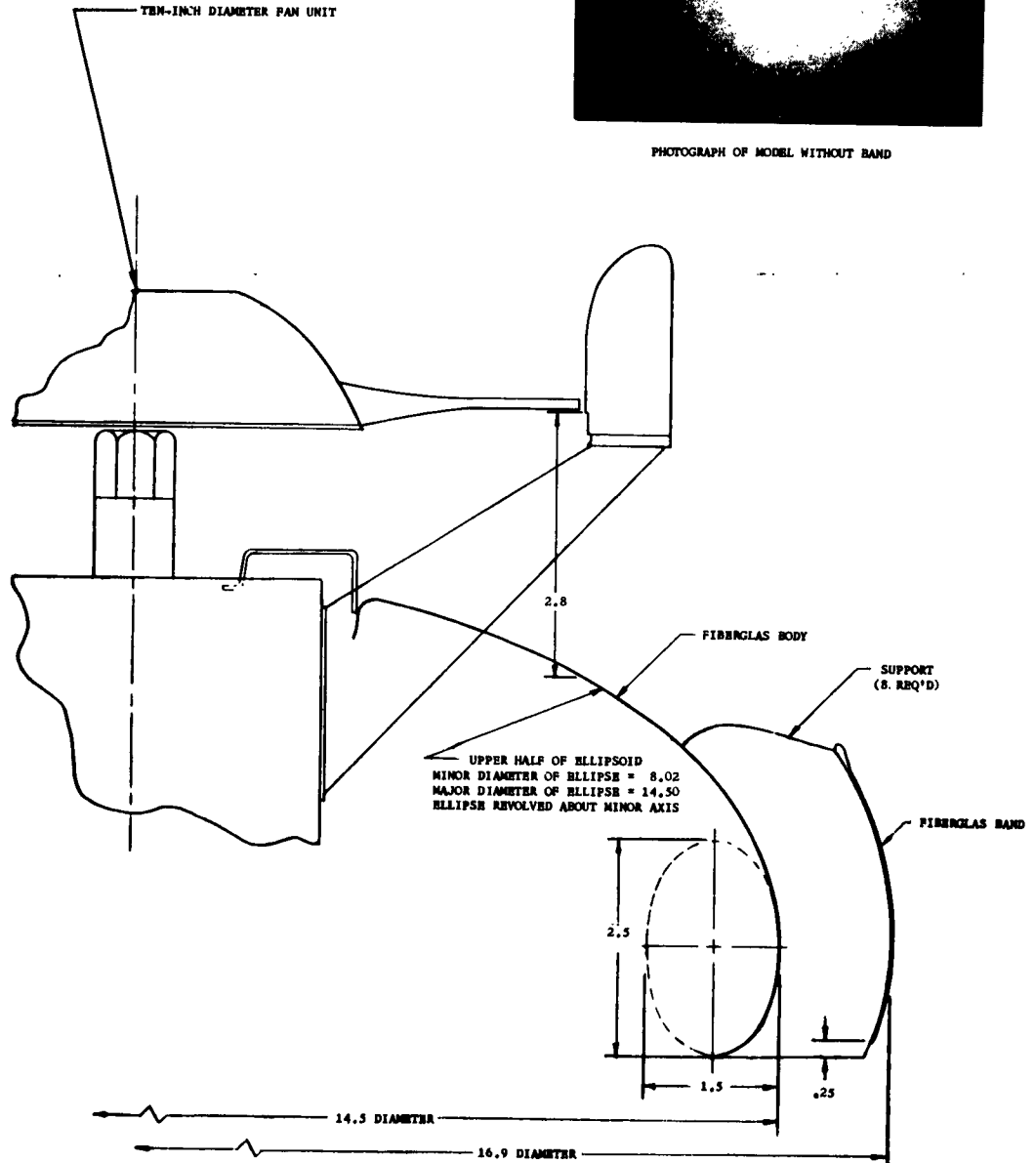


Figure 18. External Flow Model

## VI. DESCRIPTION OF EXPERIMENTAL EQUIPMENT AND PROCEDURES

### A. GENERAL

Two separate test setups were used to measure the hovering characteristics of the large and small models described in the previous section. In both setups the total lift produced by the models was measured mechanically. The experimental apparatus for the small models also provided means for determining static stability, control, and propulsion characteristics.

### B. LARGE CIRCULAR AND SQUARE MODEL TESTING

Hovering performance of the large models was measured with the equipment shown in Figure 19. The test stand is a beam balance with the model (approximately 50 pounds) on one side and a counterbalance supported by a Fairbanks beam scale (75 pound capacity, 1 ounce sensitivity) on the other side. Total model lift was the difference in apparent weight of the counterbalance; for power off and on.

Model height above the floor was adjusted to a selected level then fixed to obtain the test point. Fan rpm was monitored with a Berkeley impulse counter wired to a magnetic pickup mounted below a six pole armature on the fan shaft. Fan speed was maintained at 3000 rpm by manually adjusting the variac that supplied power to the fan motor. Motor torque was sensed with a strain gaged beam in the fan nacelle and read out visually on a meter. Shaft power as determined from torque and rpm ranged from .85 to 1.50 horsepower.

### C. SMALL MODEL TESTING

Characteristics of the small models employing the ten-inch diameter fan or fans were determined with the equipment shown in Figure 20. A variac was also used to control power to the small fans. Fan speed and power, in this case, were determined from Prony brake calibrations relating shaft speed and power to electric input (watts and volts). Electric input was recorded from visual meter readings. Power varied from 0 to .75 horsepower per fan.

Unlike the experiments with the large models, the lift of the small models (12 to 20 pounds weight) was fixed by placing a calibrated ballast weight on the end of an unloading wire, thus balancing a portion of the model's weight. As power was applied the model ascended from the ground board until it reached an equilibrium height. A torque restraint guide was calibrated to show model height above the ground board.

Determination of static stability and horizontal thrust was accomplished simultaneously with the measurement of lift, power, and height of selected configurations.

Horizontal thrust was reacted with a wippletree tether. The load in the tether was measured with a calibrated beam and poise. (See the schematic in Figure 20.) Illustrated is the tether for reacting forward thrust. A similar arrangement was used to measure lateral thrust.

For the stability and control studies, the tandem fan oval model was restrained by a single-axis pivot atop a centrally located vertical guide rod which could be aligned to permit either freedom in roll or pitch. This pivot was located at the center of gravity of the model which was adjusted to be 3.75 inches above the bottom edge of the model. Attitude was measured with protractors affixed to the model.

Static stability characteristics were determined by shifting the model center of gravity with calibrated weights, to correspond with the shifts in cushion center of pressure resulting from attitude changes.

Yawing moments produced by a heading control system were measured with a spring scale as shown in the schematic.

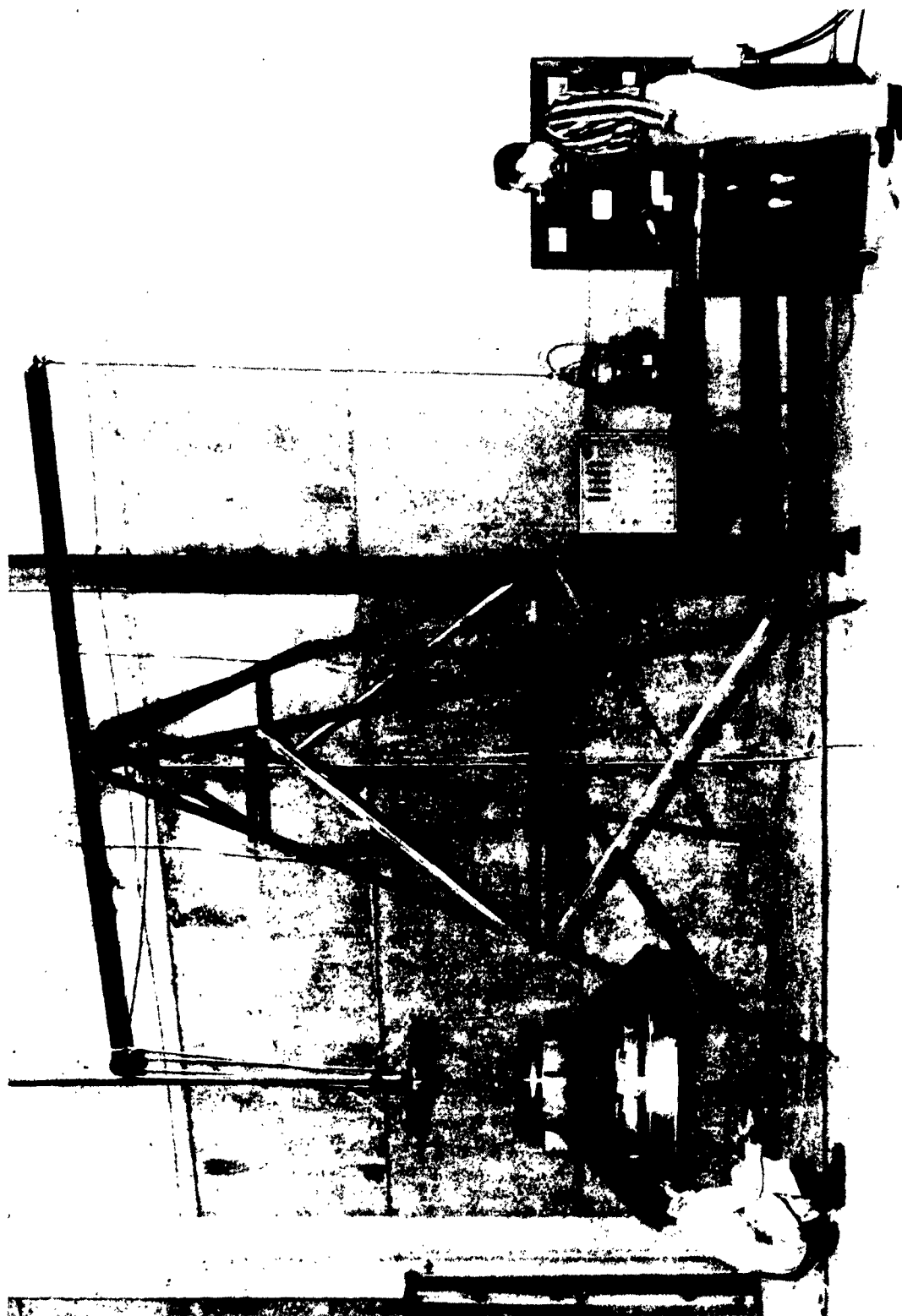


Figure 19. Test Equipment for Large Models

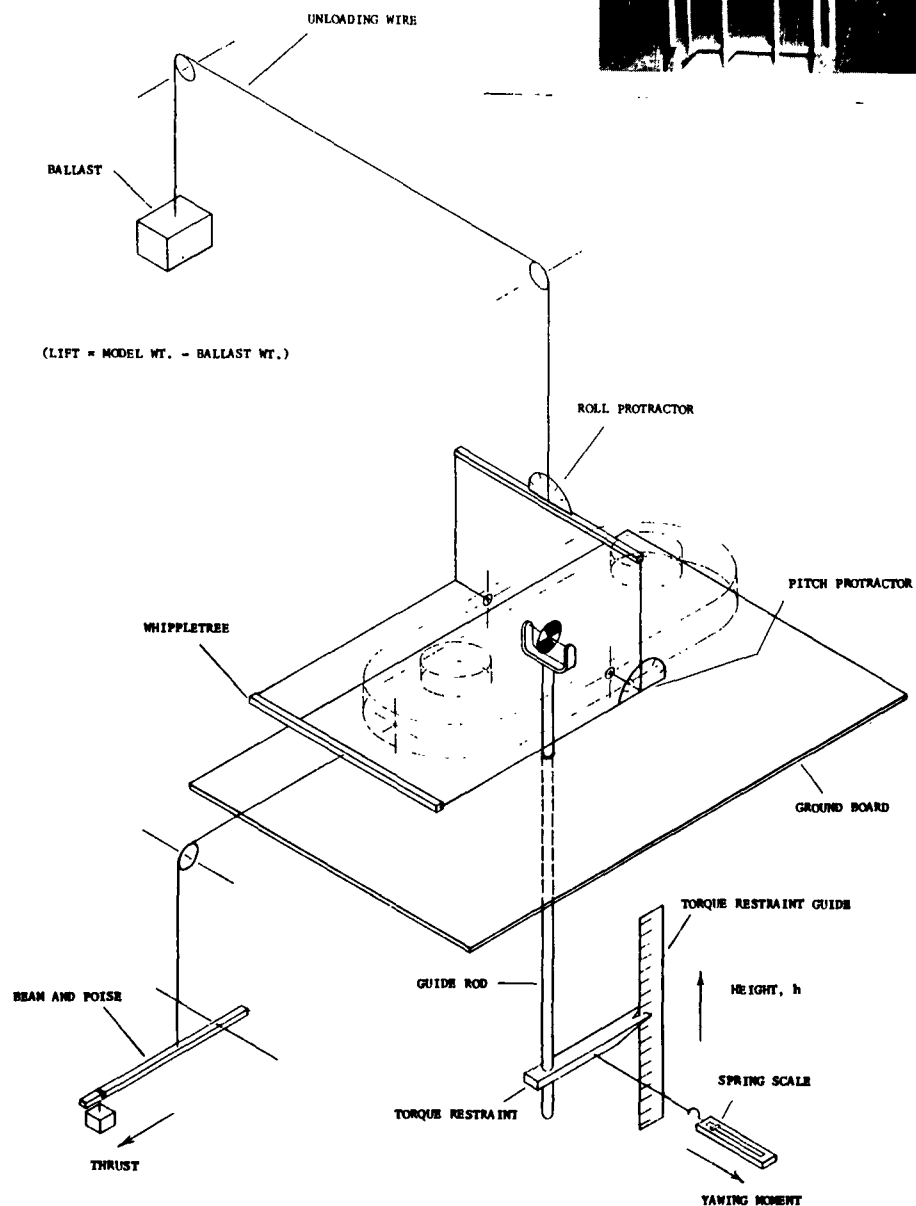


FIGURE 20. TEST STAND FOR SMALL MODELS



## VII. RESULTS

### A. GENERAL

In this section, the experimental results are presented generally in the chronological order in which they occurred. This sequence is also one of planform variation starting with circular (Configurations 1 through 9), square (Configurations 10 through 16), oval with single fan (Configurations 17 through 24), and oval with tandem fans (Configurations 25 through 30).

A considerable portion of the initial effort with the circular planform was aimed at improving the general performance of the models regardless of whether the internal arrangement was configured as a plenum or as an annular jet formed by controlled flow, a base plate, or with internal ducting. By starting with a circular planform, the problem of obtaining a uniform distribution of the jet around the periphery was purposely avoided. Based on tests with the circular planform, the significant controlled flow devices were then applied to the square planform model, and the peripheral distribution problem was introduced. This was repeated for the remaining oval model configurations. During all tests, hovering performance results were consistently recorded and are presented in this section.

Near the completion of the investigation, the oval model with tandem fans was used exclusively for quantitative investigations of various systems providing stability, controllability and propulsive force in the hovering flight regime. These systems were all of the integrated type; that is, they were incorporated with the lift system. The results presented include the effectiveness of these systems and the hovering performance penalties resulting from their use.

During the investigations, configuration combinations were tested to determine the effects of controlled flow techniques on the conventional base plate peripheral jet. In addition, the application of controlled flow techniques as applied to the External Flow Vehicle was briefly explored.

### B. HOVERING PERFORMANCE

#### 1. Jet Exit Arrangements

One of the initial set of experiments conducted was an exploration of the effects of skirt length and jet inclination angles used at the periphery of the vehicle. It was known from previous work that skirt length could affect the performance of the conventional annular jet configuration. Improved performance of the annular jet with increased jet inclination angles was, of course, expected; however, the question of inducing separation at the concave bend in the controlled flow configuration remained. Therefore, early in the experimental program, these two parameters were investigated on the circular model.

a. Skirt Length - For a number of annular jet configurations tested, with and without controlled flow, skirt length to jet thickness ratio was varied from approximately zero to 5.0. Effects of lengthening the outer skirt were observed for vertical and 45° inclined peripheral jets. The results are presented in Figures 21 and 22, respectively.

Effects of lengthening the outer skirt are shown for the vertical jet configurations in Figure 21. The hovering performance of the fully ducted annular jet increases abruptly with increases in skirt length peaking out at a skirt length of 1.0 to 1.2 inches. This is equivalent to 75 per cent of the jet exit width. Performance decreases, rises and decreases again as skirt length increases. It appears from Figure 21 that performance is relatively insensitive to increases of skirt extension beyond eight inches or about five times the jet thickness.

Within the range tested, the performance of the partial duct configuration varied less than six per cent. All of the internal arrangements tested with the 45 degree inclined jet lip performed best with a skirt extension of 5.7 inches ( $3.8 \times t_e$ ). (See Figure 22.) Note, however, that the 45 degree inclined jet lip increases base cavity depth 3.2 inches ( $2.1 \times t_e$ ). This is not included in the skirt extension length.

The performance of the controlled flow configuration employing an 11.5 inch diameter spinner spoiler was increased as much as 48 per cent at low heights by increasing skirt length. Here, again, Figures 21 and 22 show that the performance levels off as the skirt is extended beyond eight inches. During tests of this configuration, the internal flow was observed, revealing that boundary layer separation on the convex turn was reduced and flow re-attached to the ceiling sooner with the longer skirt extensions. Boundary layer separation occurred in all configurations on or just downstream of the 90 degree turn below the fan.

There are several mechanisms at work that could be responsible for the difference in performance from one internal configuration to another and from one skirt extension length to another. Three modifications were made to the fully ducted annular jet configuration in an attempt to isolate the effects of the several mechanisms affecting performance.

Performance comparisons of the fully ducted annular jet with these modifications are shown in the first plot of Figures 21 and 22, respectively. The first modification consisted of extending the inner duct wall (inner skirt) the same amount as the outer skirt extension. This reduces the transfer of energy from the jet curtain to the air mass in the cushion. The plot for the vertical jet shows that this modification improves performance at low heights but causes a loss in performance at heights above 10 per cent of the model diameter. Note, however, that

\* Denotes Configuration Number

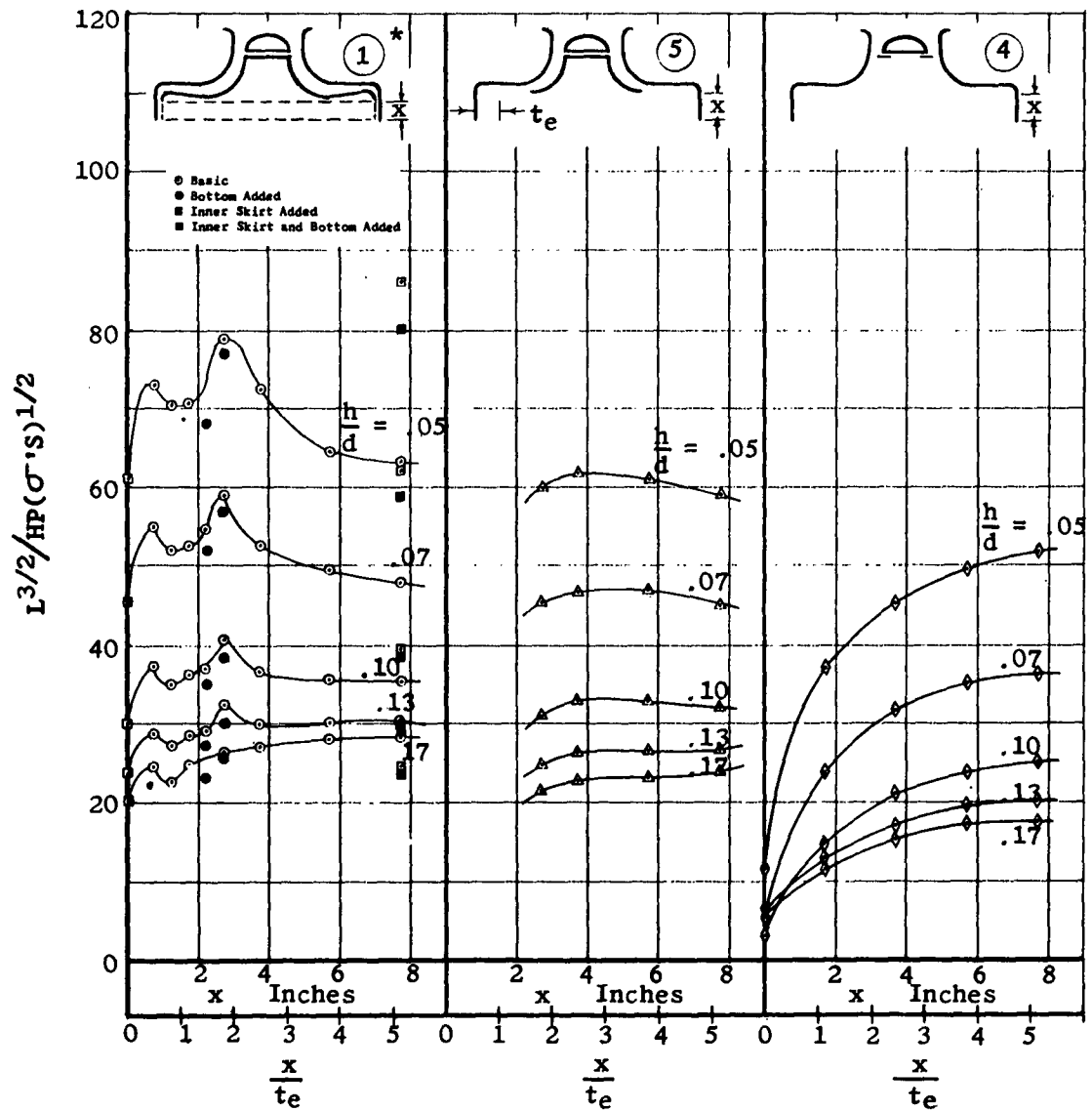


Figure 21. Effects of Skirt Length on Performance,  $\theta=0^\circ$

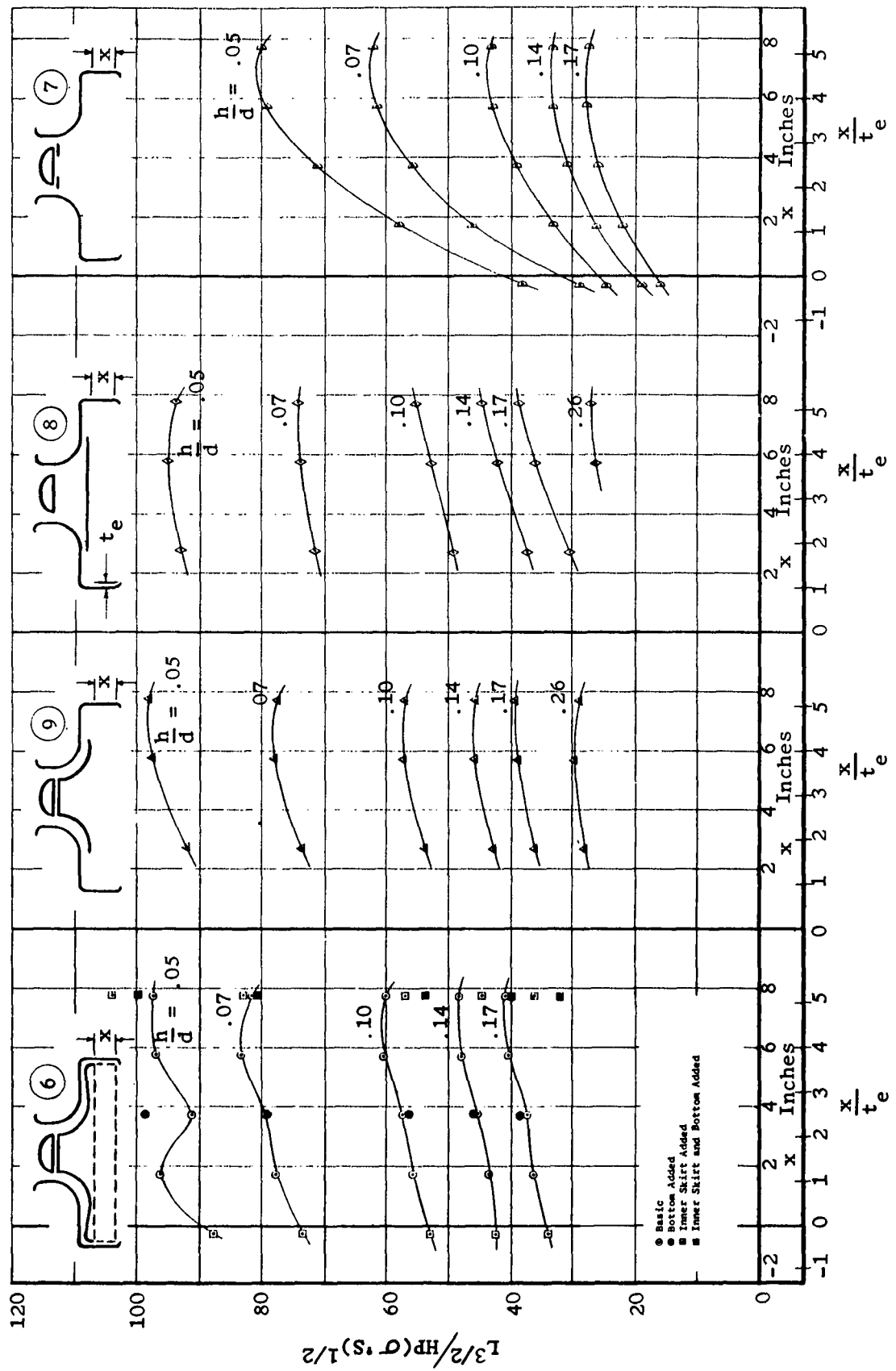


Figure 22. Effects of Skirt Length on Performance,  $\theta=45^\circ$

the crossover height was eight per cent of the base diameter for the 45 degree inclined jet; i.e., above eight per cent, the model experiences loss of performance due to the presence of the inner skirt.

The second modification was made to see if the depth of the base cavity had an effect on performance. By placing a bottom flush with the inner and outer skirt in their fully extended positions, the base cavity was eliminated entirely and the resulting configuration was that of a fully ducted annular jet with a baseplate. A third test was made with a bottom flush with the inner duct without an inner skirt. This arrangement had an intermediate depth of the base cavity. The results are significant in that they show that the insertion of a bottom, that reduces the base cavity depth or completely eliminates the base cavity, causes a loss in performance at all heights.

b. Jet Inclination Angle - It can be shown theoretically that inclining the jet inward will produce higher base pressures. However, the vehicle's internal surface area must be increased to incline the jet, thus increasing internal losses. Additional turning of the jet curtain upstream of the exit for high inclination angles also increases internal losses. Because of the possibility of a breakdown in controlled flow resulting from high internal losses, several versions of the circular models were tested with inclination angles of 0 and 45 degrees.

Using data shown in Figures 21 and 22, a comparison of the 0 and 45 degree inclined skirts was made and is shown on Figure 23 for the fully ducted annular jet configuration and one controlled flow arrangement. Also included in Figure 23 are the calculated ideal curves for the two values of jet inclination angle. The results indicate that increasing the jet inclination angle on the controlled flow configurations, at least up to 45 degrees, improves performance in the normal operating height range. From observation of the internal flow profiles on the controlled flow configuration, no breakdown of the flow was detected at the higher inclination angle.

For subsequent model tests on other than circular planform configurations, a jet inclination of at least 45 degrees was always used.

## 2. Internal Distribution Systems

a. Circular Planform Configurations - The circular models were tested in a number of configurations which included the simple plenum version as well as the annular jet as obtained with (a) a complete contoured inner duct lining (the fully ducted annular jet), (b) a baseplate (typical of many annular jet configurations), and (c) various controlled flow configurations.

The controlled flow techniques used included (a) a partial duct under the fan to allow the flow to complete the convex bend without separating, (b) a spinner tab below the plane of the fan to initiate

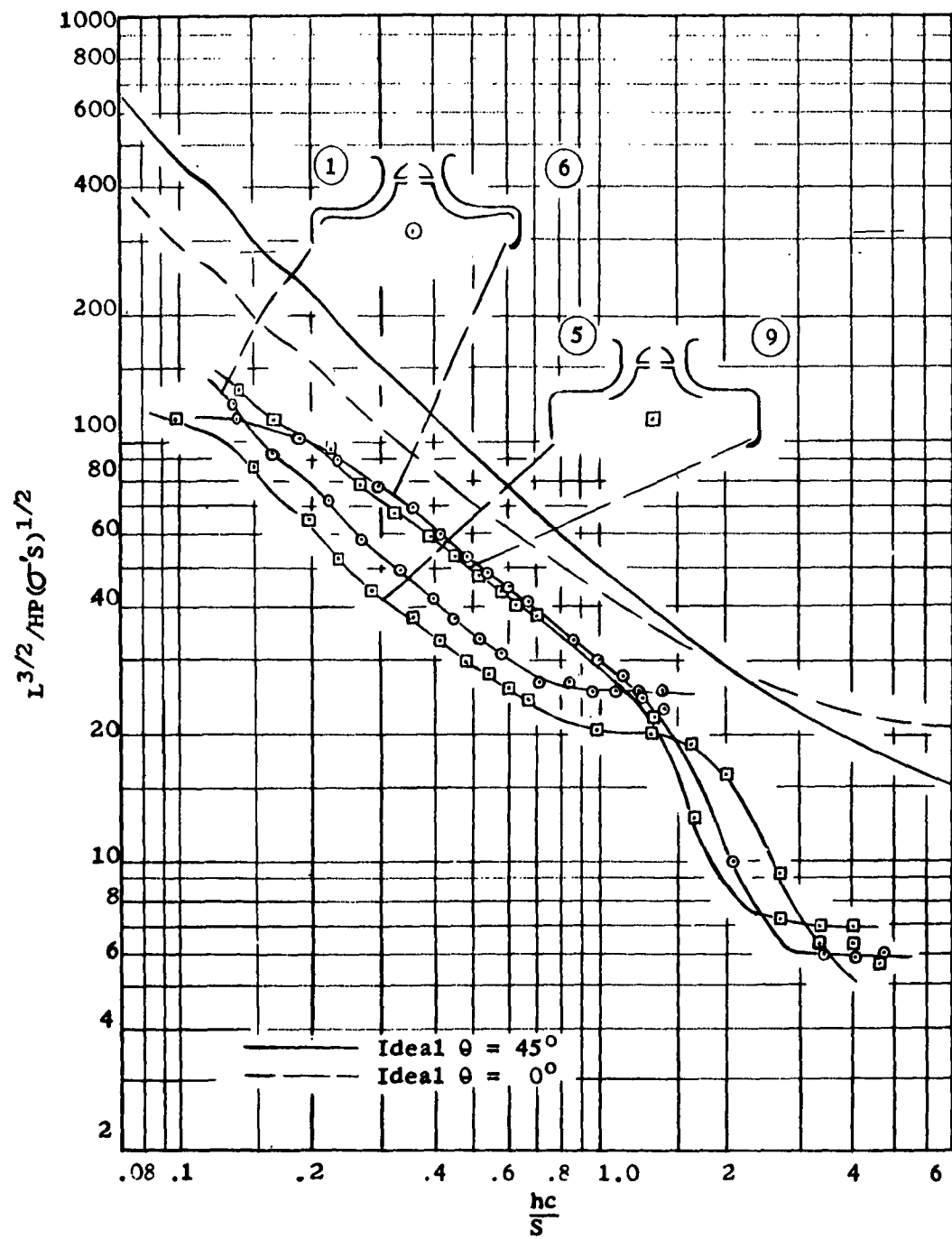


Figure 23. Effects of Jet Inclination on Performance

a favorable velocity distribution on the convex bend, and (c) a deflector plate below the fan which was a simple device to approximate the partial duct.

In Figure 24, the performance results are summarized for some of the above configurations (1 through 5) when tested with optimum skirt length and zero geometric inclination angle at the periphery. The ideal annular jet performance for zero jet inclination angle is shown for reference in Figure 24. It will be noted that the plenum version has an extension added to the fan shroud projecting toward the cushion cavity. Without this extension, the configuration would appear as the simplest possible, or ideal, version of the controlled flow configuration.

Such a configuration was tested (results not shown) early in the program, and it was found that the flow was unstable on the convex bend. Stable flow for the total air mass could not be maintained and performance measurements were erratic. The fan shroud extension was necessary to stabilize the flow in the plenum configuration. It can be seen from Figure 24 that the performance of the plenum is, as expected, inferior to the other configurations for all practical values of height. Additionally, the two versions of the controlled flow configurations can be seen to fall between the fully ducted annular jet and the "practical" annular jet using a base plate. It should be noted here, however, that the base plate annular jet model was not optimized with regard to the height of the base plate plenum. Consequently, internal recirculating flows tended to increase, more than would be ordinarily expected, the internal losses of this configuration.

In Figure 25, only annular jet configurations (6 through 9) with jet inclinations of 45 degrees are compared; the plenum with its poorer performance is not considered. The figure shows three controlled flow devices compared with the fully ducted annular jet configuration. It is significant that at this higher jet inclination angle, the two best controlled flow configurations have nearly the same performance as the fully ducted annular jet. The controlled flow version using a partial duct most nearly represents the flow conditions of the "ideal" controlled flow configuration. Whether or not the ideal controlled flow configuration (Coanda turning on the convex bend) would be better than the partially ducted configuration because of reduced skin contact area could not be determined. If the performance parameter of the fully ducted annular jet at an  $h/d$  of .1 is used as a reference (100.0 percentile), the relative performance of the two best controlled flow configurations is as follows:

	Fully Ducted Annular Jet	(Configuration 6)	100.0%
"Controlled Flow"	Partially Ducted Annular Jet	(Configuration 9)	93.5%
	Deflector Plate Annular Jet	(Configuration 8)	87.0%

The spinner tab configuration succeeded in stabilizing the flow on the convex bend, but separation occurred on the ceiling of the cushion cavity

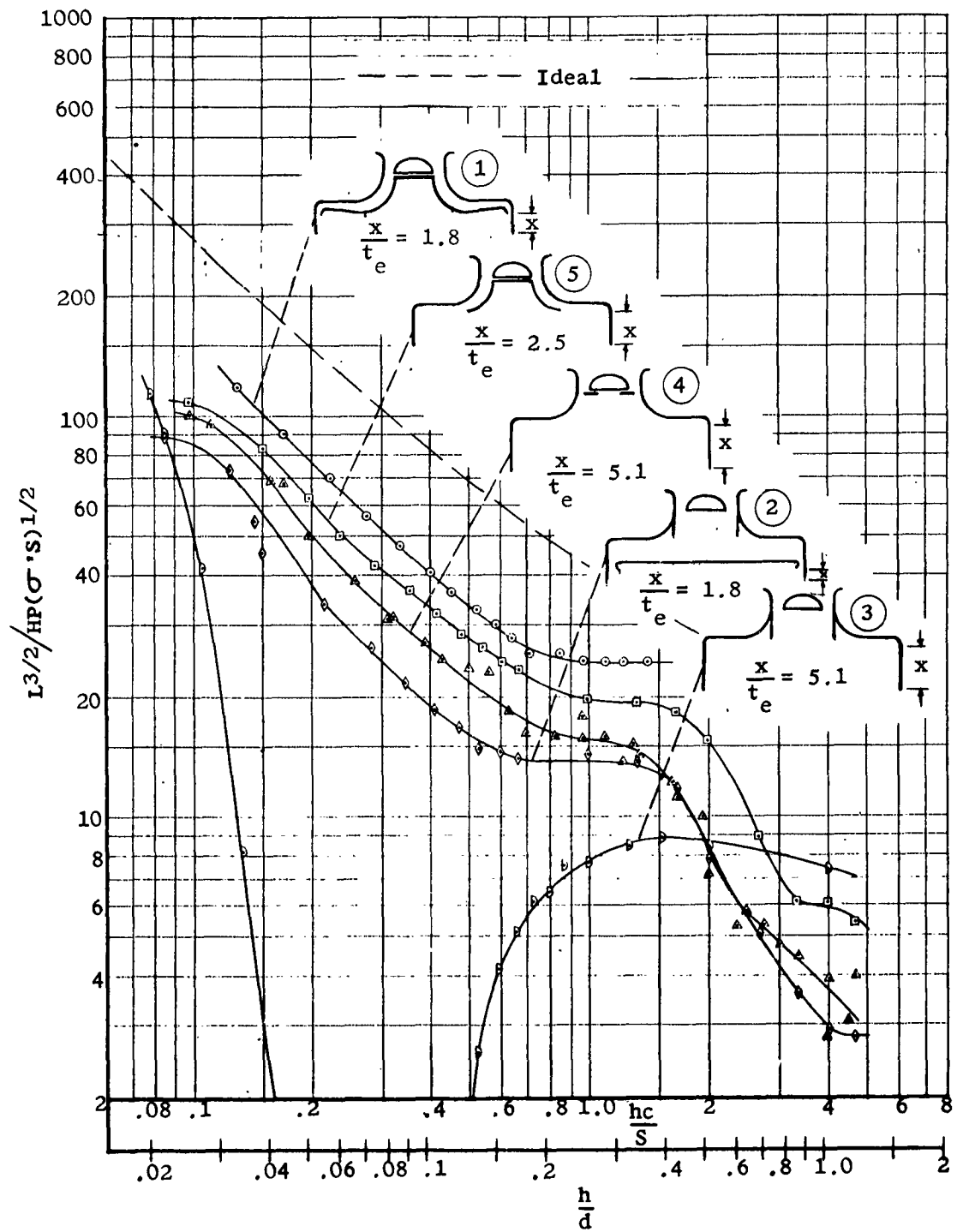


Figure 24. Circular Model Performance, Optimum Skirt Length,  $\theta=0^\circ$



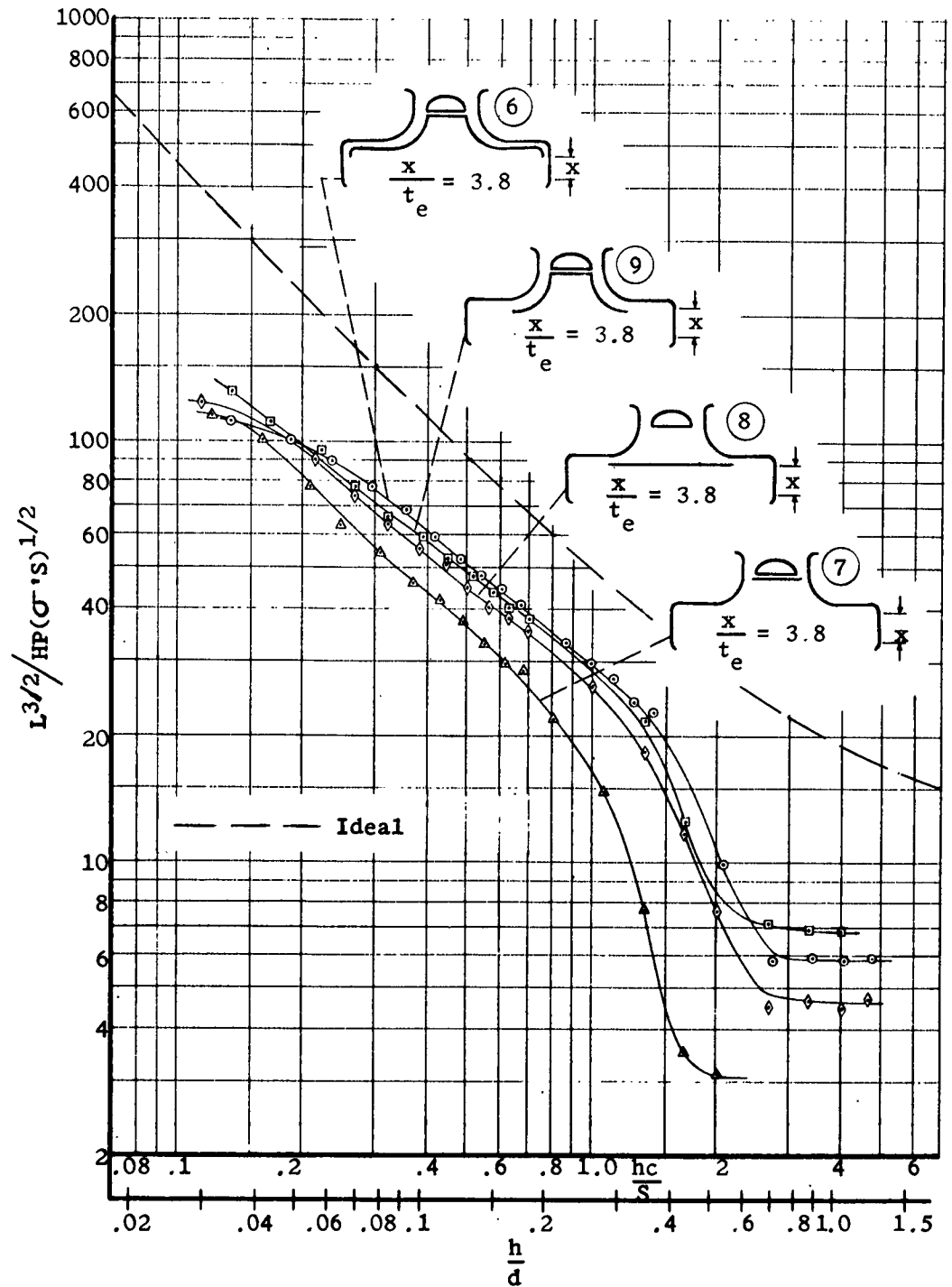


Figure 25. Circular Model Performance, Optimum Skirt Length,  $\theta=45^\circ$

downstream of the convex bend which explains its considerably poorer performance.

b. Square Planform Configurations - Proper distribution of air to the jet periphery was first introduced as a problem with the square planform model. With this planform, the model was tested in the base plate configuration (10), the plenum configuration (11), and in various controlled flow configurations based on devices tested on the circular planform model. One square controlled flow configuration used a spinner tab (12). Others used the deflector plate under the fan (13) and a partial duct (14). Another device was used in an attempt to combine effectively a turning aid with a planform distribution control. This device was named a contoured orifice and was tested as Configuration 16. Configurations 13, 14, 15, and 16 also included planform distribution vanes running generally radially from the turning aids under the fan to the jet exit at the periphery (shown in Figure 9). Configurations 13 and 15 were also tested without the full length vanes. All configurations were tested with a fixed jet inclination angle of 45 degrees and a fixed skirt length of 6.0 inches to correspond with the optimum skirt length for the circular model.

Hovering performance for the several configurations of the square model is compared in Figure 26. As with circular planform models, the plenum can be seen to have the worst performance by a significant factor. The base plate version also has relatively poor performance and for the same reason as did the circular base plate model (internal recirculation). All the controlled flow versions had better performance than the base plate annular jet; and, again, the spinner tab was poorest of the controlled flow configurations. The remaining arrangement with full length vanes and either deflector plate, partial duct, or contoured orifice (Configurations 13, 14 and 16 respectively) all had nearly identical performance. When the full length vanes were removed from Configuration 13, no reduction in performance was noted, whereas removing the vanes from 16 caused an 8 per cent reduction in efficiency. It was apparent that the square model configured with the simple deflector plate performed as good as any controlled flow arrangement tested in that model.

To determine the effect of controlled flow techniques on the performance of a base plate peripheral jet configuration, the partial duct was combined with a base plate as Configuration 15. The improvement in performance over Configuration 10 (base plate only) is shown in Figure 27. It is expected that this occurred primarily because of the non-optimum design of Configuration 10.

c. Single Fan Oval Planform Configurations - The tests with the oval model were aimed at applying the controlled flow concept to a more practical vehicle planform. The silhouette proportions of this model with a fixed jet inclination angle of 45 degrees were also more representative of full scale vehicle design.

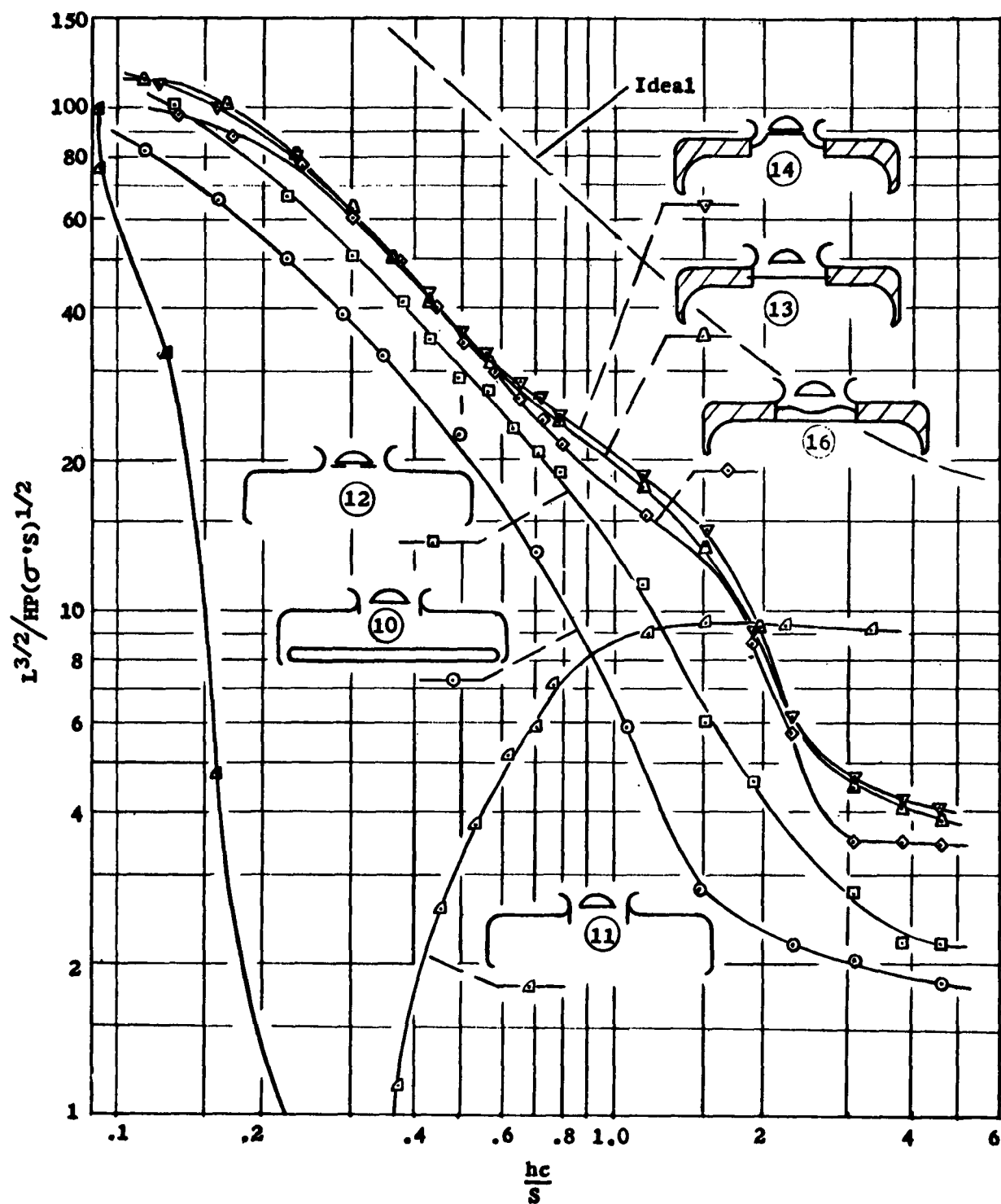


Figure 26. Square Model Performance,  $\theta=45^\circ$

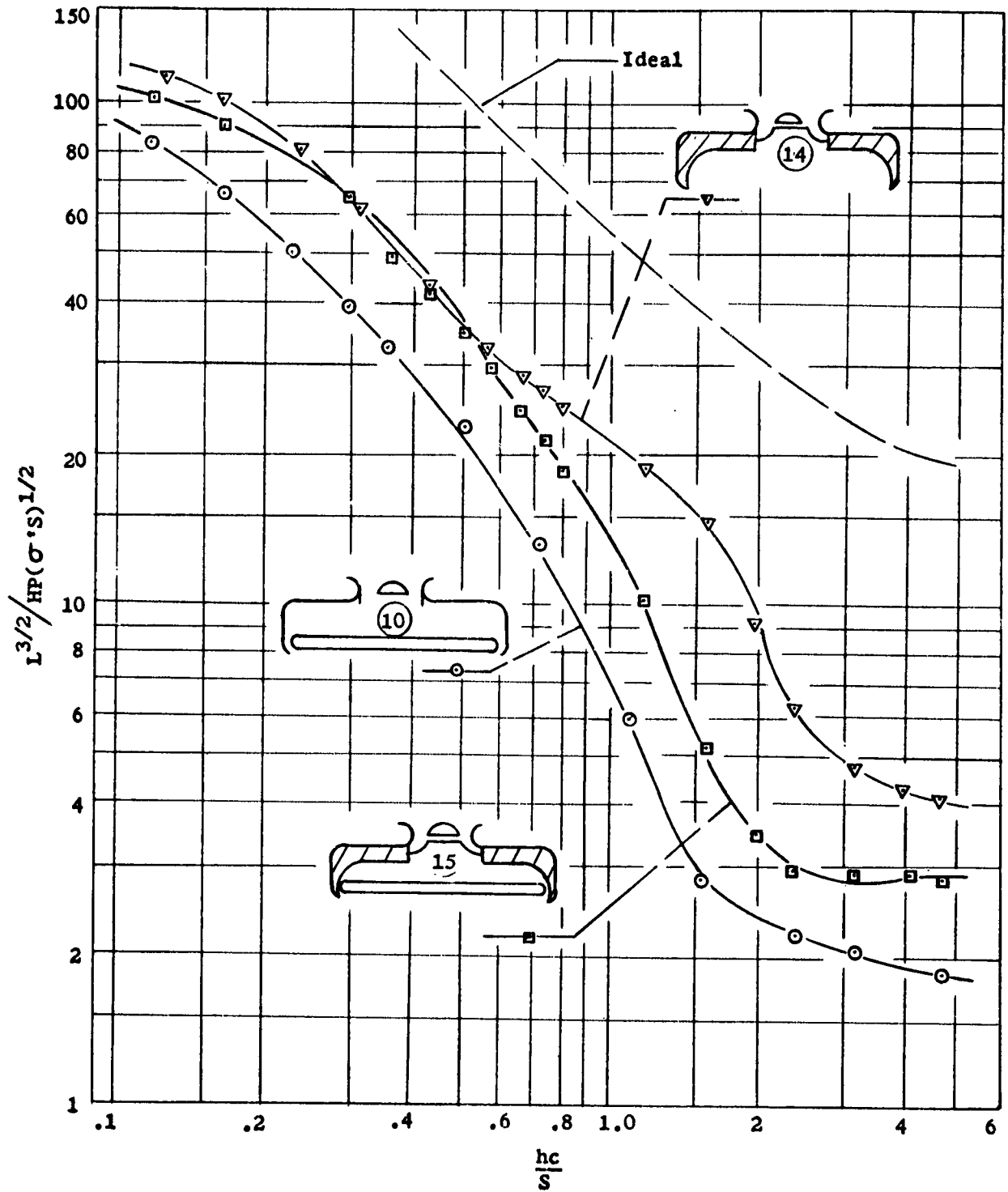


Figure 27. Square Model Performance, Controlled Flow Applied to Base Plate Configuration,  $\theta=45^\circ$

The oval model with a centrally located fan unit was not tested in the plenum configuration; however, tests were conducted in the conventional base plate peripheral jet arrangement (Configuration 17). Controlled flow techniques were also tested but mainly by utilizing the simple deflector plate device under the fan. The use of this device was based on the favorable results obtained on the larger circular and square planform models. The application of controlled flow techniques to the base plate peripheral jet was tested on Configuration 18 which was the combination of Configuration 17 with the deflector plate.

The controlled flow versions all included the deflector plate under the fan. To this basic configuration were added full length vanes (Configuration 19), or short fins at the concave bend (Configuration 20).

In Configuration 22, the short fins were replaced by an oval ring in an attempt to govern the planform distribution by confining the flow to a given thickness at the concave bend. The propeller, defined on page 29, which was specially designed for inducing higher velocities near the tip, was substituted for the standard propeller used on Configurations 20 and 22 and the new combinations were called Configurations 21 and 23, respectively.

Finally, the effects of applying a base plate to Configuration 23 were determined. The resulting combination was called Configuration 24.

Figure 28 compares the performance of the base plate version of the peripheral jet (Configuration 17) with each of the three controlled flow configurations where planform distribution techniques are varied (Configurations 19, 20 and 22). It should be noted that without the full length vanes, short fins or oval ring, the distribution was characterized by overfeeding along the sides, resulting in slanting of the air in the side curtains fore and aft from the middle of the model.

Figure 28 shows a large variation in performance depending on which planform distribution system was used. The arrangement with the full length vanes was tested first.

These vanes were laid out to give even volume distribution around the periphery of the model. Flow visualization revealed that this system did in fact produce the best distribution. However, boundary layer separation was evident on the longer vanes. The poor performance of this system as compared to the others is attributed to the additional drag and turbulence created by the vanes.

The best controlled flow performance, shown in Figure 28, is for a system of 36 short turning fins on the ceiling. These fins are rectangular with an aspect ratio of .7. These turning fins caused the flow to impinge on the side walls normal to the periphery. Another technique was used in conjunction with the turning fins. This was

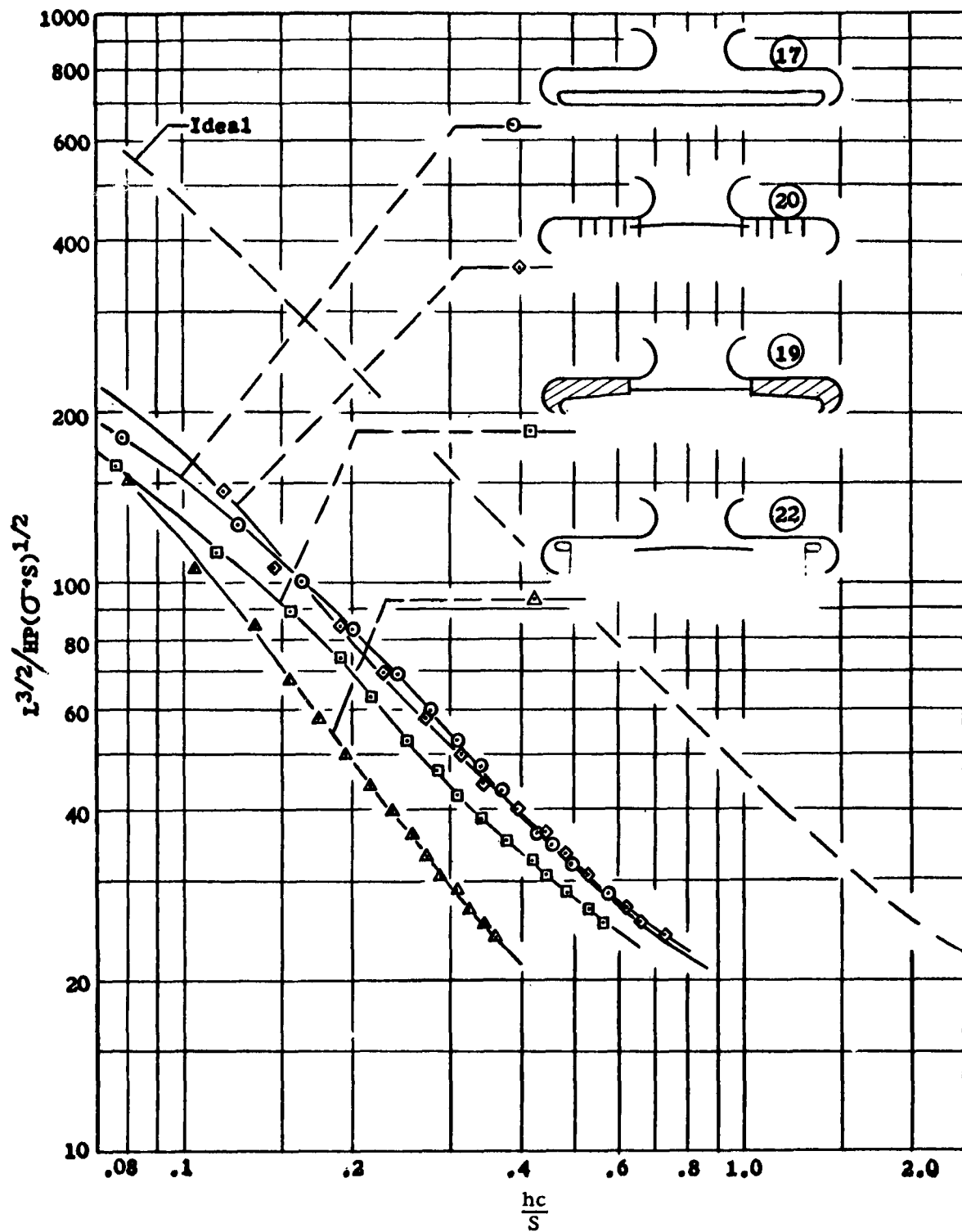


Figure 28. Single Fan Oval Model Performance,  $\theta=45^\circ$

warping of the deflector plate. The deflector plate was warped so as to reduce the flow to the sides, thereby preventing overfeeding of the side jets.

The oval model tested as a peripheral jet with a base plate exhibited good planform air distribution. This was a result of the contraction of the flow in the jet nozzle. The third planform distribution system, the oval ring, evaluated this method for achieving planform distribution in a controlled flow configuration. The warped deflector plate was also used in this system.

The performance of the oval ring arrangement does not compare favorably in Figure 28. However, the model possessed roll stability in this configuration. All other oval model configurations exhibited roll instability.

A technique aimed at improving the quality of controlled flow by creating a non-uniform velocity through the fan was tried by testing the oval model with a specially designed propeller. The performance of the fan power unit alone (without the air cushion vehicle afterbody) was tested and compared when using the standard propeller and the special propeller.

The performance of the two propellers is compared in Figure 29 for the unshrouded condition and in Figure 30 when acting as a ducted fan. In both cases the vehicle height-size parameter  $h_c/S$  is based on the minimum area of the duct less the spinner area.

Figure 29 shows that the unducted "Coanda" propeller is poorer than the standard propeller without a duct. But Figure 30 shows that the "Coanda" propeller produces more thrust in the presence of the ducted inlet than does the standard propeller.

Two configurations of the single fan oval model were tested with each set of blades. It was necessary to use a deflector plate below the fan to establish controlled flow in both of these configurations. Flow would not remain attached on the convex bend for the full 90 degrees without the deflector plate, regardless of which set of blades was installed. However, the performance of the Coanda propeller with the deflector plate was considerably higher than the performance of the standard propeller with the plate. Model performance with each set of blades is compared in Figure 31. Performance increases as high as 45 per cent are shown in Figure 31 for the Coanda blades. A comparison of the blades made in Figures 29 and 30 shows that their performance is nearly equal. The improvement in over-all model performance must be associated with a reduction in internal losses resulting from a velocity profile compatible with a Coanda bend.

In Figure 32, the effect of adding a base plate to a controlled flow configuration is shown. In this particular case,

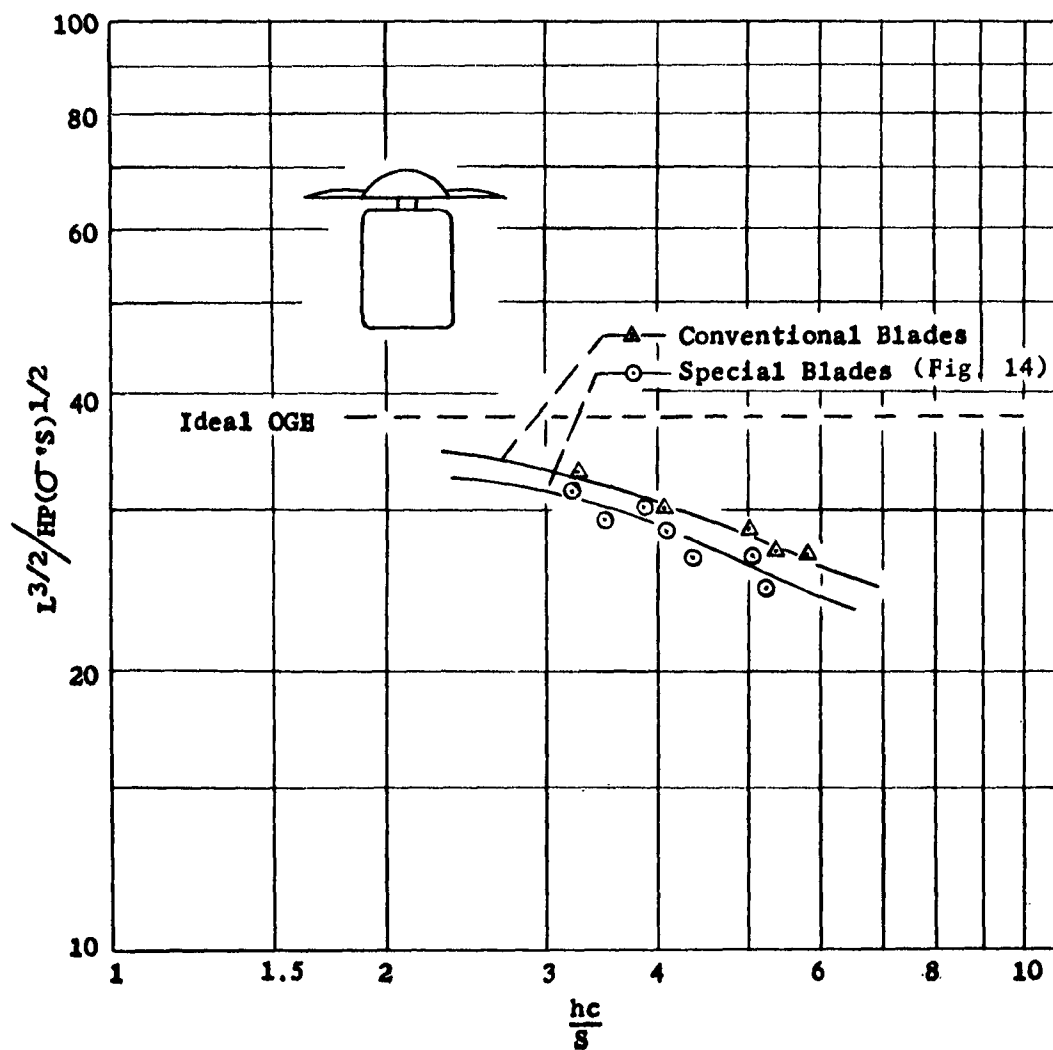


Figure 29. Ten-Inch Diameter Fan Performance



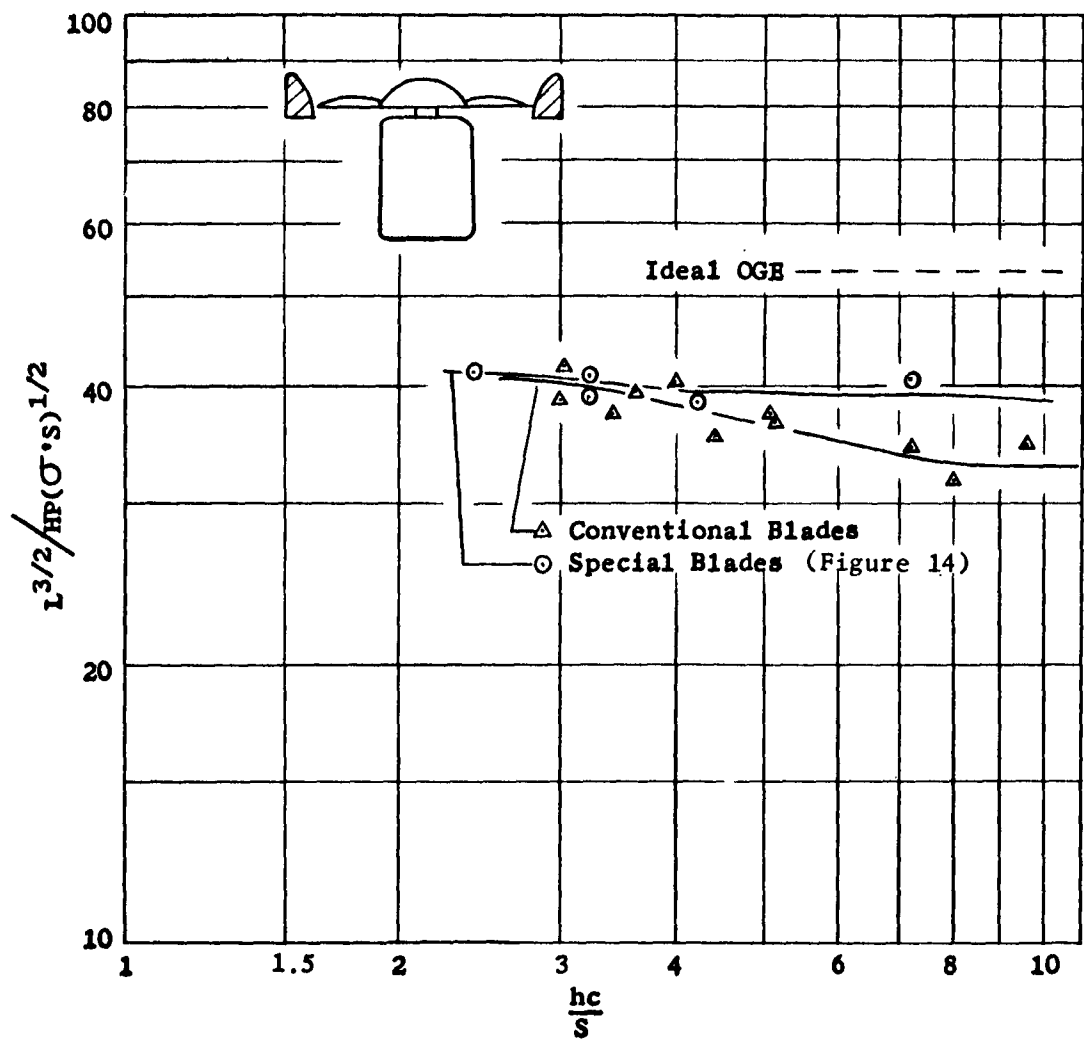


Figure 30. Ten-Inch Diameter Ducted Fan Performance

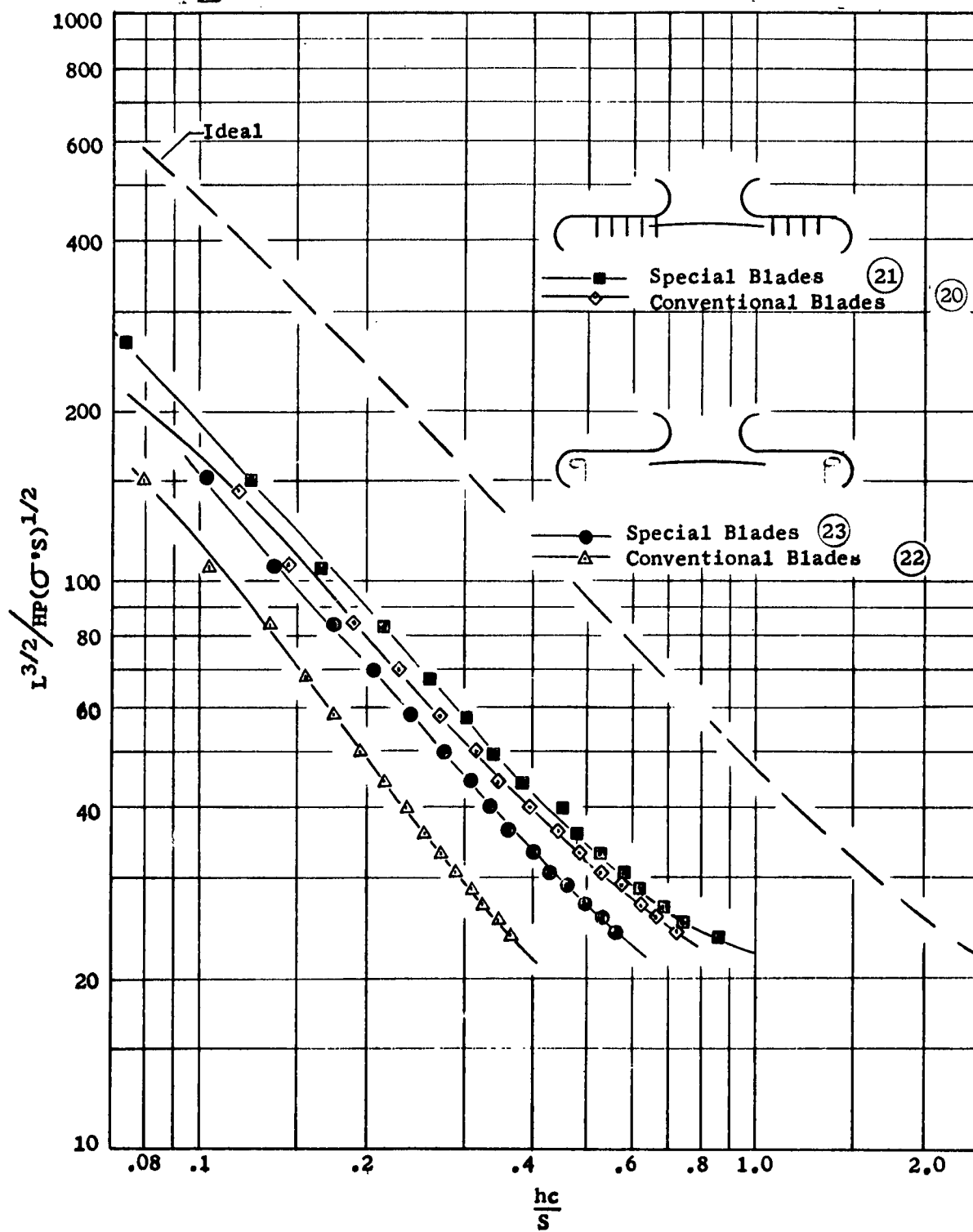


Figure 31. Single Fan Oval Model Performance, Special and Conventional Blades,  $\theta=45^\circ$

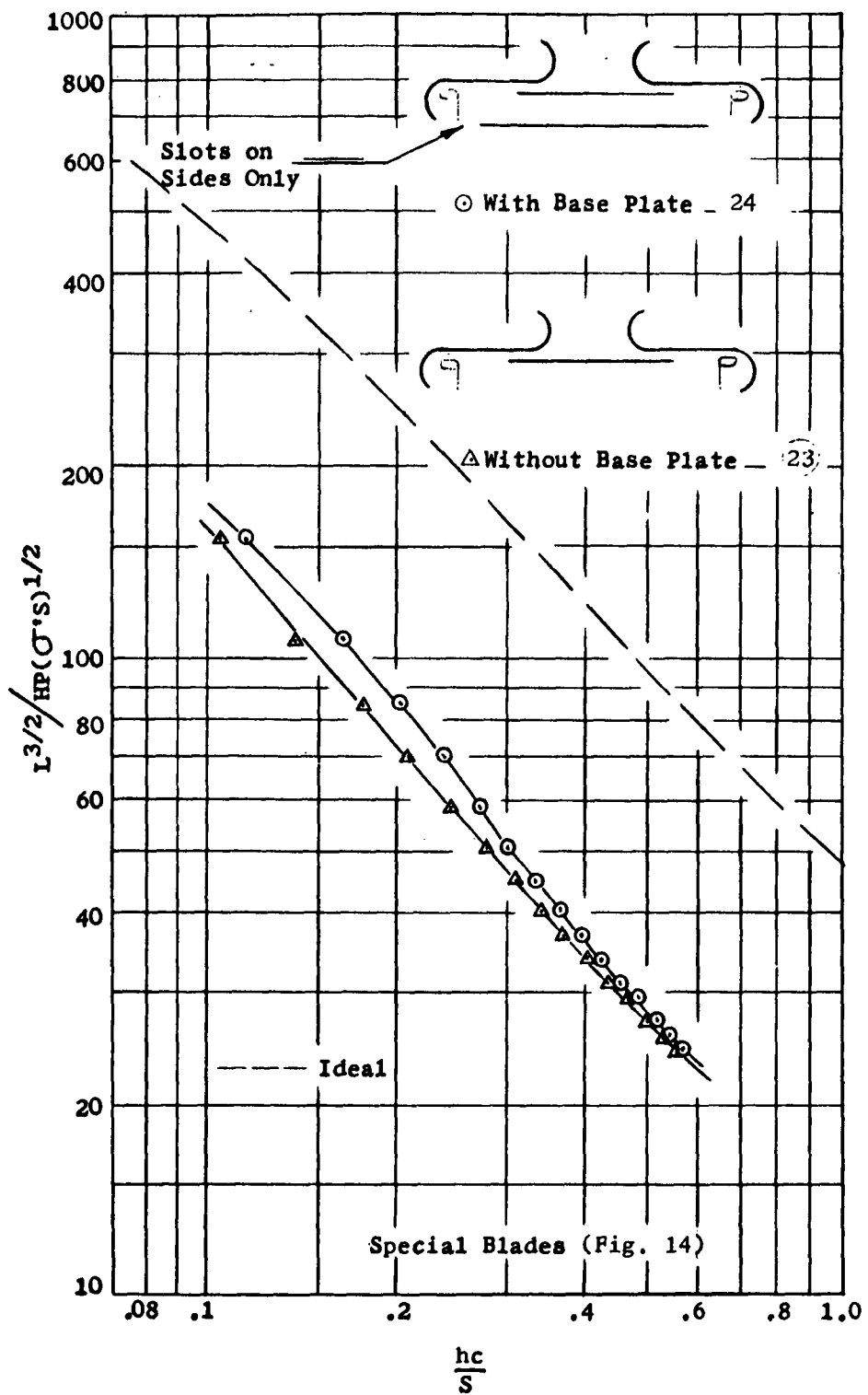


Figure 32. Single Fan Oval Model Performance, Controlled-Flow Configuration with Base Plate Added,  $\theta=45^\circ$

the performance was increased approximately 15 per cent by the addition of the base plate.

d. Tandem Fan Oval Planform Configurations - An oval model was tested with tandem fans for comparison with results of previous tests with single fan models.

The planform area of this model is equal to the planform area of the single fan oval model. However, a fixed jet inclination of 60 degrees rather than 45 degrees was used. This resulted in slightly less planform area for the tandem model. The tandem fan oval model was tested in the plenum version (Configuration 25), in a base plate version (Configuration 26), and in two deflector plate configurations. The first included two circular plates, one under each fan (Configuration 27), and the second incorporated one larger, oval shaped deflector plate under both fans (Configuration 28).

A comparison of the two controlled flow configurations is presented in Figure 33. A flow splitter supported from the ceiling was positioned between the fans to turn the opposing fan air amidships toward the sides (see Figure 16). This assembly was used in both of the controlled flow configurations tested. The sketches in Figure 33 depict the difference in the two configurations. The best performance was achieved with the oval shaped deflector plate extending under both fans. This plate was warped to optimize the planform distribution.

The circular plates under each fan were also warped to control planform distribution. However, the individual plates do not extend to the flow splitter; a portion of the flow impinging on the splitter turned down (rather than outboard toward the sides), forming a centerline jet across the model. To alleviate this situation, a turning vane system was developed. This system is shown in Figure 34; however, its performance is not shown in Figure 33.

There were no vanes required in the ends of the model. (See Figure 34.) Due to the location of the fans, flow to the ends is essentially radial. Vertical flow stream lines defined with tufts were observed at all points on the skirt wall, indicating the absence of local overfeeding. Thus, the vertical jet across the model was eliminated. However, the performance of this arrangement was equal to but not better than the performance of the single deflector plate arrangement, even though some overfeeding of the side jets existed in the single plate arrangement. Again, as with the single fan oval model, additional drag from the turning vanes absorbed any possible performance gain from improved distribution.

Two sets of performance data have been presented in Figure 33 for the single deflector plate arrangement. The curve for 30 pounds lift shows better performance than does the 20-pound lift

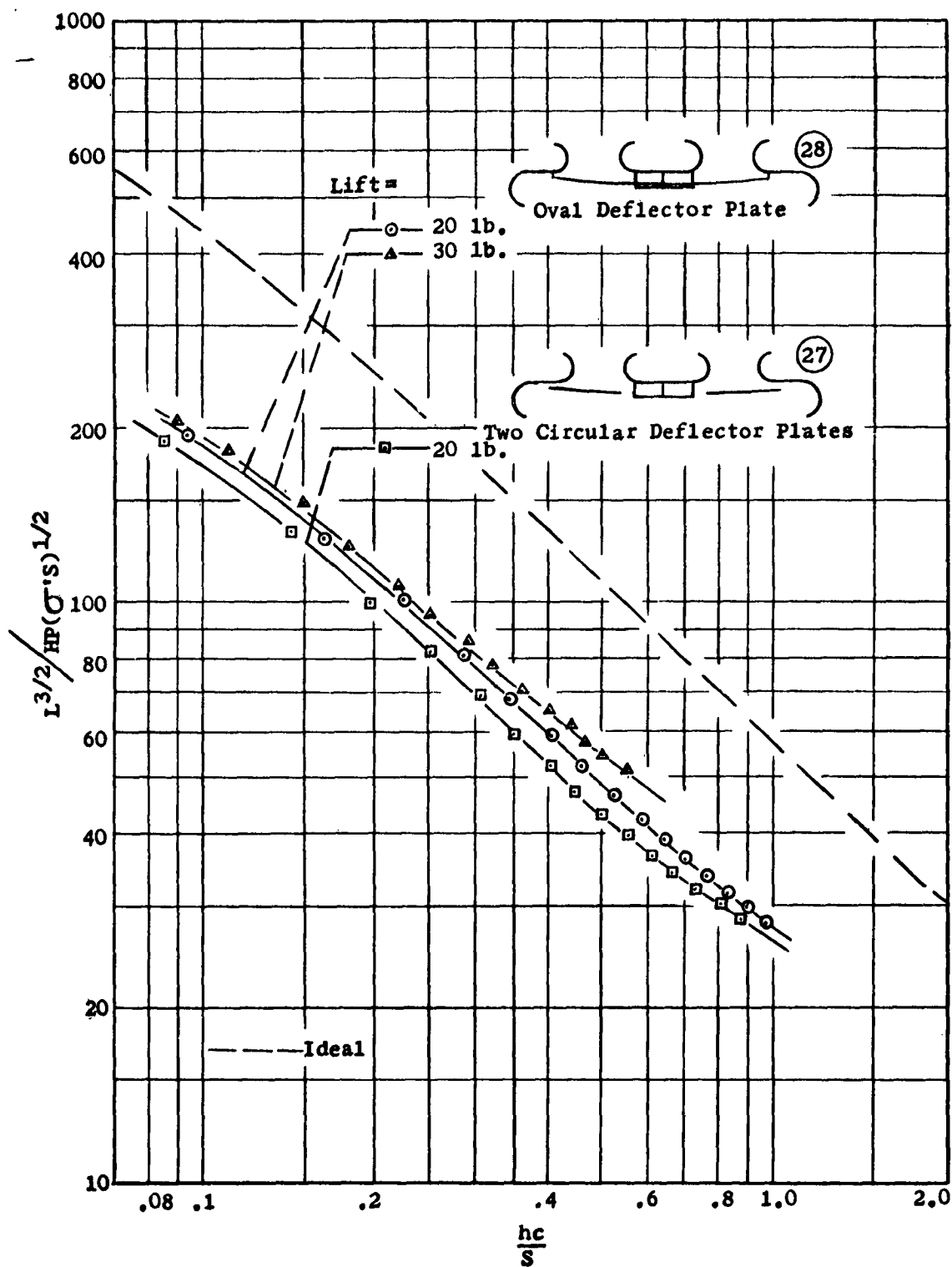


Figure 33. Tandem Fan Oval Model Performance, Controlled-Flow Configurations,  $\theta = 60^\circ$

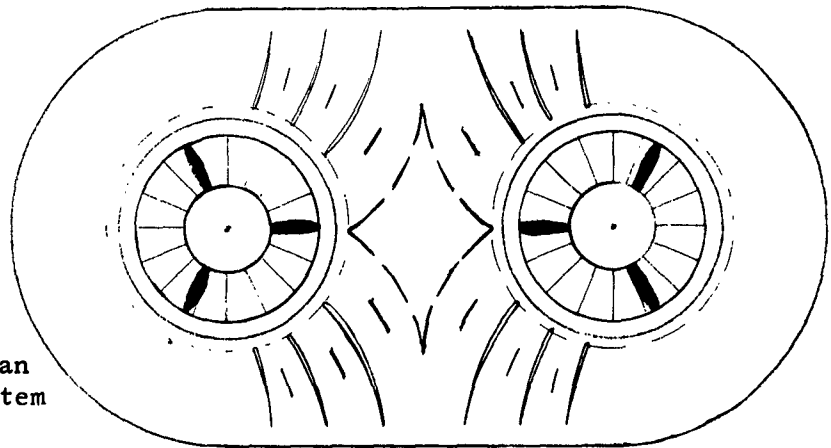


Fig. 34. Twin Fan  
Turning Vane System

case. This indicates that the blade section was operating below its optimum L/D coefficient at 20 pounds of lift. However, to observe the model at relatively high heights, a model lift of 20 pounds was selected for stability and control tests described in a later section.

A comparison of the best controlled flow arrangements with the plenum and annular jet base plate configurations is made in Figure 35 for the tandem fan model at a lift of 20 pounds.

### 3. External Flow System

For a conventional air cushion vehicle, the concept of ideal controlled flow involves the Coanda process on an internal surface under the fan. However, another possible application of this phenomenon is on the External Flow Vehicle. In this case, air from a ducted fan or propeller would be discharged over the external surface of the vehicle. The flow would follow the vehicle contour to the periphery, where it would leave the vehicle in a peripheral jet curtain as shown in Figure 36. The ideal performance parameter,  $(M_p)_i$ , can be defined by equation (1), since the conditions at the jet exit plane can be identical to that for the conventional peripheral jet. The losses in the device are caused by the skin friction on the external surface (comparable to internal duct losses with the conventional peripheral jet) and by the possible premature separation of the flow near the jet periphery due to an adverse pressure gradient acting on the unconfined flow vein. The ability of the Coanda phenomenon to prevent separation, and therefore a breakdown of the jet curtain, is a necessary requirement for further consideration of this concept since, ideally, it has the same performance as a conventional air cushion vehicle.

Certain characteristics of this device present interesting possibilities (see Reference 4). The accessibility of the fan or air supply unit suggests using an existing lifting device such as a jet engine, flying jeep, or helicopter as the air pumping system. Since the air pumping system could be an entire vehicle in itself and the

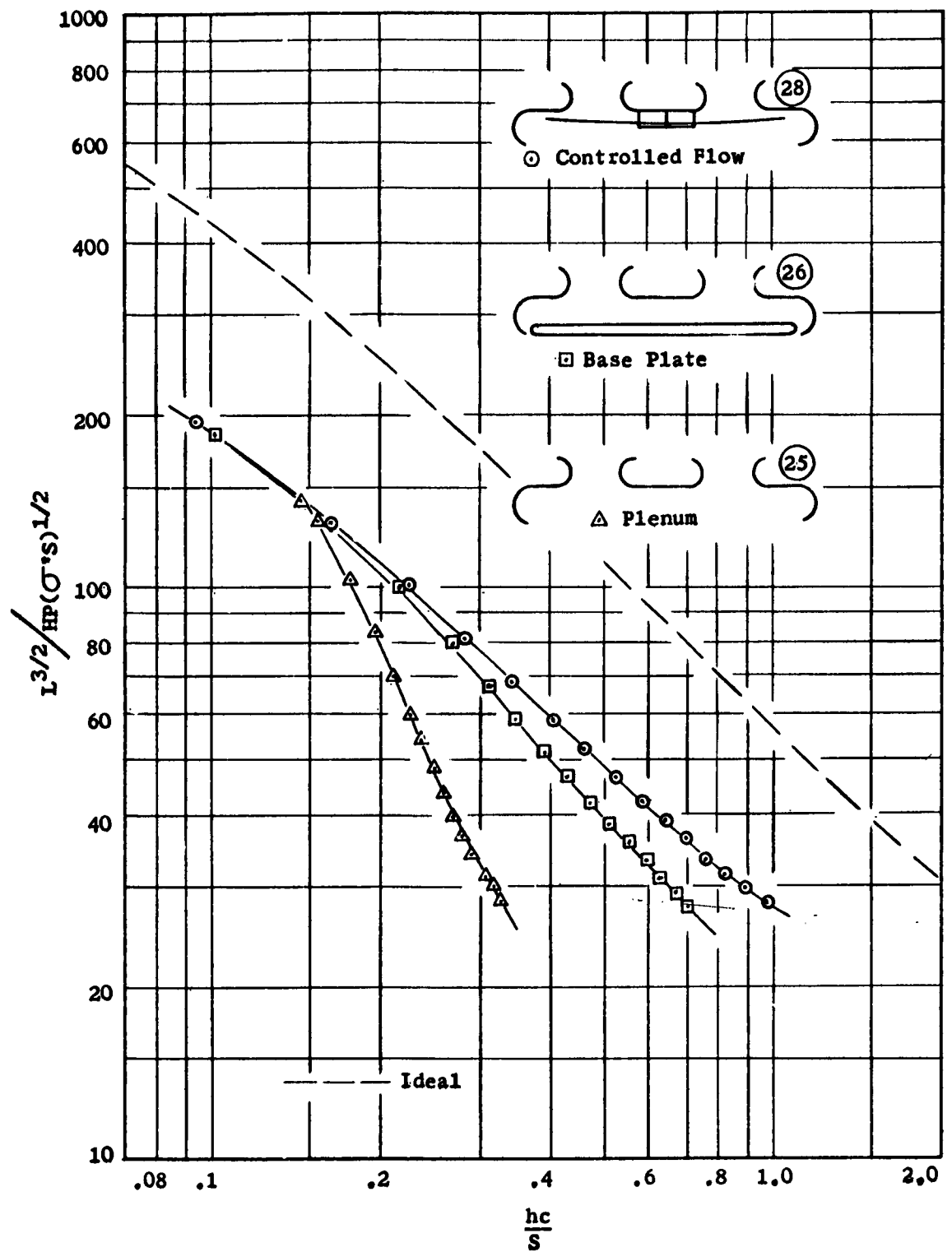


Figure 35. Tandem Fan Oval Model Performance, Controlled-Flow and Conventional Configurations  $\theta=60^\circ$

remainder of the structure an "accessory," the performance of the primary lift unit has been used as a reference in evaluating the external flow model performance. Test results are presented herein in terms of the augmentation ratio defined as

$$A = \frac{\text{Lift of the External Flow Air Cushion Vehicle}}{\text{Lift of the Fan Unit Out of Ground Effect}}$$

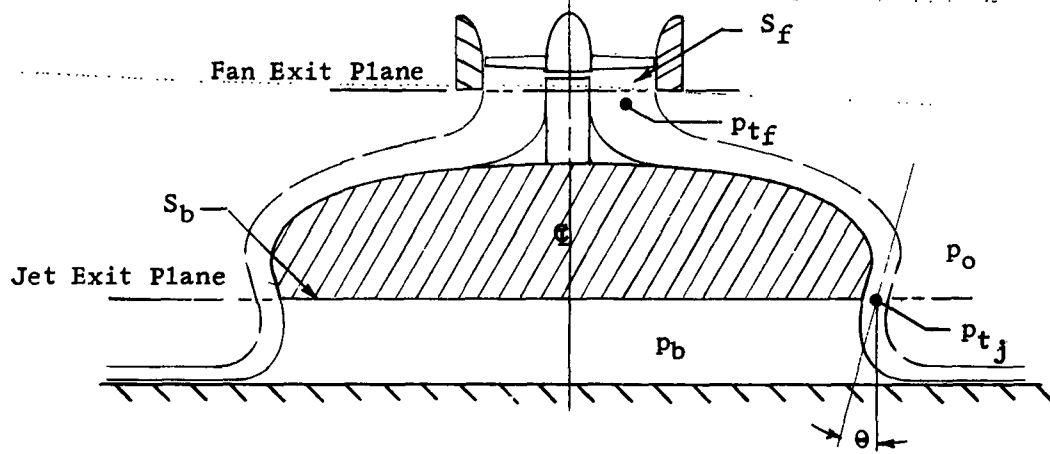


Figure 36. Ideal External Flow Schematic

Referring to Figure 36, the lift of the External Flow Air Cushion Vehicle is expressed as the total lift due to the jet at the jet exit plane plus the base pressure times base area. When powered with a ducted fan, the total vehicle lift is

$$L = 2 P_{tj} S_f \cos \theta + P_b S_b.$$

The jet lift is transferred to the vehicle by the Coanda process and the jet area is assumed to be equal to the fan area. The lift of the fan unit out of ground effect is  $2P_{tf} S_f$ . Therefore, the Augmentation Ratio is

$$\begin{aligned} A &= \frac{2P_{tj} S_f \cos \theta + P_b S_b}{2P_{tf} S_f} \\ &= \frac{P_{tj}}{P_{tf}} \left[ \cos \theta + \frac{1}{2} \frac{P_b}{P_{tj}} \frac{S_b}{S_f} \right] \end{aligned} \quad (2)$$

The ratio of base pressure to total pressure at the jet exit,  $P_b/P_{tj}$ , is shown in Figure 37 as a function of the height parameter,  $h/t_e$ , and is taken from curves of  $P_b/P_{tj}$  presented in Reference 5.



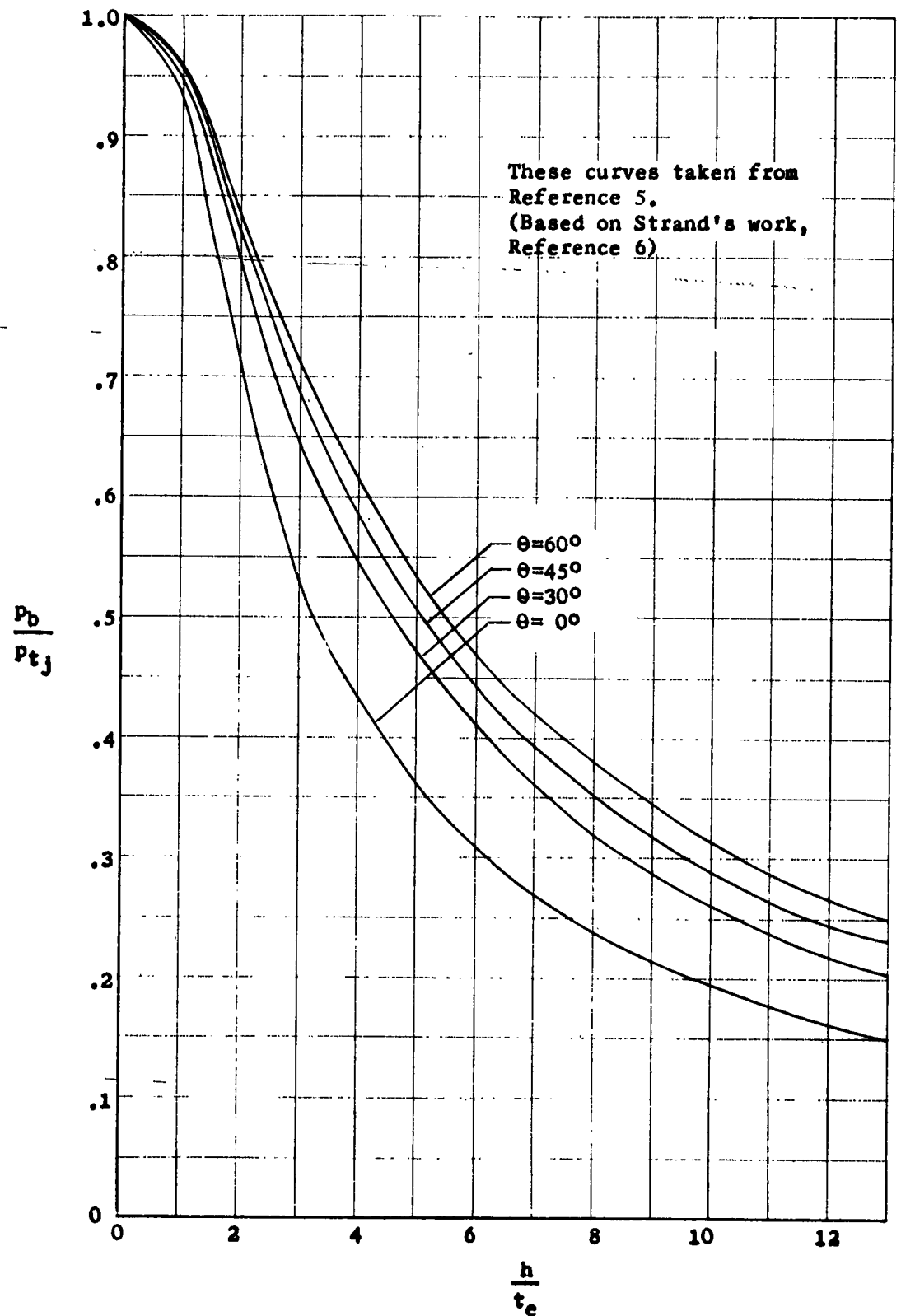


Figure 37. Theoretical Base Pressure to Jet Total Pressure Ratios.

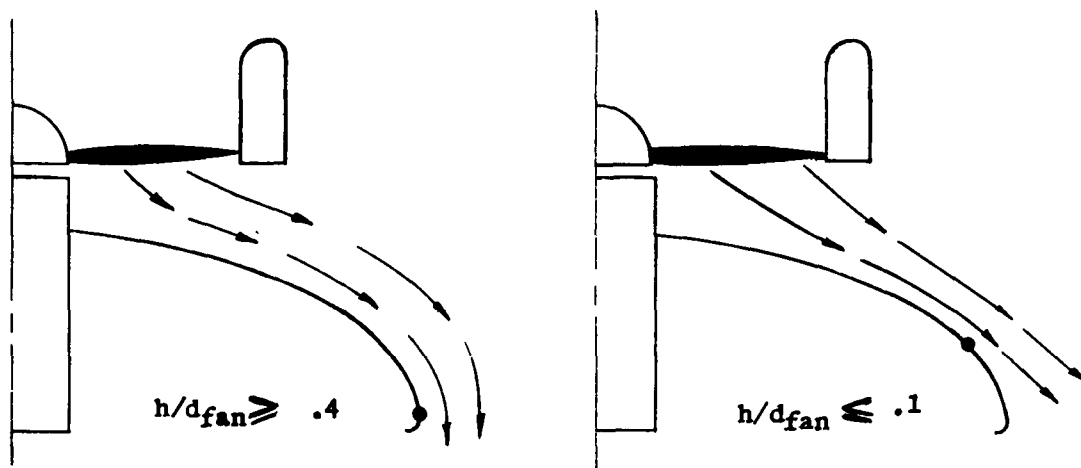
These curves were developed with Strand's conformal mapping method of Reference 6.

In the ideal case  $p_{t_j} = p_{t_f}$ , and so the ideal augmentation ratio can be predicted from equation (2) by using Figure 37 and the vehicle geometry only.

In the actual case, a difference in total pressure exists between the fan exit and jet exit due to losses, and the term  $p_{t_j}/p_{t_f}$  should be determined experimentally.

Ideal and experimentally determined augmentation ratios are presented in Figure 38 for two versions of the external flow model: the basic model and the model with a band at the jet periphery. The basic model (described in Figure 18) consisted of a ten-inch diameter ducted fan mounted over a circular planform body with a semielliptical silhouette.

Initial tests with the basic model showed that at an  $h/d_{fan} < .4$ , the flow breaks away from the body. The point of break-away progresses upstream as the height decreases. The flow conditions at either end of the height range are depicted in the sketches below:



The band encircling the body was incorporated to prevent the flow from breaking away from the body upstream of the jet exit.

In Figure 39, the ratio  $A/A_i$  (or  $p_{t_j}/p_{t_f}$ ) is shown as a function of the height parameter  $h/t_e$ . This figure can be used in estimating the actual augmentation ratios of larger external flow vehicles of somewhat similar proportions.

For determining over-all efficiencies of the external flow vehicle, equation (1) may be used for calculating the ideal performance parameter as stated previously. However, an approximate method is presented here which is based on the performance of the primary

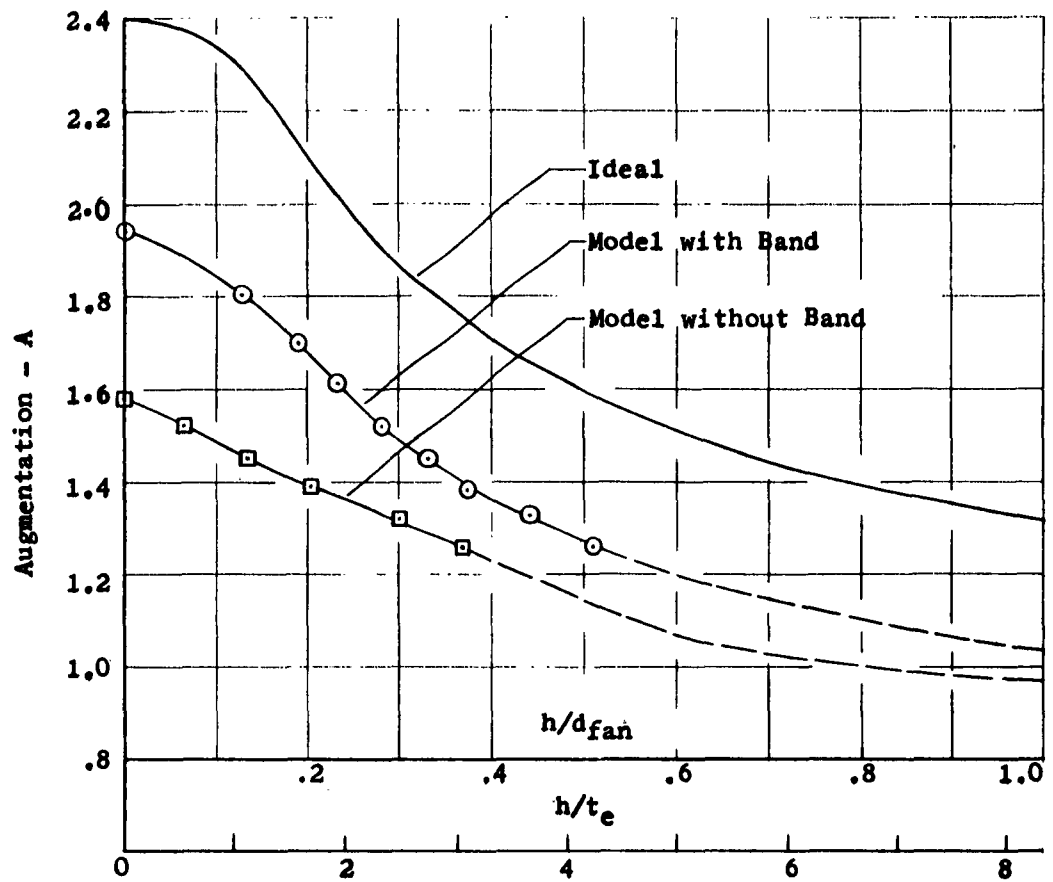


Figure 38. External Flow Model Augmentation,  $\theta=0^\circ$

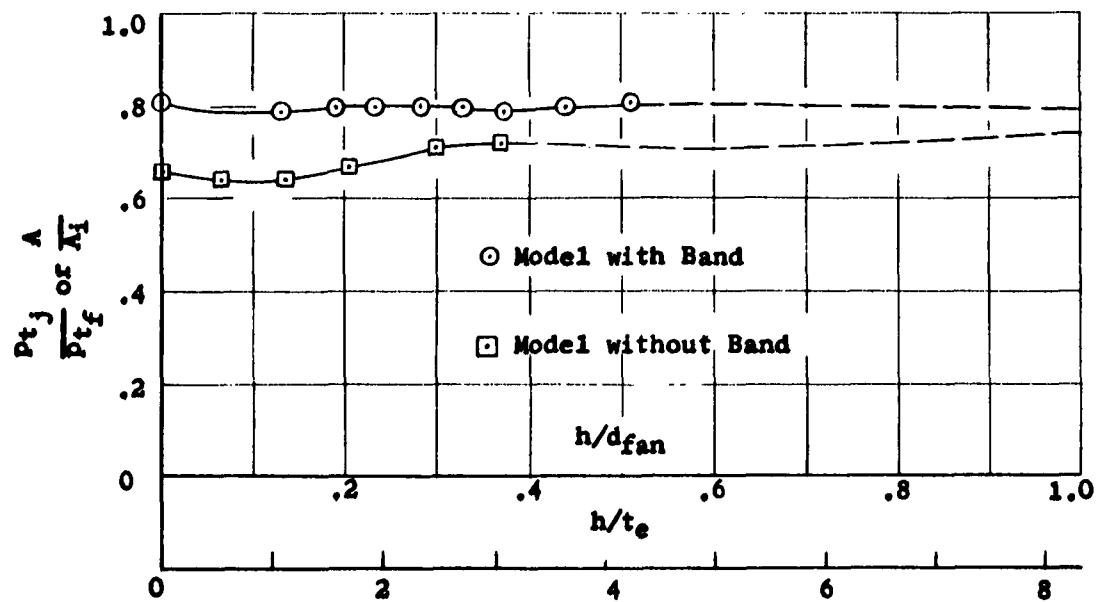


Figure 39. External Flow Model, Jet Total Pressure to Fan Total Pressure Ratios

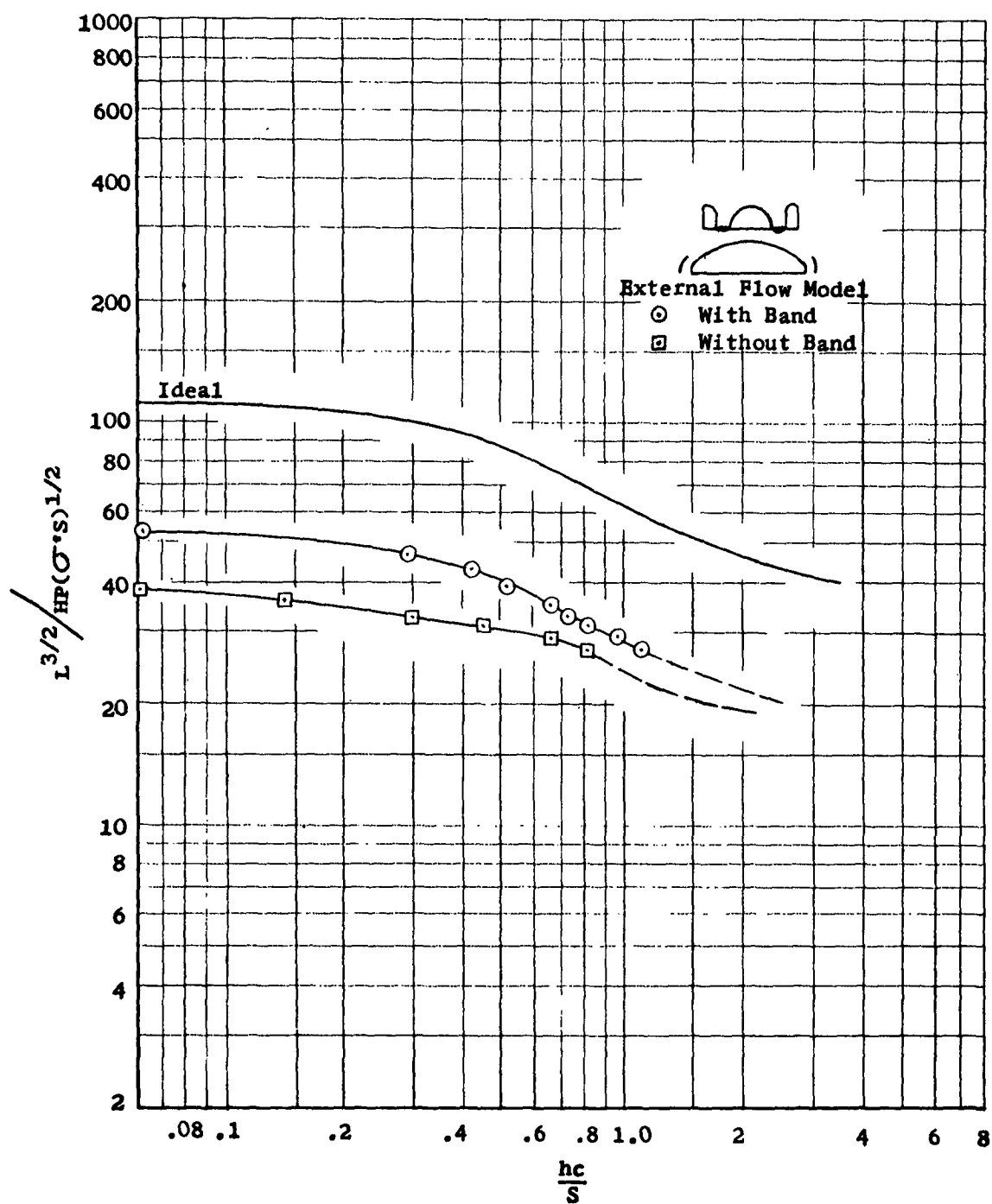


Figure 40. External Flow Model Performance,  $\theta=0^\circ$

lift system. In this case, it is assumed to be a ducted fan unit. The derivation also permits estimating actual, as well as ideal, values of the performance parameters.

For a ducted fan out of ground effect

$$\frac{L_f^{3/2}}{HP (\sigma' S_f)^{1/2}} = 53.6 M'$$

For the external flow vehicle, substitute

$$L_f^{3/2} = \frac{L^{3/2}}{A^{3/2}} \quad \text{where } A \text{ is from equation (2), and}$$

$$S_f^{1/2} = \frac{S^{1/2}}{(S_b/S_f + \cos \theta)^{1/2}};$$

therefore,

$$\begin{aligned} \frac{L^{3/2}}{HP (\sigma' S)^{1/2}} &= \frac{53.6 M' A^{3/2}}{(S_b/S_f + \cos \theta)^{1/2}}; \\ &= \frac{53.6 \left[ M' (P_{tj}/P_f)^{3/2} \right] \left[ \cos \theta + \frac{1}{2} \left( \frac{P_b}{P_{tj}} \right) \left( \frac{S_b}{S_f} \right) \right]^{3/2}}{(S_b/S_f + \cos \theta)^{1/2}}. \end{aligned} \quad (3)$$

The ideal performance parameter is obtained by setting the quantity  $M' (P_{tj}/P_{tf})^{3/2}$  equal to unity. The variation of the performance parameter with height occurs mainly through the term  $(P_b/P_{tj})$  as evaluated in Figure 37. The experimental values of the performance parameter as obtained with the two versions of the external flow model are shown in Figure 40 along with the ideal value based on equation 3.

### C. STATIC STABILITY

To determine the utility of the controlled flow configured vehicle, its stability and controllability must also be assessed in addition to its performance as a lift producing device.

Experiments to develop and evaluate stability augmenting devices for a typical controlled flow configuration were conducted with the tandem

fan oval model. This model was selected because it is more representative of current air cushion vehicles than any of the other models used in the hovering performance studies.

Each of the augmenting devices tested effects some form of compartmentation of the cushion. By dividing the cushion into compartments, cushion pressure can vary from one compartment to another as the model rolls or pitches, resulting in a shift in cushion center of pressure to resist the roll or pitch. This variation in compartment pressure is derived from a change in effectiveness of the peripheral curtain adjacent to the compartment as the clearance height of the jet exit increases or decreases. Static stability characteristics have been determined as total cushion center of pressure shift corresponding to pitch and roll attitude. Center of pressure shifts were measured at three or more initial hover heights for each configuration observed. In conducting the tests, fan power was adjusted to hover the model at a given height in a level attitude. No changes were made in fan power as the model was tilted. This resulted in a decrease in the mean hover height as the model tilted.

Initial stability tests were concerned with defining the characteristics of the model before incorporation of stability augmenting devices. Static stability of the model configured as a plenum and annular jet was also measured. Characteristics of these basic configurations are discussed below and will be compared later with characteristics resulting from incorporation of the augmenting devices in the controlled flow configuration. Performance penalties associated with each of the stabilizing devices are also presented.

## 1. Static Stability Results

a. Basic Configurations - Static stability of the tandem fan oval model was determined with the model in three basic internal configurations: the plenum, base plate peripheral jet, and deflector plate controlled flow arrangement. Hovering performance of these configurations (discussed previously) is compared in Figure 35.

The lateral and longitudinal static stability of these configurations are compared in Figures 41 and 42. Data presented in these figures are for base loadings of 3.65 pounds per square foot. The controlled flow arrangement was also tested at 1.83 and 5.48 pounds per square foot. Stability characteristics were nearly identical within this range of base loadings. Because of the insensitivity to base loadings, only the results of the model tests at 3.65 pounds per square foot are presented in this report for comparing stability characteristics using the various stabilizing devices.

Figures 41 and 42 show that stability generally decreases with increases in height for each of the internal arrangements. These

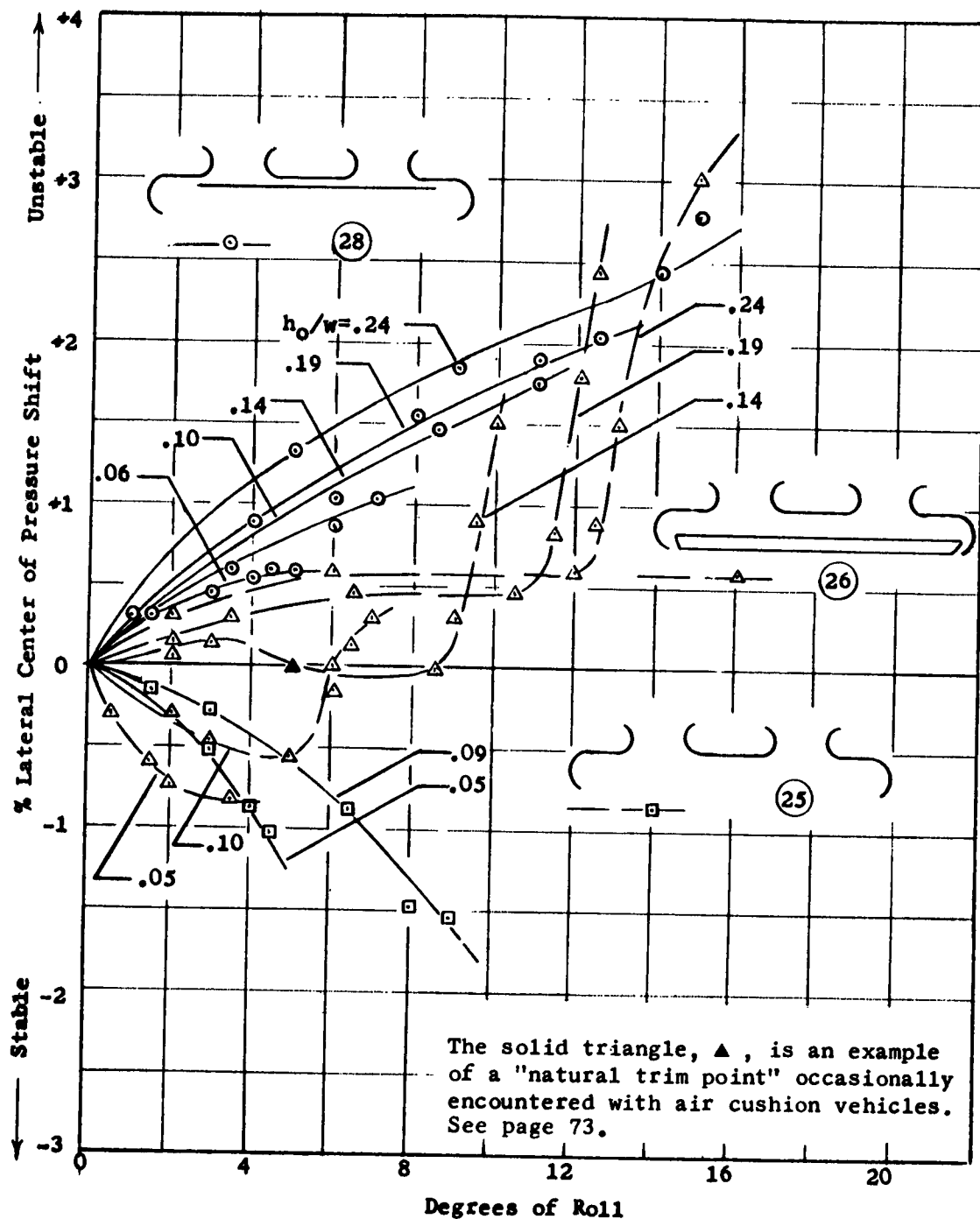


Figure 41. Tandem Fan Oval Model, Static Lateral Stability, Basic Configurations

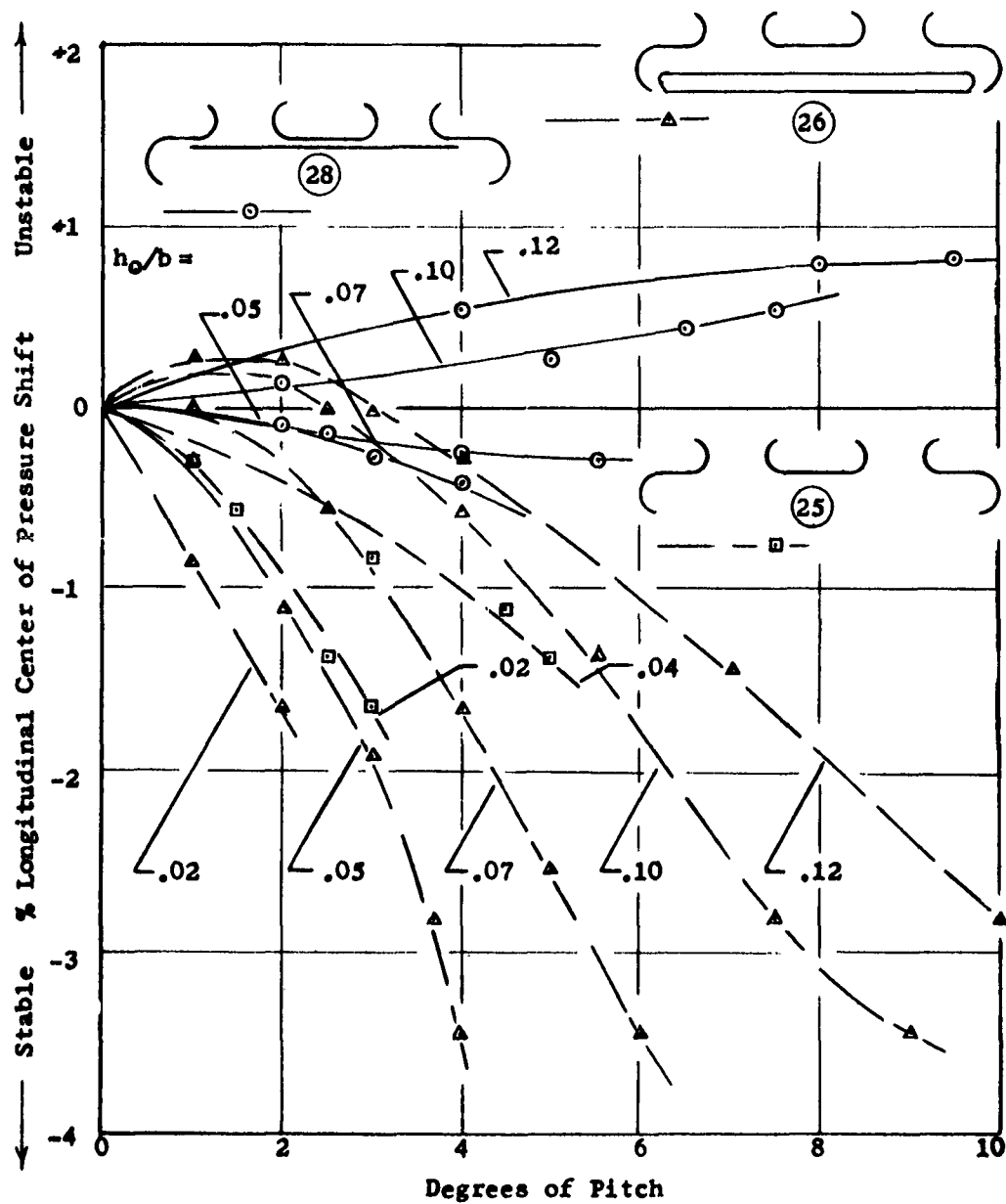


Figure 42. Tandem Fan Oval Model, Static Longitudinal Stability, Basic Configurations



figures also reveal that lateral stability is poorer than longitudinal for the controlled flow and base plate peripheral jet arrangements. In general, the plenum's characteristics are better than the peripheral jet, and the base plate peripheral jet is better than the controlled flow version. It is shown in Figure 35 that the order of relative hovering performance is the exact reverse.

A stability characteristic typical of the air cushion vehicle is the occasional existence of a "natural trim point" defined as the stable tilt angle at which the cushion-induced moments go to zero (see example in Figure 41).

b. Controlled Flow with Additional Inner Side Jets - The first device tested for augmenting stability created an additional jet curtain on either side, inboard of the original peripheral jet curtain. This device is illustrated schematically in Figure 43. This device, in effect, splits the peripheral curtain along either side into two jets. A longitudinal compartment is formed between the jets on each side of the model. Lateral stability is derived from a difference in pressure between these compartments resulting from rolling.

The new lateral stability characteristics with this device installed are compared in Figure 43 with the characteristics of the basic controlled flow configuration. A noted improvement in stability is shown. However, the model still becomes unstable in roll above  $h/w$  ratios of 12 per cent.

The effects of this device on longitudinal stability are apparent in Figure 44. The model becomes unstable at even lower heights with this device installed. However, the device forms a double jet along the sides only. The jet curtain has not been altered at the ends of the model.

c. Controlled Flow with Additional Outer Jet - An additional outer jet was formed around the basic model; that is, the single peripheral jet of the basic configuration was split, forming complete concentric jets.

Lateral and longitudinal stability are both enhanced by this modification. Comparisons of lateral and longitudinal stability are made in Figures 45 and 46.

Figure 45 shows that the modification produces roll stability for all angles, only at low heights ( $h/w < .05$ ). At higher heights, the characteristics are essentially the same as the basic configuration, unstable, for small angles of roll. However, the model has been successfully stabilized at higher angles of roll.

An improvement in longitudinal stability is apparent in Figure 46. The data show that the model possesses static longitudinal stability at  $h/b = .1$  or an  $h/w$  of .2.

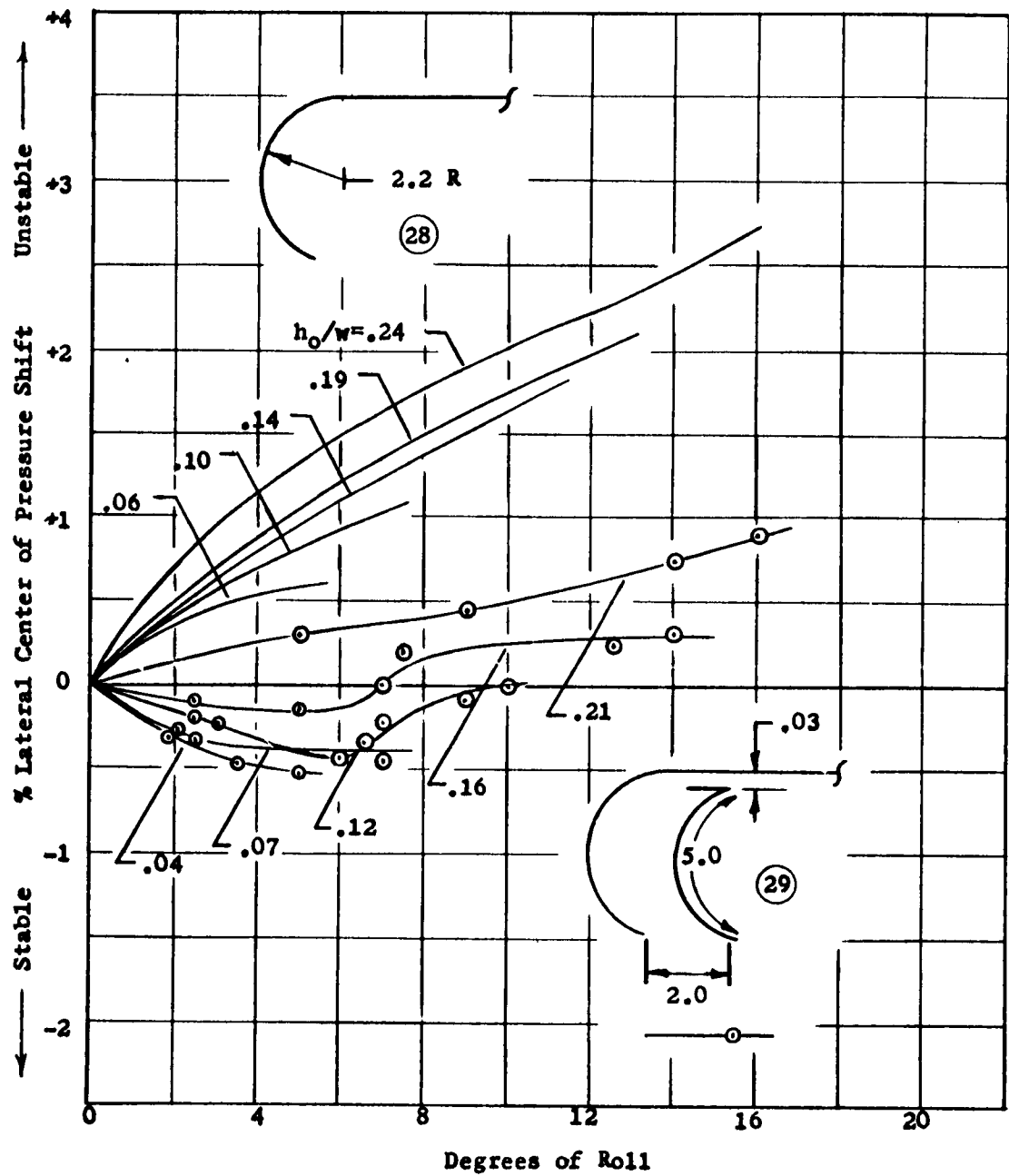


Figure 43. Tandem Fan Oval Model, Static Lateral Stability, Controlled Flow Configuration with Concentric Side Jets

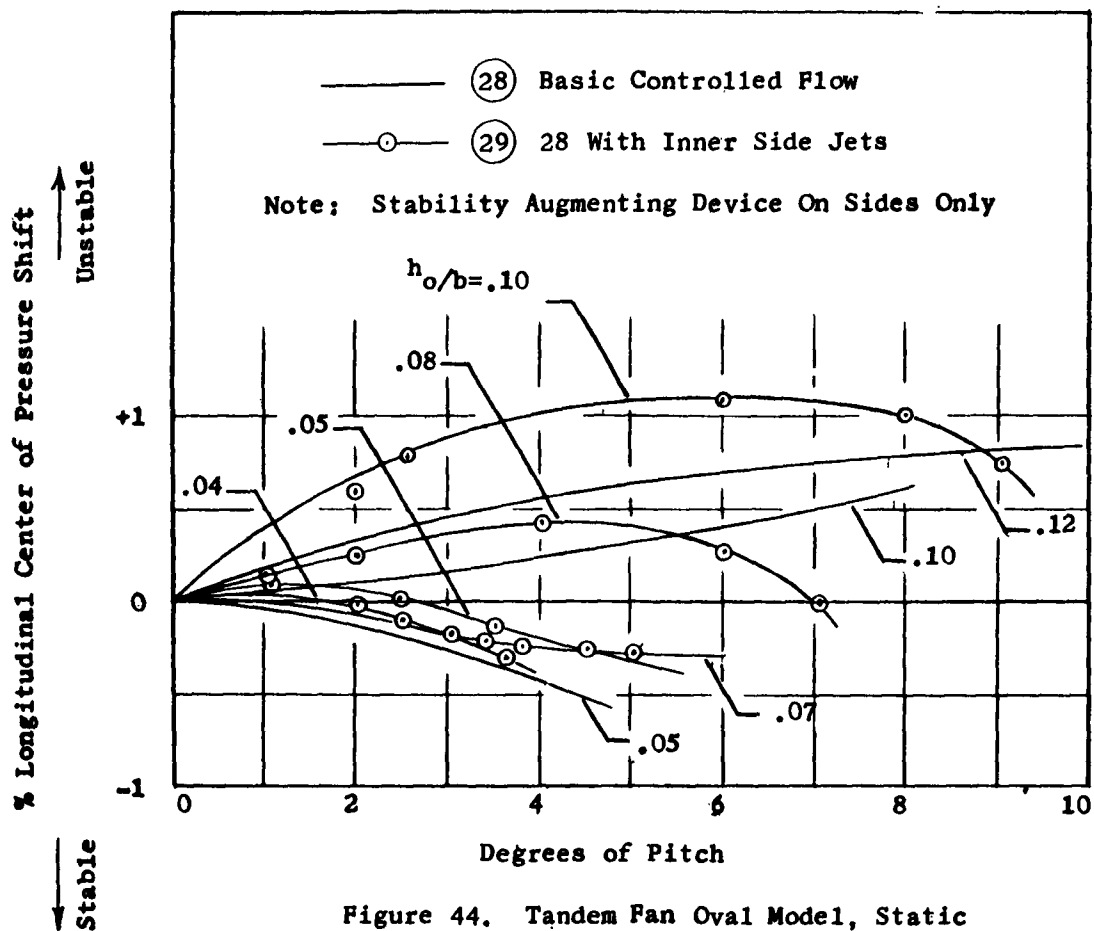


Figure 44. Tandem Fan Oval Model, Static Longitudinal Stability, Controlled Flow Configuration With Concentric Side Jets

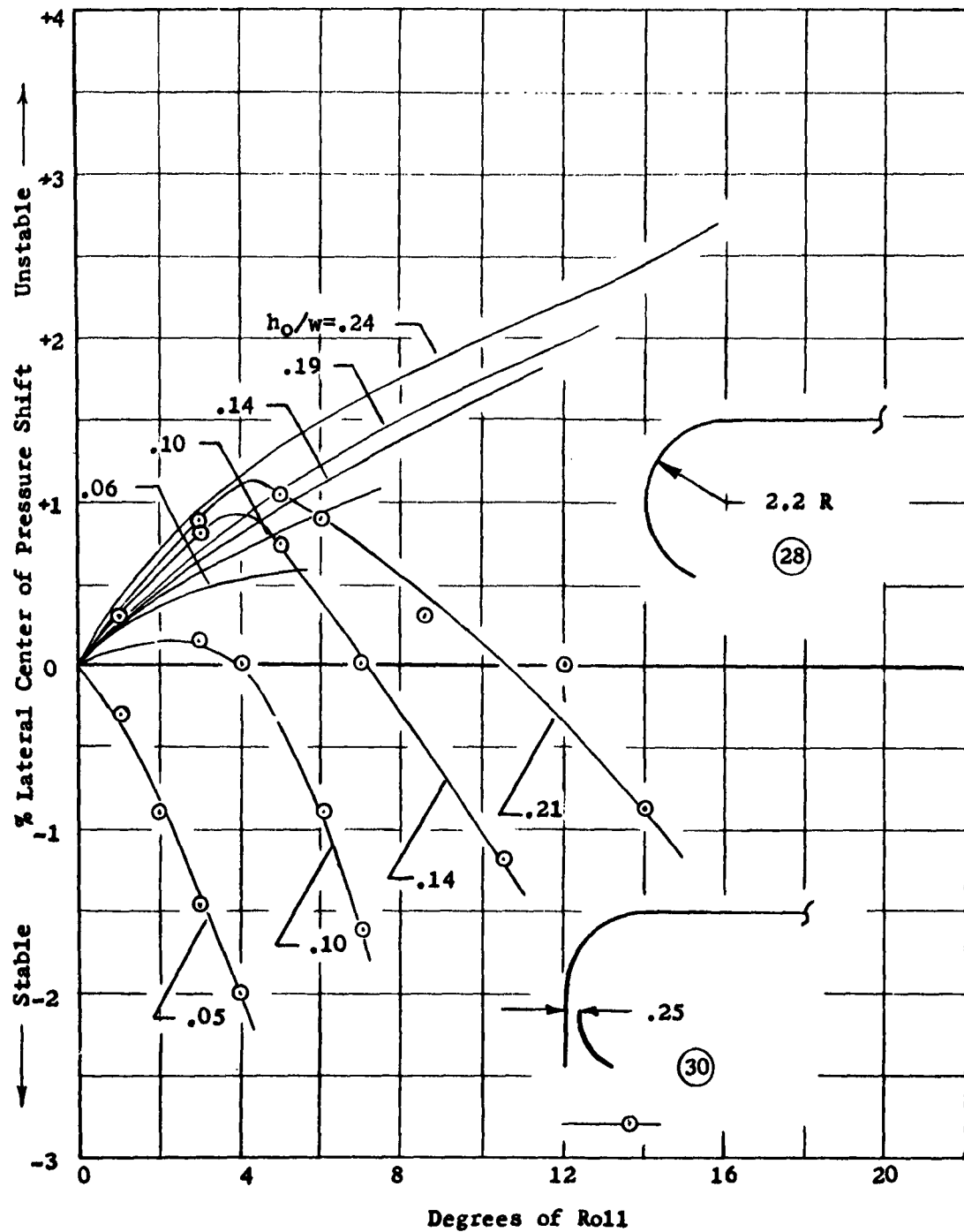


Figure 45. Tandem Fan Oval Model, Static Lateral Stability, Controlled Flow Configuration with Concentric Outer Jet

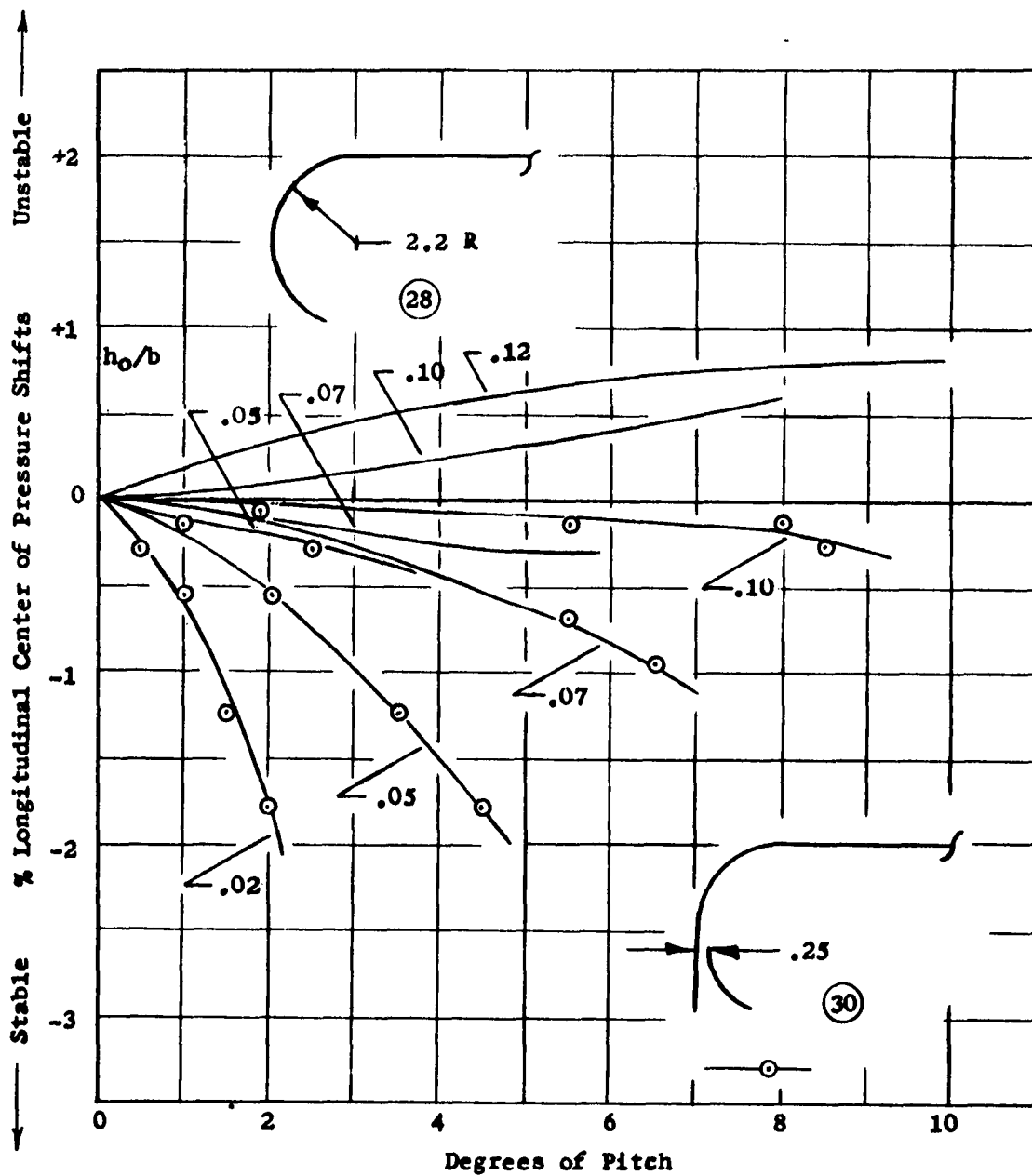


Figure 46. Tandem Fan Oval Model, Static Longitudinal Stability, Controlled Flow Configuration with Concentric Outer Jet

In both Figures 45 and 46, the per cent center of pressure shifts are based on the base width ( $w$ ) and base length ( $b$ ) of the basic configuration. However, in creating the outer jet, the overhang of the fuselage has been utilized to increase the cushion area.

d. Controlled Flow With an Athwartship Fence - The last device evaluated was a rigid vertical fence across the base cavity amidships. The bottom of this fence was even with the edges of the model's side skirt. The effects of this device are shown in Figure 47. Longitudinal center of pressure shifts were measured at one initial height with this device. However, qualitative observations revealed that pitching caused larger center of pressure shifts at lower heights.

Since this device does not alter the peripheral jet, changes in pitch attitude affect only the characteristics of the complex flow system in the air cushion. Cushion flow was not affected by the athwartship skirt when the model was rolled. Hence, lateral stability characteristics with this device are identical to those of the basic controlled flow configuration.

## 2. Performance Penalty With Stability Augmenting Devices

Two plots are used to show the cost of stability augmentation in terms of hovering performance. The hovering performance for the basic model and the model with each of the devices installed is plotted versus  $h_{0c}/S$  in Figure 48. Performance for the annular jet with a base plate and plenum is also shown for reference. Since the loss in clearance height due to tilting varied with each configuration, a plot of the variation of mean height/initial height ratio with attitude is shown in Figures 49 and 50 for roll and pitch. The plot for roll is for  $h_0/w = 15$  per cent. Loss in mean height from rolling was less at  $h_0/w = 5.0$  per cent and greater at  $h_0/w = 15$  per cent. The plot for pitch is for  $h_0/b = 7.5$  per cent ( $h_0/w = 15$  per cent). The mean height of the configurations with stability augmenting devices decreased more rapidly with pitch at higher initial heights and less rapidly at lower heights. Effects of changing initial heights were exactly opposite for pitch of the basic configurations.

Test results in Figures 43 and 45 show that stability is enhanced by splitting the jet curtain into two jets, but splitting the jets reduces hovering performance (reference Figure 48). To provide a tool for mathematically evaluating split jet arrangements, an equation was derived for the ideal hovering performance of a concentric jet air cushion. This equation was derived using assumptions similar to those of Chaplin. The new equation is for any planform with continuous concentric jets. The complete derivation of this equation is included in Appendix III of this report.

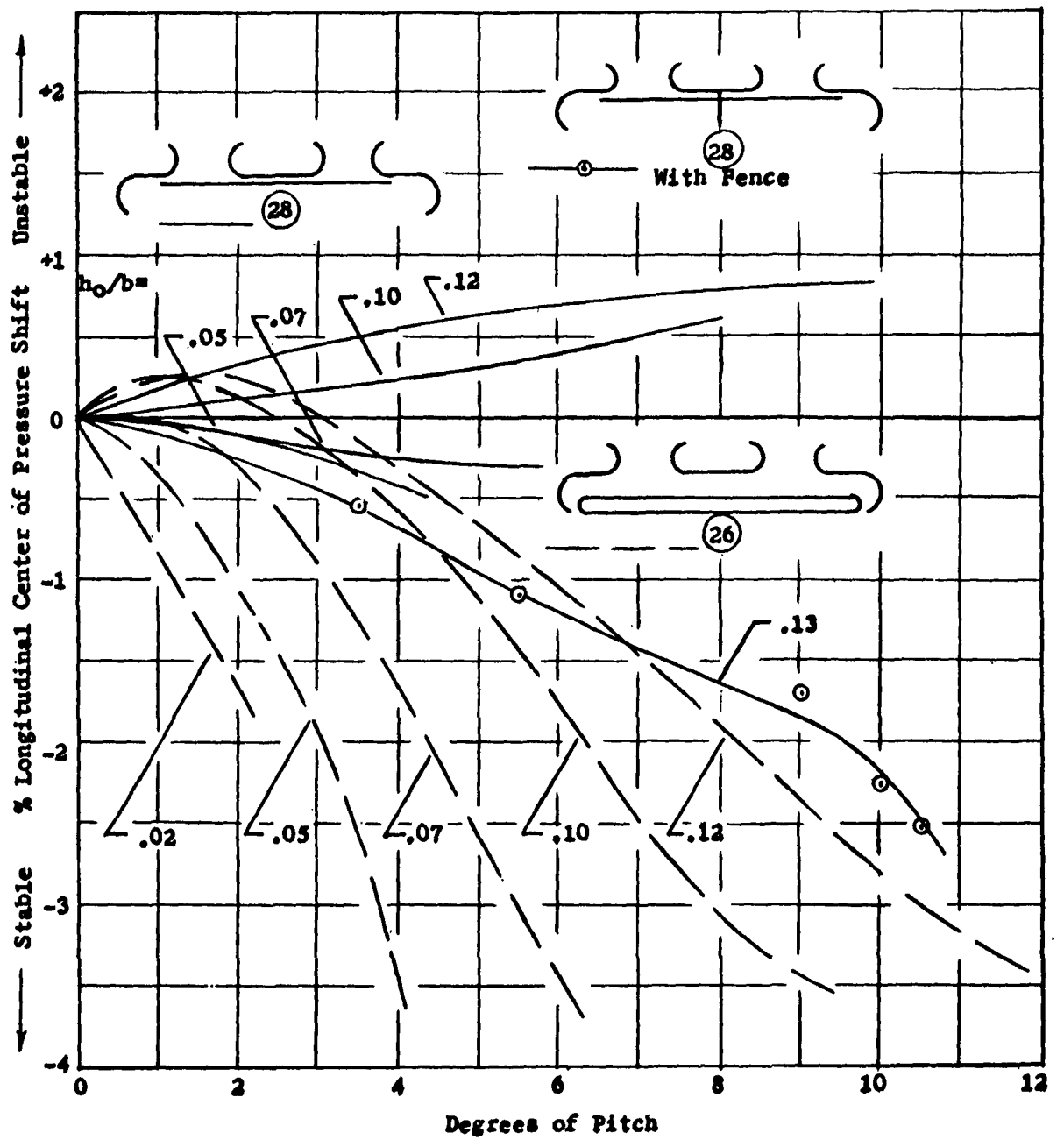


Figure 47. Tandem Fan Oval Model, Static Longitudinal Stability, Controlled Flow Configuration with Athwartship Fence

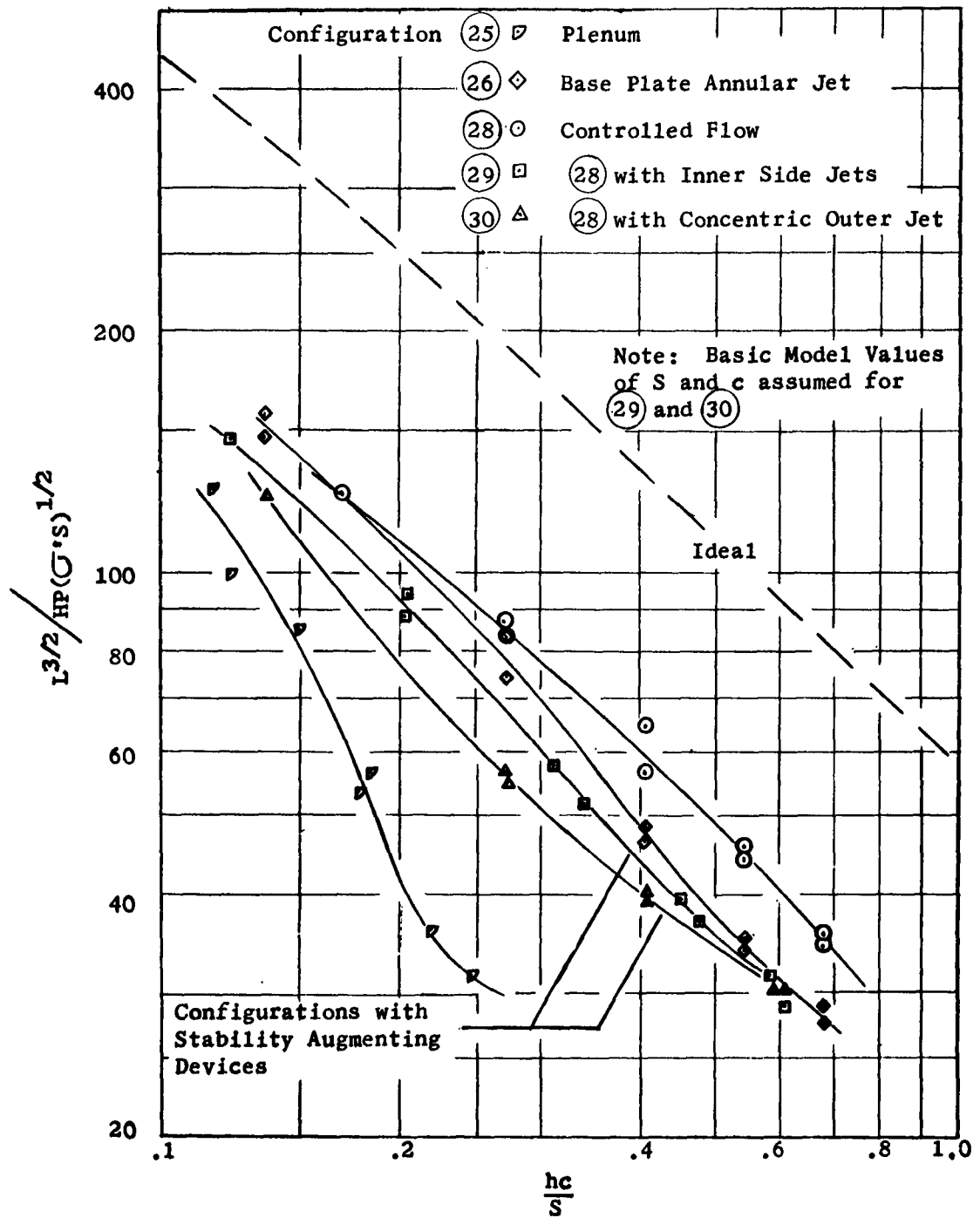


Figure 48. Tandem Fan Oval Model Performance, Basic Configurations and Stabilized Configurations



$$\text{Clearance Height} = h_o \times \frac{h_m}{h_o} - .179 \times \text{Degrees of Roll}$$

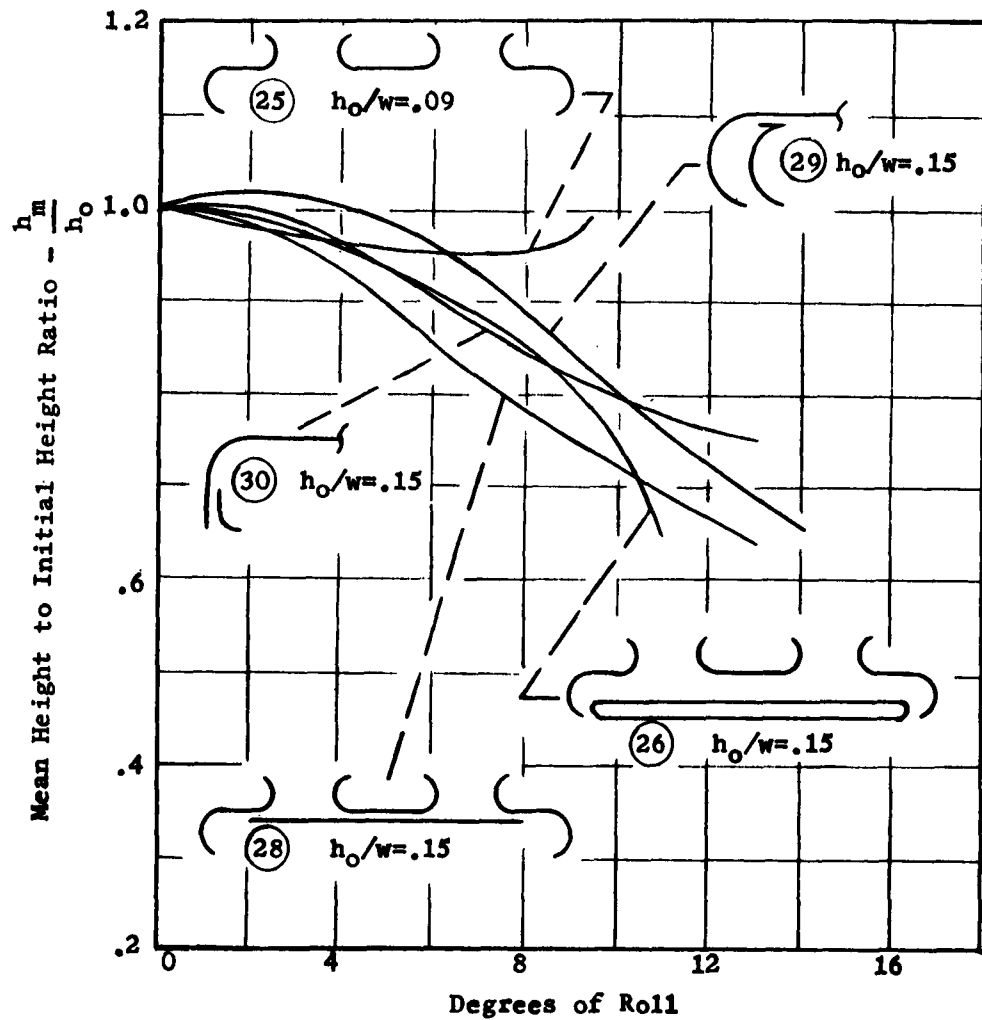


Figure 49. Tandem Fan Oval Model, Variation in Mean Hover Height with Roll

$$\text{Clearance Height} = h_o \times \frac{h_m}{h_o} - .36 \times \text{Degrees of Roll}$$

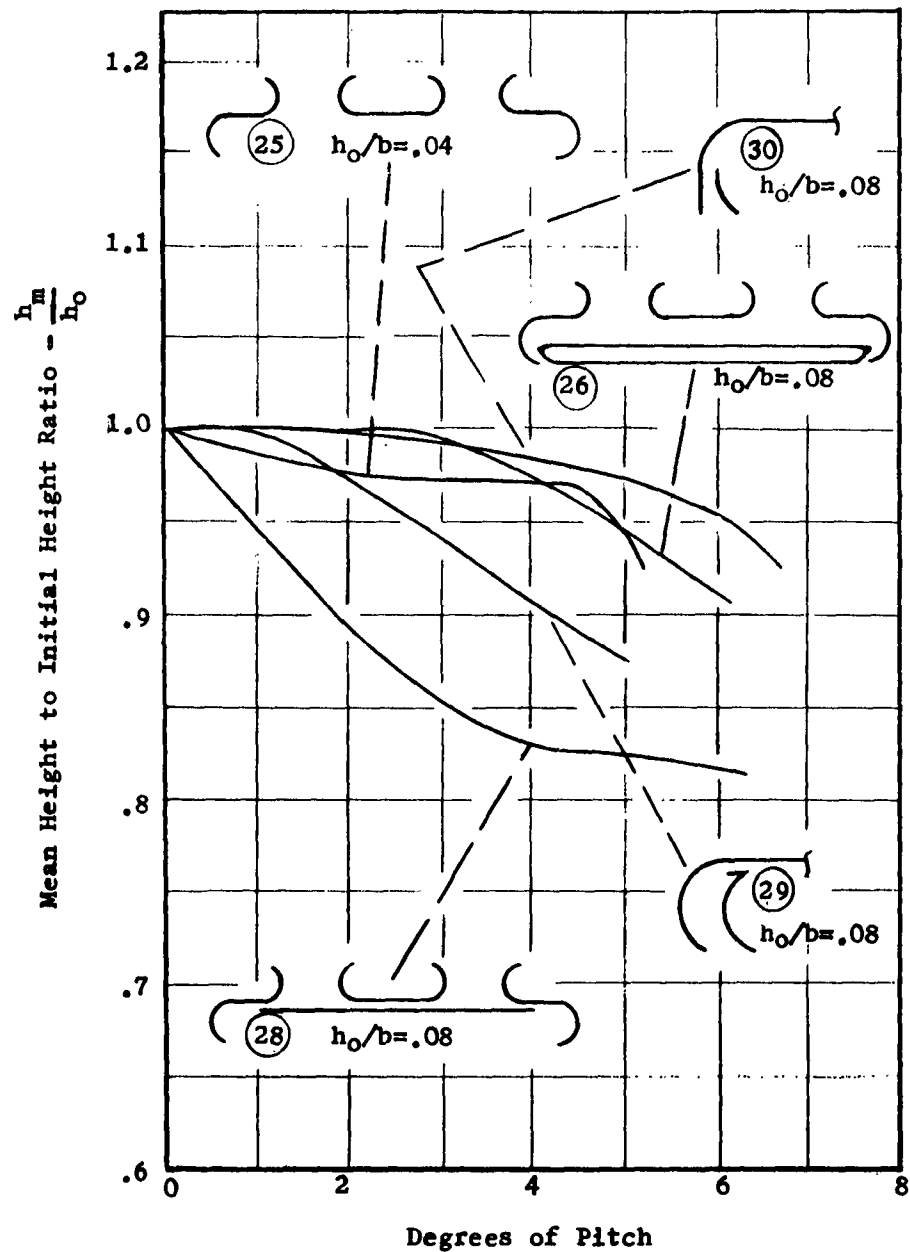


Figure 50. Tandem Fan Oval Model, Variation in Mean Hover Height with Pitch

Ideal performance has been determined with the concentric jet equation for the controlled flow model with an additional outer jet. Figure 51 compares the ideal performance with the experimental performance for the case where inner and outer jet areas are equal. Also shown for reference is the ideal and experimental performance of the basic configuration.

#### D. CONTROL

Almost all current air cushion vehicle designs incorporate an integrated control system for at least one mode of control. Therefore, it was considered appropriate to determine characteristics of the controlled flow air cushion vehicle with integrated control systems.

Many integrated control schemes are possible with the controlled flow air cushion vehicles. The accessibility of the jet curtain (provided by the open base cavity) suggests control systems that alter the characteristics of the jet, some of which are:

1. Slanting the jet (forward or aft)
2. Changing the jet inclination (in or out)
3. Changing the jet area
4. Splitting the jet

Control effected by slanting the jet has received considerable attention by investigators working with conventional peripheral jet arrangements. For instance, the Marine Corps GEM III research vehicle is controlled in this manner. The second and third methods have been investigated to a lesser degree, but little attention has been given to splitting the jets. Lateral thrust, lateral center of pressure trim, and roll attitude control systems were investigated in this program with this method of control. Longitudinal control was not studied; however, the lateral system principles tested could also be utilized for longitudinal control.

A system for controlling heading was tested that effected a change in the curtain slant angle and is particularly adaptable to controlled flow configurations. This system is described along with a discussion of the experimental results.

##### 1. Lateral Control System

Two lateral control systems were tested. They consisted of differential adjustment of the lateral stability devices discussed previously. These devices split the peripheral jet curtain, forming twin jets along the sides. Control is effected by altering the relative strength of these jets, by diverting more or less flow into the outer jet. Thus the jet reaction is acting at a greater or lesser

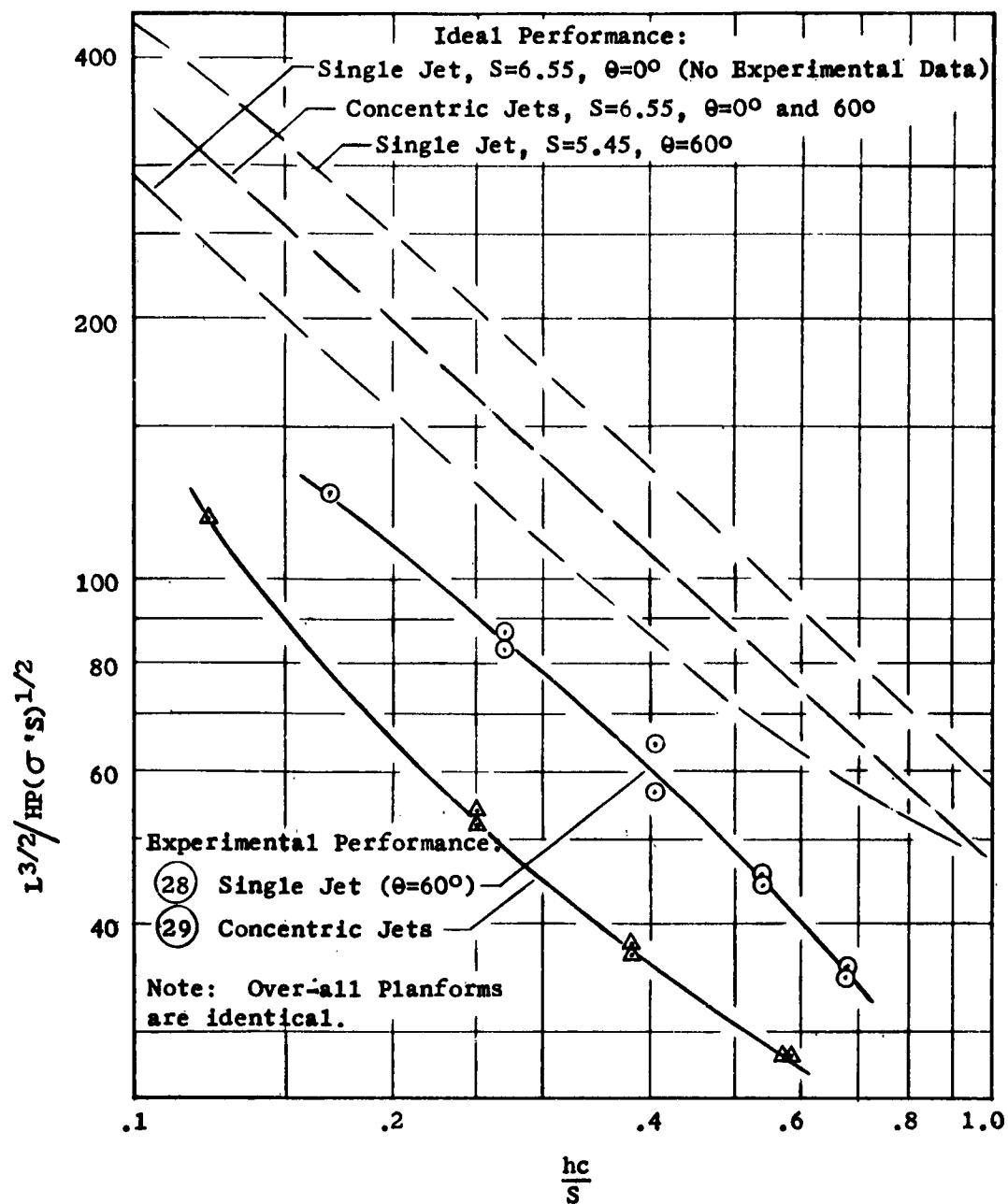


Figure 51. Tandem Fan Oval Model Performance, Ideal and Experimental Comparison for Single and Concentric Jet (Controlled Flow) Configurations

distance (longer or shorter moment arm) from the center of gravity. Other phenomena are involved, such as a change in base pressure between the side jets, but the lateral displacement of the jet thrust is the primary mechanism at work.

The functions performed by the lateral system are discussed below with the test results.

a. Trim Control - The strengths of the additional stability jets were varied differentially from side to side. The resulting center of pressure shifts for the model restrained to level flight simulate the use of differential side jet settings for trimming off-center loads. The level attitude lateral center of pressure shifts for differential side jet settings are shown in Figure 52. This figure shows that differential settings of the additional outer vertical jet produce three times the shift in center of pressure as does differential setting of the additional inner side jet. Effects of differential settings on hover height are also shown in Figure 53 on a plot of mean height/initial height versus differential control setting. This plot shows that differential setting of the additional inner side jets results in up to 23 per cent increase in hover height. Height losses from differential settings of the additional outer jets are less than 3 per cent.

b. Lateral Thrust and Roll Attitude - Differential setting of the additional jets was effective in shifting the trim attitude. Roll angles corresponding to differential settings are shown for each device in Figure 54. Since the model was not stable for angles above an h/w of 10 per cent, data are not shown in Figure 54 for heights greater than that value. Lateral thrusts corresponding to the roll attitudes established by differential side jet settings are shown in Figure 55 for both devices. No loss in mean hover height resulted from rolling the model with differential side jet settings. This is significant since rolling the model by shifting the cg does result in a mean hover height loss.

## 2. Heading Control System

A simple device for producing yawing moments was tested in the tandem fan oval model. This device consisted of one internal vertical vane at each end of the model (see Figure 56). The vanes were positioned coincident with the model's centerline for zero moments. To produce a moment, the downstream ends of the vanes were displaced laterally in opposite directions. The upstream ends of the vanes were cantilevered to the model, thus allowing control of the curvature of the vane. Data were taken with the curvature of the vane adjusted to maximum effectiveness prior to stall. Moments were measured in one direction only. Test results with three vane arrangements are presented in Table 7.

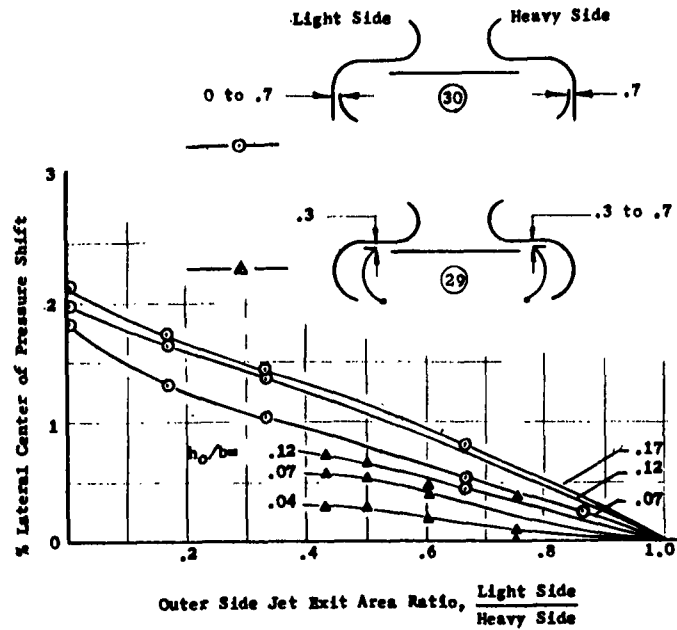


Figure 52. Tandem Fan Oval Model Trim Control, Control Capability

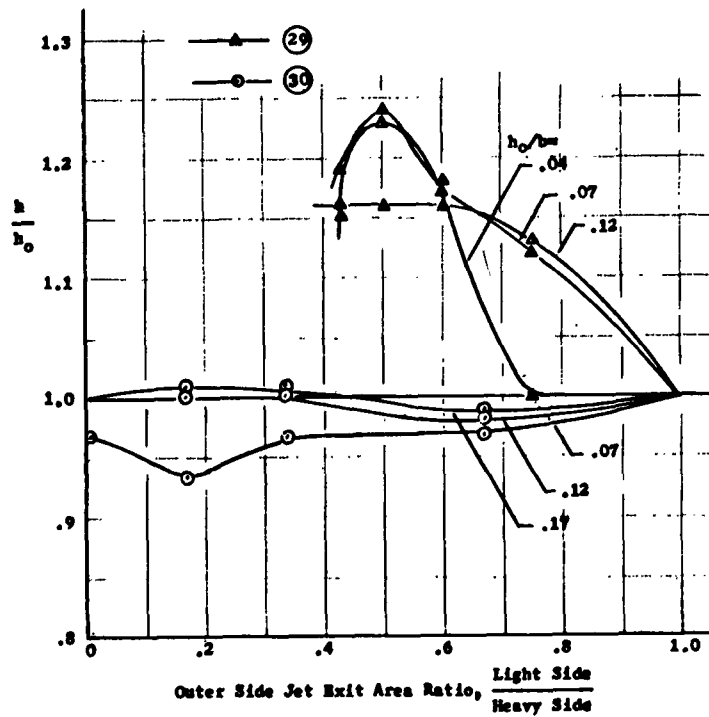


Figure 53. Tandem Fan Oval Model Trim Control, Effect on Hover Height

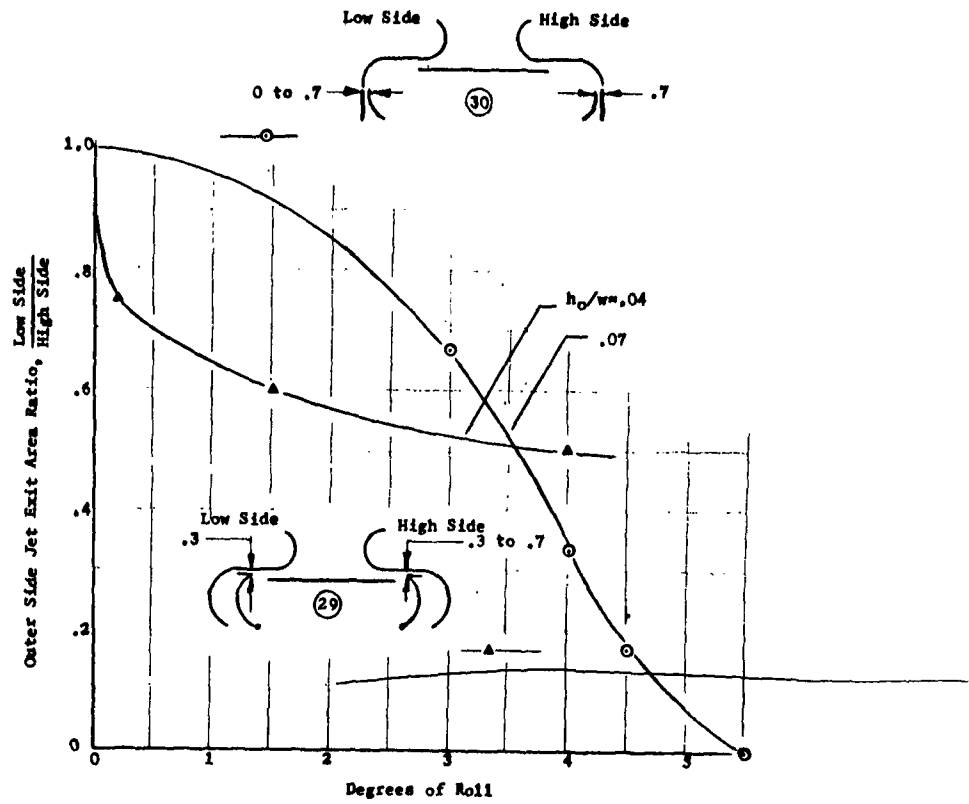


Figure 54. Tandem Fan Oval Model Lateral Control, Trim Attitude

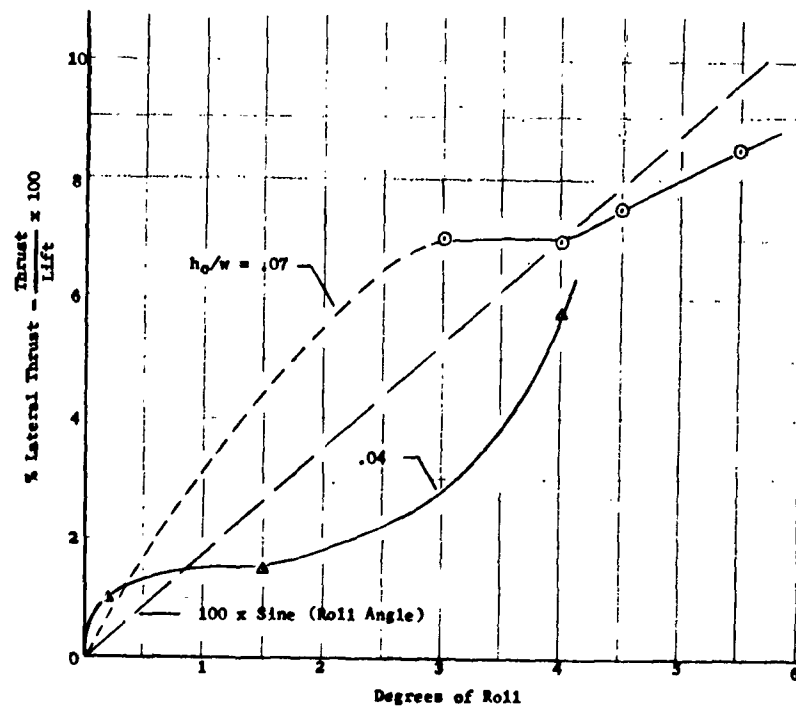


Figure 55. Tandem Fan Oval Model Lateral Control, Lateral Thrust

Configuration No. 28 With End Vanes

End Vane  
(Both Ends)

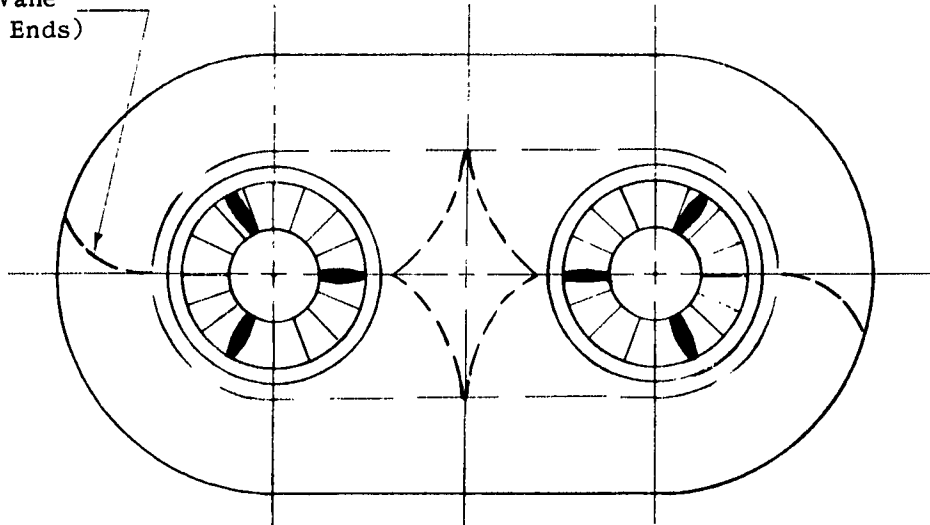


Figure 56. Heading Control System

Table 7

Maximum Heading Control Moments for Yaw Vanes Installed in the Tandem Fan Oval Model, Configuration No. 28

Test Conditions	Side Elevation Showing Control Vane	Moment
Lift=20 lbs $\frac{h}{b} = .715$		.208 ft/lbs
Lift=20 lbs $\frac{h}{b} = .715$		.188 ft/lbs
Lift=20 lbs $\frac{h}{b} = .715$		.055 ft/lbs



It is expected that the maximum yaw control moment derivative will be the same for vehicles similar to the model at the same h/b ratio of 0.72 per cent.

#### E. PROPULSION

The characteristics in hovering of a propulsion system integrated with a controlled flow lifting system were studied.

In this system, forward thrust is produced by decreasing the effectiveness of the rear jet curtain. The resulting decrease in local pressure at the rear induces a generally rearward flow of air in the cushion cavity which results in a decrease in vehicle hover height. The effectiveness of the front jet curtain is excessive at lower heights. Thus a portion of the front jet flows under the vehicle and exits in the rear. Resulting thrust consists of a slight rearward component of the side jet, a decrease in rearward thrust from the front jet, plus the forward thrust from the portion of the front jet exiting at the rear.

To simulate the flow system described above, flaps and ports (see Figure 17) in the rear skirt of the model were adjusted to exhaust air rearward. Resulting thrust and loss of height are presented in Figure 57 for three initial hover heights. Power was held constant as flaps and ports were adjusted. Higher thrusts were not realized because of the proportions of the ports and control flaps. More lift energy could have been converted into forward thrust, had these devices been larger. However, within the limits of the test, internal flow observations revealed no adverse effects on internal distribution from employment of this forward thrust system.

The flow observations clearly indicated that the air discharging from the sides remained nearly normal to the sides with little slant back evident. The side jet air necessary to support the cushion pressure exits normal to the side. The excess air in the side jet flows into the base cavity and exits under the rear skirt as does the excess air in the front jet.

The theoretical and experimental results in Figure 57 are for the model in level attitude and for a control system that affects only the rear portion of the peripheral curtain. In conducting the tests, it was necessary to shift the center of gravity of the model to maintain a level attitude. For example, with the aft ports full open, a nose-up moment would result.

Another series of tests was conducted (data not shown) to determine if the vehicle attitude could be controlled by altering the

peripheral curtain along the sides and at the front during the application of forward thrust. In this test, the model was configured with the additional outer jet except at the stern. Attitude was maintained level by adjusting the local strength of the outer jet. As a result of further reducing the effectiveness of the forward curtain by slanting it aft to reduce the nose-up pitching moment, an excess of air was available for propulsion. The resulting forward thrust was higher than that shown in Figure 57. This indicates that a forward thrust system can be devised which will maintain the vehicle attitude during an application of forward thrust.

A forward thrust system which, in addition to a rear port, included slanting the side jets aft by means of "beta" vanes was investigated theoretically and the predicted height loss versus thrust is shown as the dashed curve in Figure 57. It should be noted that the predicted performance using "beta" vanes exceeds the predicted performance for the configuration with a rear port only. Such a system, therefore, appears to offer promise for future applications.

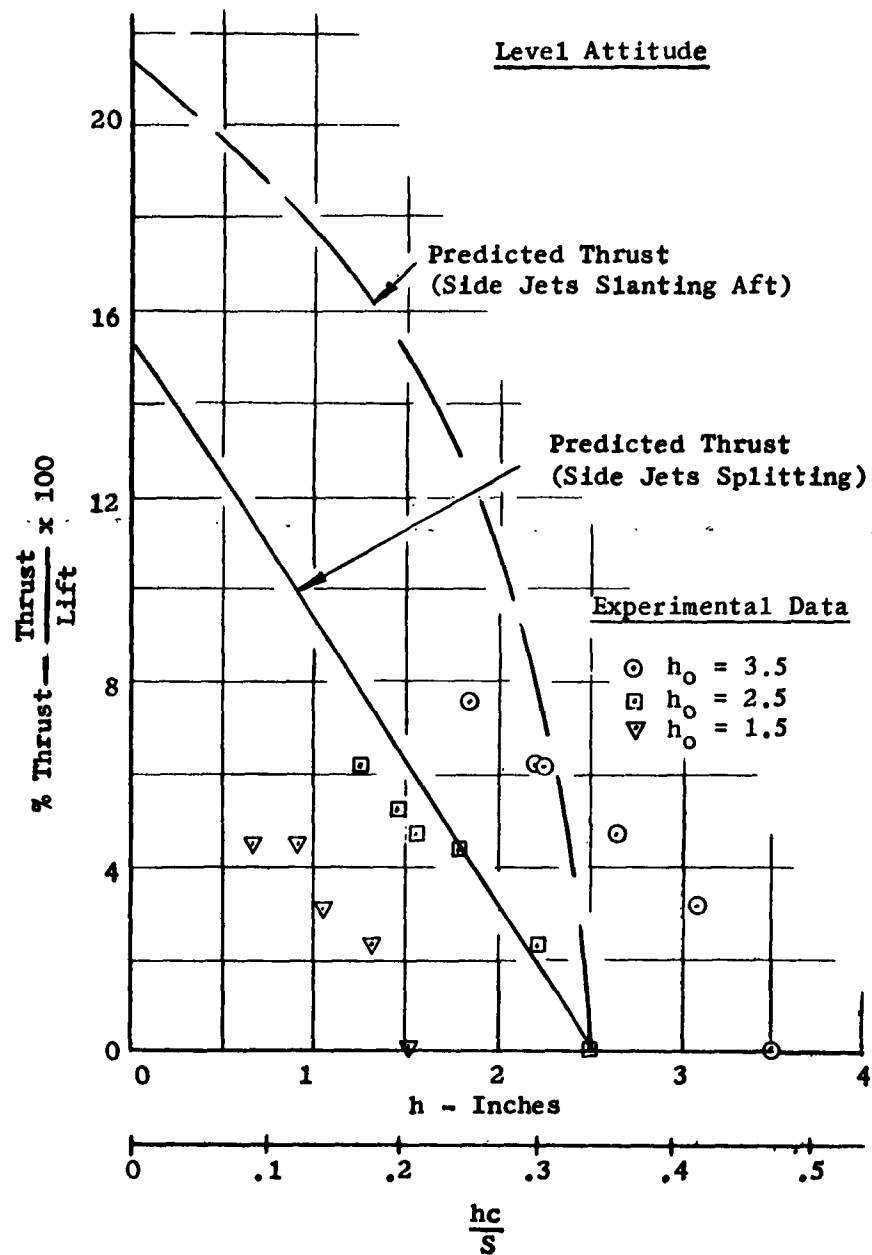


Figure 57. Tandem Fan Oval Model Propulsion System, Variations in Height with Thrust

## VIII. EVALUATION

The purpose of this section is to extract from the results presented in the previous section, the data considered pertinent for evaluating the merits of controlled flow configurations and to discuss what are judged to be the significant characteristics of the controlled flow system. The results have generally verified the findings by other investigators, that attempts to improve the static stability characteristics of air cushion vehicles by modifying the air distribution system will generally entail a performance loss. Therefore, discussion of the controlled flow concept in this section is divided into two parts. The first part is concerned with the relative hovering performance of the controlled flow system without regard to stability characteristics; in the second part, stability, control and propulsion characteristics as provided by the basic air distribution system are considered as factors in evaluating the concept.

### A. DISCUSSION AND COMPARISON OF THE CONTROLLED FLOW CONCEPT; HOVERING PERFORMANCE CRITERION

#### 1. Devices for Achieving Controlled Flow

Controlled flow is described as the ability to establish a peripheral jet on an air cushion vehicle without the use of a base plate or internal ducting. The quality of controlled flow achieved depends on the proper distribution of the jet around the periphery of the model and is, therefore, intimately related with the vehicle planform shape and silhouette.

Ideally, controlled flow would be established by a free vortex flow of the air after it leaves the fan and while it executes the first (or convex) bend. In such a case, a minimum of ducting would be required to guide the flow on the remainder of its journey to the exit periphery and skin friction would be minimum.

An attempt was made during the program to predict analytically the curve shape for the convex bend and the velocity gradients required to insure that the entire flow vein would remain attached during this Coanda process. Time did not permit a complete analytical or experimental investigation of the optimum contour. However, a special propeller was designed and tested which, by very nearly generating the proper velocity distribution on the convex bend, improved the performance of the test model. This indicates that more progress can be made towards achieving a stable free vortex flow. The ideal Coanda flow was not established as such. However, the question of whether or not the flow could be made to follow the outer walls of the cushion cavity in an operational type planform and silhouette has been answered in the affirmative, and the performance loss compared to a fully ducted annular jet has been found to be small. It should be noted that although the controlled flow systems tested did not involve "pure" Coanda

flow on the first bend below the fan, those devices used for causing the flow to execute this turn do not involve an appreciable loss and are simple in nature.

Three basic devices were used to produce controlled flow in the performance tests:

- A spinner tab to cause an abrupt contraction in the vein just below the fan and ahead of the first turn.
- A deflector plate below the fan to prevent the vein from separating on the first bend.
- A partial annular duct below the fan to eliminate the need for Coanda flow.

In planforms other than circular, the deflector plate was warped and thereby utilized to produce improved peripheral, or planform, air distribution at the first bend. When short vanes were also used at the downstream bend, this combination resulted in the best performance for noncircular planform controlled flow configurations. The net result of adding these flow control devices was to achieve peripheral jet flow characteristics without resorting to extensive internal ducting or a base plate.

It was then possible to compare the controlled flow configuration as applied to various planforms with the more conventional arrangements of the peripheral jet.

## 2. Performance Comparison

Of the several configurations tested and discussed in the previous sections of this report, those listed below are the significant ones and have been selected for a final hovering performance comparison for the reasons stated:

Configuration 6, Circular Model, Fully Ducted Annular Jet - This configuration was selected for this comparison because it had the best performance of all models tested.

Configuration 9, Circular Model, Partially Ducted Annular Jet - This configuration more closely approaches the internal flow geometry of the ideal controlled flow configuration for a circular planform than all the models tested.

Configurations 2, Circular, Square, Single Fan Oval, and Tandem Fan  
10, 17, and 26 Oval Planforms (respectively), with Base plates - These models are representative of practical design approaches for peripheral jet vehicles of various planforms.

Configuration 8, Circular, Square, Single Fan Oval and Tandem Fan  
13, 20, and 28 Oval Planforms (respectively), with Deflector Plates -  
These models are representative of practical design  
approaches for approximating ideal controlled flow  
in various planforms.

Table 8 summarizes the experimental values of the performance  
parameter,  $M_p$ , for each of the above configurations at representative  
values of the height parameter,  $h_c/S$ .

It has been established that the ideal hovering efficiency for  
the controlled flow configurations can be predicted using equation (1).  
This arises from the fact that the ideal flow characteristics at the  
peripheral jet exit are the same regardless of internal configuration.  
The actual performance, then, primarily depends on losses associated  
with the particular internal arrangement used. Therefore, Table 8  
also contains both the ideal values of the performance parameter as  
calculated from equation (1) and the resulting measured efficiencies.  
A complete performance comparison should also include the forward flight  
characteristics, which were beyond the scope of this investigation;  
however, certain conclusions regarding relative hovering performance  
are apparent from examining the data of Table 8, namely:

- The fully ducted annular jet shows slightly better performance  
than the partially ducted annular jet configuration. This in-  
dicates that losses due to skin friction are not as great as  
those associated with the partially ducted version with uncon-  
fined internal flow. The difference in performance is small and  
the partially ducted configuration is much simpler in construc-  
tion.
- The partially ducted annular jet is only slightly better in  
performance than the controlled flow version using a flat de-  
flector plate below the fan. The latter is certainly a further  
simplification of the internal structure and results in little  
performance penalty.
- Controlled flow versions using a deflector plate were equal to  
or better than all versions of the peripheral jet configuration  
with base plates when compared with the same planform. This in-  
dicates that the simpler controlled flow internal arrangement is  
more desirable than the "practical" peripheral jet configuration.

The difference between deflector plate and base plate versions of  
the oval models is slight, whereas on the circular and square  
models, the deflector plate versions are noticeably better. This  
is mainly due to the fact that the base plate versions of the cir-  
cular and square models had too large a plenum cavity, which gave  
rise to erratic internal flow conditions and do not represent  
optimized design of the base plate configurations.

However, it is significant that on the more refined oval models, the simpler internal geometry of the controlled flow version was as good or better than peripheral jet configurations with a base plate.

- The circular planform configurations, in general, had the best performance, followed by the oval planform configuration with two fans. The latter represents a more practical arrangement for full-scale vehicles and the performance penalty is slight.

### 3. Application of Controlled Flow Techniques to Peripheral Jet Configurations with Base Plates

As discussed in the previous paragraph, the performance of the circular and square models using base plates indicated non-optimum design which resulted from the plenum arrangement above the base plate. The flow was observed to be unstable on the convex bend immediately below the fan and would intermittently separate and attach. To stabilize the flow for measurements in the base plate configuration, a clean separation from the convex bend was induced by extending the cylindrical surface of the fan shroud to be flush with the ceiling of the plenum cavity. The flow pattern thus established and associated losses explain the relatively poor showing of Configurations 2 and 10.

By introducing a partial duct below the fan on the square model (a controlled flow technique), the internal flow pattern was improved and the efficiency was increased. With the oval models, the base plate configuration was more nearly optimized and no improvement was apparent by adding a control flow device.

This study indicates that too deep a plenum cavity above the base plate in a conventional peripheral jet design can noticeably reduce the over-all efficiency. Control flow techniques may then be applied to improve vehicle hovering performance.

### 4. Application of Controlled Flow Techniques to External Flow of Air Cushion Vehicles

The external flow air cushion vehicle concept is predicated on utilizing Coanda flow over the external surface (ellipsoidal silhouette investigated) to induce the vein of air to the jet exit. The jet curtain at the periphery then behaves, ideally, as a conventional annular jet. Since the ideal controlled flow concept employs the Coanda phenomenon internally, it follows that the same techniques might have application on the external flow air cushion vehicle.

Theoretical considerations of the ideal flow characteristics around the external surfaces during hovering indicate that again the ideal performance may be predicted by equation (1). The losses associated with this configuration are primarily due to flow separation from the external surface just upstream of the jet exit. The main attempt made to prevent this separation near the jet exit during a

brief investigation of the external flow concept consisted of attaching a circular shroud near the jet periphery. This succeeded in improving the performance deeper in ground effect and reduced the height at which separation occurred.

The results of performance tests with the external flow configuration are compared in Figure 58 with results for the fully ducted annular jet, a plain ducted fan with extended shroud, and the open rotor version discussed in Reference 4.

At heights above values of  $h/d$  of .1, the test results indicate higher performance for the external flow configuration than that obtained with the fully ducted annular jet. Below this value of height, the flow begins to separate from the external surface and efficiency drops off. With more effective techniques applied to prevent separation of the flow from the vehicle surface, performance which is competitive with the standard annular jet configuration could be obtained in the lower height, higher base loading range. The effect of forward speed on the external flow pattern has not been investigated, but ram-wing concepts may offer possible solutions as the external flow is swept aft.

An interesting by-product of this investigation is the relatively high performance obtained with the 10-inch diameter ducted fan power unit (with extended shroud) in ground effect. It was found to be superior to the conventional air cushion vehicle at heights down to an  $h/d$  of .06.

#### 5. Recommendations

On the basis of the hovering performance criterion comparisons made above, it is recommended that the controlled flow internal arrangements be considered when

- a base plate is not mandatory (for flotation, etc.) on a peripheral jet air cushion vehicle. The advantages to be gained would be reduced terrain interference with the vehicle bottom and performance equivalent to or better than a peripheral jet configuration with base plate.
- a deep internal plenum cavity is formed between the fan exit and the base plate in a peripheral jet configuration. The principal advantage in such a case will be to improve the internal flow profile within the plenum, thereby improving the over-all efficiency. A "deep" plenum is considered to be one in which the upper surface of the base plate is at least between .25 and .30 fan diameters below the ceiling of the cavity.
- simplicity of internal construction is desired. In comparison, only the plenum configuration, with relatively poor performance, is simpler. The fully ducted peripheral jet can be expected to have better performance but at the expense of complicated internal ducting.



B. DISCUSSION AND COMPARISON OF THE CONTROLLED FLOW CONCEPT; STABILITY, CONTROL, AND PROPULSION CRITERIA

To evaluate further the controlled flow concept, considerations of stability, controllability and propulsive force characteristics in hovering flight are included in the following paragraphs. Questions remain regarding forward flight characteristics; these, however, were beyond the scope of this investigation.

1. Stability, Control and Propulsion Devices; Controlled Flow Configurations

As discussed in the results, three devices were investigated which improved the stability of the basic controlled flow version of the oval model with two fans. These were

- an inner concentric jet formed by splitting the main flow at the periphery of the vehicle.
- an outer concentric jet formed by extending a vertical shroud from the extremity of the vehicle and venting a portion of the main flow through it.
- a fence running across the model in the cushion cavity.

The concentric jet versions were modified easily to provide integrated roll control systems. Application of the same principles would also provide longitudinal control. Yaw control vanes near the deflector plate were successfully combined with the controlled flow concept. In addition, a propulsive system was tested and the results compared with predicted results based on a theoretical method developed for this purpose. The general conclusion based on these results indicates that the propulsion and control systems can be integrated with the controlled flow lift system without causing the internal flow to break down during application of control or propulsion.

2. Comparisons

Table 9 summarizes the stability characteristics of the tandem fan oval model in the conventional base plate configuration, the basic controlled flow configuration, and the inner and outer concentric jet configurations. It can be seen that the base plate peripheral jet and the inner concentric jet version of the controlled flow have very nearly the same stability characteristics in roll; that is, stability exists at very small angles, then deteriorates as the tilt angle increases. The outer concentric jet version, on the other hand, has what is judged to be a more desirable characteristic than the standard peripheral jet or inner concentric jet. This configuration possesses positive stability at all tilt angles except for a narrow range ( $\pm 2$  degrees) near zero tilt angle. This is a significant improvement over the standard peripheral jet configuration. The stabilized controlled flow configuration suffered a reduction in hovering performance ranging from 28

to 33 per cent depending on height compared to the base plate version of the peripheral jet. This represents the cost of stabilization as determined during this investigation. Further investigation with controlled flow concepts may easily point the way toward still better improvements in stability with less of a performance penalty. When stabilized, the controlled flow configurations as tested during this investigation lose their performance advantages over the base plate peripheral jet configuration. However, the stability characteristics are superior and they still retain terrain clearance advantages which may prove useful in air cushion vehicle design.

### 3. Recommendations

It is recommended that further consideration be given to stabilization techniques involving a concentric jet arrangement on controlled flow configurations. This combination produced an improvement in stability characteristics but at a significant cost in hovering power requirements. It is also recommended that further optimization of handling qualities and performance be accomplished through experimentation with scale models of the vehicle under consideration.

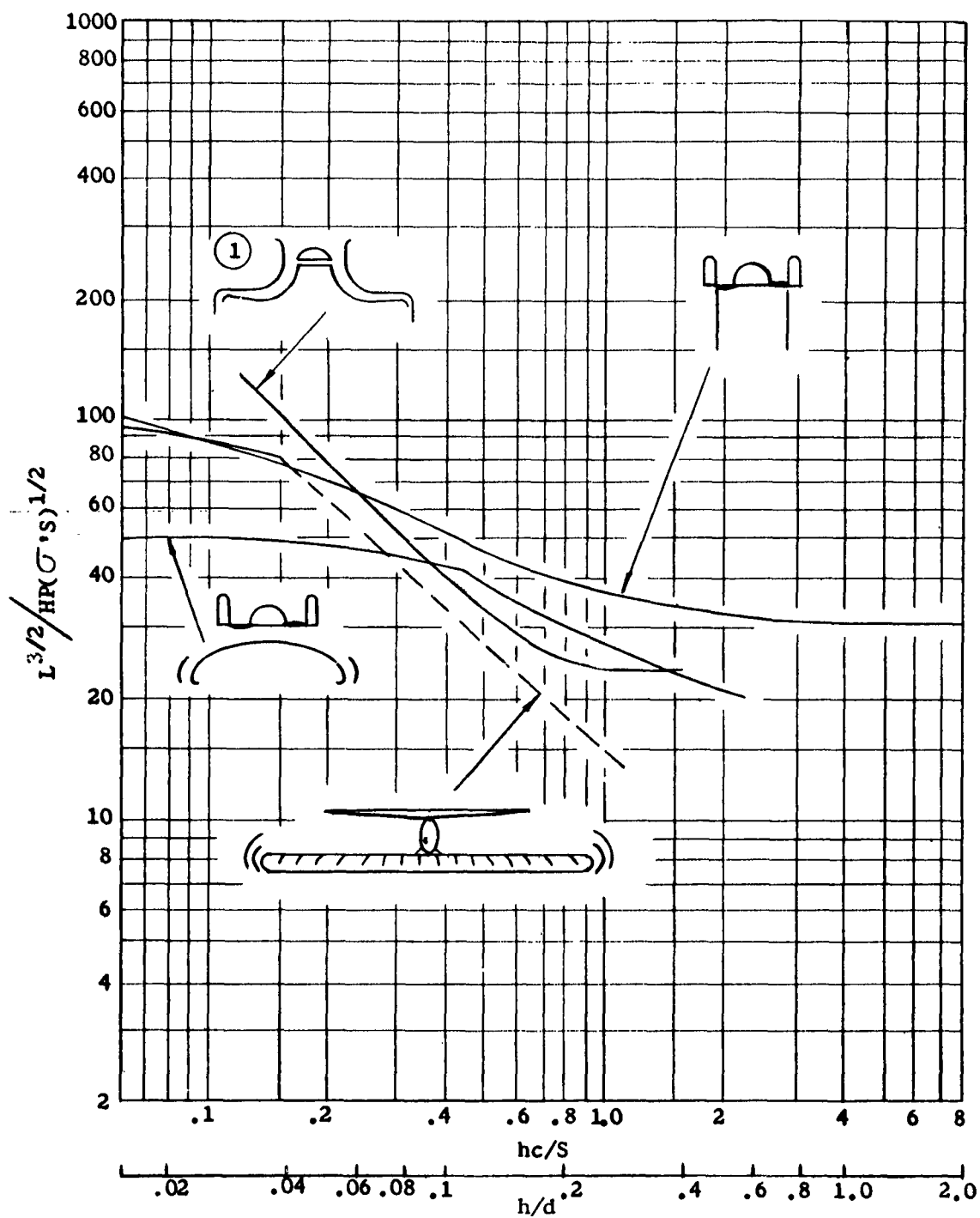


Figure 58. Experimental Hovering Performance: Peripheral Jet, Ducted Fan, and External Flow Models

TABLE 8

SUMMARY OF PERFORMANCE FOR SELECTED MODELS

Configuration	No.	hc/S = .2					hc/S = .4					hc/S = .6				
		(M <sub>p</sub> )	(M <sub>p</sub> ) <sub>i</sub>	η	G	(M <sub>p</sub> )	(M <sub>p</sub> ) <sub>i</sub>	η	G	(M <sub>p</sub> )	(M <sub>p</sub> ) <sub>i</sub>	η	G	(M <sub>p</sub> )	(M <sub>p</sub> ) <sub>i</sub>	G
Circular - Base Plate	2	38.0	150	25.3	1.41	18.5	84.0	22.0	2.90	14.5	60.5	22.3	3.70			
Circular - Fully Ducted	6	98.0	225	43.5	.55	62.0	115	53.9	.86	44.5	79.0	56.4	1.20			
Circular - Def Plate	8*	95.0	225	42.2	.56	53.0	115	46.1	1.01	39.0	79.0	49.4	1.37			
Circular - Partial Duct	9*	98.0	225	43.5	.55	58.0	115	50.4	.92	43.0	79.0	54.4	1.25			
Square - Base Plate	10	55.0	243	22.6	.97	27.5	129	21.3	1.95	16.2	84.5	19.2	3.30			
Square - Deflector Plate	13*	90.5	243	37.2	.59	45.0	129	34.9	1.19	29.5	84.5	35.0	1.82			
Sgl Fan Oval - Base Plate	17	83.0	250	33.2	.65	39.5	117	33.7	1.35	27.5	78.0	35.3	1.95			
Sgl Fan Oval - Def Plate	20*	79.0	250	31.6	.68	39.5	117	33.7	1.35	28.0	78.0	35.9	1.91			
Tand Fan Oval - Base Plate	26	106	250	42.4	.51	50.0	135	37.0	1.07	32.5	92.5	35.2	1.65			
Tand Fan Oval - Def Plate	28*	110	250	44.0	.49	59.5	135	44.0	.90	41.0	92.5	44.4	1.31			
*Controlled flow configurations																

TABLE 9

SUMMARY OF STABILITY CHARACTERISTIC FOR CONVENTIONAL AND CONTROLLED FLOW  
TANDEM FAN OVAL MODEL CONFIGURATIONS

Configuration	No.	Roll		Pitch	
		Stable Heights, h/w	Stable Attitudes	Stable Heights, h/b	Stable Attitudes
Base Plate Only	26	up to .10	up to 5°	up to .07	all
Def Plate Only	28	unstable all	unstable all	up to .07	all
Inner Conc Jet	29	up to .16	up to 5°	up to .05	above 1°
Outer Conc Jet	30	up to .10	above 2°	up to .10	all

## IX. REFERENCES

1. Contract DA 44-177-TC-744, Investigation of Controlled-Flow Phenomena for Air Cushion Vehicles, U. S. Army Transportation Research Command, June 28, 1961.
2. Barclay, Hartley W. (ed), "Ford Has GEM," Automotive Industries, Vol. 126, No. 7, dated April 1, 1962.
3. Wernicke, K. G., Performance Testing of a Five-Foot Air Cushion Model, Paper No. 28, Princeton University, Department of Aeronautical Engineering, Symposium on Ground Effect Phenomena - A Compilation of the Papers Presented October 21 - 22 - 23, 1959.
4. Wernicke, R. K., Experimental Investigation of an Unusual GEM Configuration Involving the Use of a Helicopter, Bell Helicopter Company Report No. 8034-099-002 dated June 7, 1961.
5. Carmicheal, Bruce H.; Dobson, Frank A.; Rawlings, William L., State of the Art Summary Air Cushion Vehicles, Aeronutronic, A Division of Ford Motor Company, Publication No. U-926 dated June, 1960.
6. Strand, T., Exact Inviscid Incompressible Flow Theory of Static Peripheral Jets in Proximity to the Ground, Convair Engineering Research Report ERR-SD-002, November 27, 1959.
7. Chaplin, Harvey R., Ground Cushion Research at the David Taylor Model Basin - A Brief Summary of Progress to Date and A Preliminary Design Technique for Annular Jet GEM's, Paper No. 4, Princeton University, Department of Aeronautical Engineering, Symposium on Ground Effect Phenomena - A compilation of the Papers Presented October 21 - 22 - 23, 1959.

## APPENDIX I

### ANALYSIS OF THE TWO-DIMENSIONAL POTENTIAL FLOW VELOCITY PROFILES ON CONVEX AND CONCAVE BENDS

#### A. GENERAL

A straightforward analysis for the controlled flow investigation is presented here of two-dimensional potential flow velocity and pressure profiles in a vein of air moving along convex and concave bends. The outer streamline (away from the wall) is exposed to a constant pressure along its length (base pressure in the cushion cavity). The purpose of the analysis is to define the pressure coefficient and streamline velocity at the wall at any point along the wall downstream of the fan. This information is required for the investigation of boundary layer separation points presented in Appendix II. Further, this analysis provides a definition of the ideal vein thickness at any point downstream of the fan which is useful for experimental investigations of various controlled flow techniques. The distance along the wall is implied only, since the path is expressed in terms of the local radius of curvature of the wall. This analysis concludes with two graphs, one for the convex bend and one for the concave bend. Each graph presents the pressure coefficient at the wall, velocity at the wall, and the local vein thickness in terms of local radius of curvature and the inlet conditions.

#### B. ANALYSIS

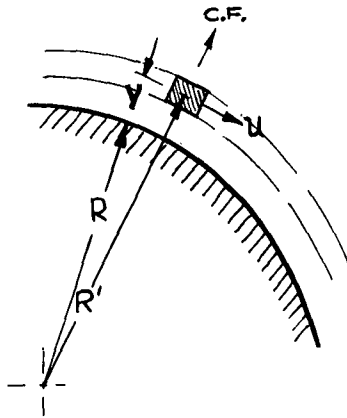
1. <u>Definitions</u>	<u>Units</u>
$a$ = Inlet Width	ft
$C_p$ = Pressure Coefficient	-
$P_T$ = Total Bernoulli Head	lb/ft <sup>2</sup>
$p$ = Static Pressure	lb/ft <sup>2</sup> <u>abs</u>
$p_s$ = Static Pressure	lb/ft <sup>2</sup> <u>gage</u>
$R$ = Radius of Curvature of Bend	ft
$R'$ = Radius of Curvature of Center of Mass of a Fluid Element	ft
$t$ = Vein Width Downstream of Inlet	ft
$u$ = Velocity of Fluid Element	ft/sec
$u_w$ = Velocity Along the Wall	ft/sec

$V_p$	= Velocity of Fluid at Inlet (Uniform)	ft/sec
$y$	= Radial Distance From Surface to Element Under Consideration	ft
$\rho$	= Fluid Mass Density	$\frac{1b\text{-sec}^2}{ft^4}$

## 2. Convex Bend Velocity Profile

Consider the convex bend shown in the accompanying sketch. Let the radius of curvature to the center of mass of a fluid element be  $R'$ .

The forces acting normal to the stream-line (in the radial direction) are those due to the centrifugal force and the pressure gradient. We are neglecting the viscous forces (potential flow) and the body force field. The force equilibrium equation for the fluid element in question is therefore the following:



$$\frac{dp}{dy} = \frac{\rho u^2}{R'} \quad (I-1)$$

Observe that centrifugal separation of the fluid can take place if the pressure force is smaller than the centrifugal force.

If we assume the flow to be parallel to the wall and the radius of curvature constant, then a potential flow with a uniform initial Bernoulli head,  $P_T$ , possesses a pressure  $p$  at a point where the velocity is  $u$  and such that

$$p = P_T - \frac{1}{2} \rho u^2 \quad (I-2)$$

From this latter equation, we obtain

$$\frac{dp}{dy} = -\rho u \frac{du}{dy} ; (P_T = \text{const}) \quad (I-3)$$

In equation (I-1),  $R' = R + y$  where  $y$  is the radial distance from the wall to the element in consideration. Combining (I-1) and (I-3), we get:

$$-\rho u \frac{du}{dy} = \frac{\rho u^2}{R + y} \quad (I-4)$$

and therefore, by separation, ( $R = \text{const}$ )

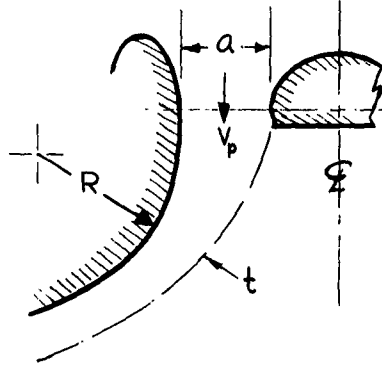
$$\frac{du}{u} = -\frac{dy}{R + y} \quad (I-5)$$

On integration, we get

$$u = \frac{K}{y + R} , \text{ where } K = \text{const of integration.} \quad (\text{I-6})$$

Equation (I-6) is the well-known free (potential) vortex equation for the flow on an incompressible inviscid fluid around a bend.

We now consider the specific case of a fluid vein attached to the wall of a plenum chamber. The sketch defines the parameters of a



two-dimensional case. At the inlet section,  $R' = R + a$  and the velocity of the fluid is  $V_p$ . At any downstream section,  $R' = R + t$  where  $t$  is the vein thickness at that station. Hence, at the boundary (streamline farthest from wall), equation (I-6) becomes

$$u = \frac{K}{R + t} .$$

Since the outer streamline is one at a constant pressure, then its velocity is constant and equal to  $V_p$  (Bernoulli). Therefore,

$$V_p = \frac{K}{R + t} , \text{ and} \quad (\text{I-8})$$

$$K = V_p (R + t) . \quad (\text{I-9})$$

If the equation of continuity is applied at the inlet section and at a section downstream where the vein thickness is  $t$ , we have

$$V_p a = \int_R^{R'} u \, dy . \quad (\text{I-10})$$

But from (I-6) and (I-9),

$$u = \frac{V_p (R + t)}{R + y} . \quad (\text{I-11})$$

Substituting into (I-10), we obtain

$$V_p a = \int_0^{R' - R} \frac{V_p (R + t)}{R + y} \, dy . \quad (\text{I-12})$$

We now note that  $t$  is constant at any given section but varies from section to section. Integrating (I-12),



$$V_p a = V_p (R + t) \left[ \ln (R + y) \right]_0^{R' - R} \quad (I-13)$$

and

$$\frac{a}{R + t} = \ln R' - \ln R, \quad (I-14)$$

which yields

$$\frac{R'}{R} = e^{a/R'} ; \quad (R' = R + t). \quad (I-15)$$

Upon noting that  $R' - R = t$ , it can be shown that

$$\frac{t}{a} = \frac{1}{a/R'} - \frac{1}{a/R} \quad (I-16)$$

and it is obvious that

$$\frac{a}{R} = \frac{R'}{R} \frac{a}{R'} \quad (I-17)$$

If the pressure coefficient,  $C_p$ , along the wall is defined as the excess over atmospheric and  $V_p$  is the velocity giving the dynamic head contributed by the fan, then along the wall,

$$p_s = \frac{1}{2} \rho V_p^2 - \frac{1}{2} \rho u_w^2 \quad (I-18)$$

and

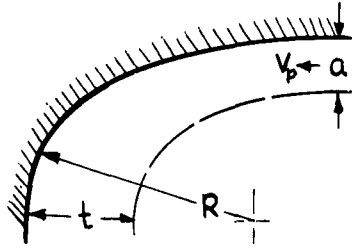
$$C_p = \frac{p_s}{\frac{1}{2} \rho V_p^2} = 1 - \left( \frac{u_w}{V_p} \right)^2 = 1 - \left( \frac{R'}{R} \right)^2 \quad (I-19)$$

The relationships expressed in equations I-15, I-16, I-17 and I-19 are summarized in Figure 59 for flow along a convex bend.

### 3. Concave Bend Velocity Profile

For the concave bend, equation (I-7) from the section on convex bend becomes

$$u = \frac{k}{R'} = \frac{k}{R - t} \quad (I-20)$$



Again the farthest streamline is one of constant pressure and thus constant velocity. We see, therefore, that

$$v_p = \frac{K}{R'} = \frac{K}{R - t}$$

and

$$K = v_p (R - t) \quad (I-21)$$

Thus

$$u = \frac{v_p (R - t)}{R - y} \quad (I-22)$$

From continuity,

$$v_p a = \int_t^0 u \, dy ; \text{ and upon integration there} \quad (I-23)$$

results

$$v_p a = -v_p (R - t) \left[ \ln (R - t) - \ln R \right] \quad (I-24)$$

$$\frac{a}{R - t} + \ln (R - t) = \ln R \quad (I-25)$$

$$(R - t) = R e^{-a/R - t} \quad (I-26)$$

But  $R - t = R'$ ; therefore,

$$\frac{R'}{R} = e^{-a/R'} \quad (I-27)$$

It can be shown that

$$\frac{t}{a} = \frac{1}{a/R} - \frac{1}{a/R'} \quad (I-28)$$

The relationships expressed by equations I-22, I-27, and I-28 are presented in Figure 59 for the concave bend.

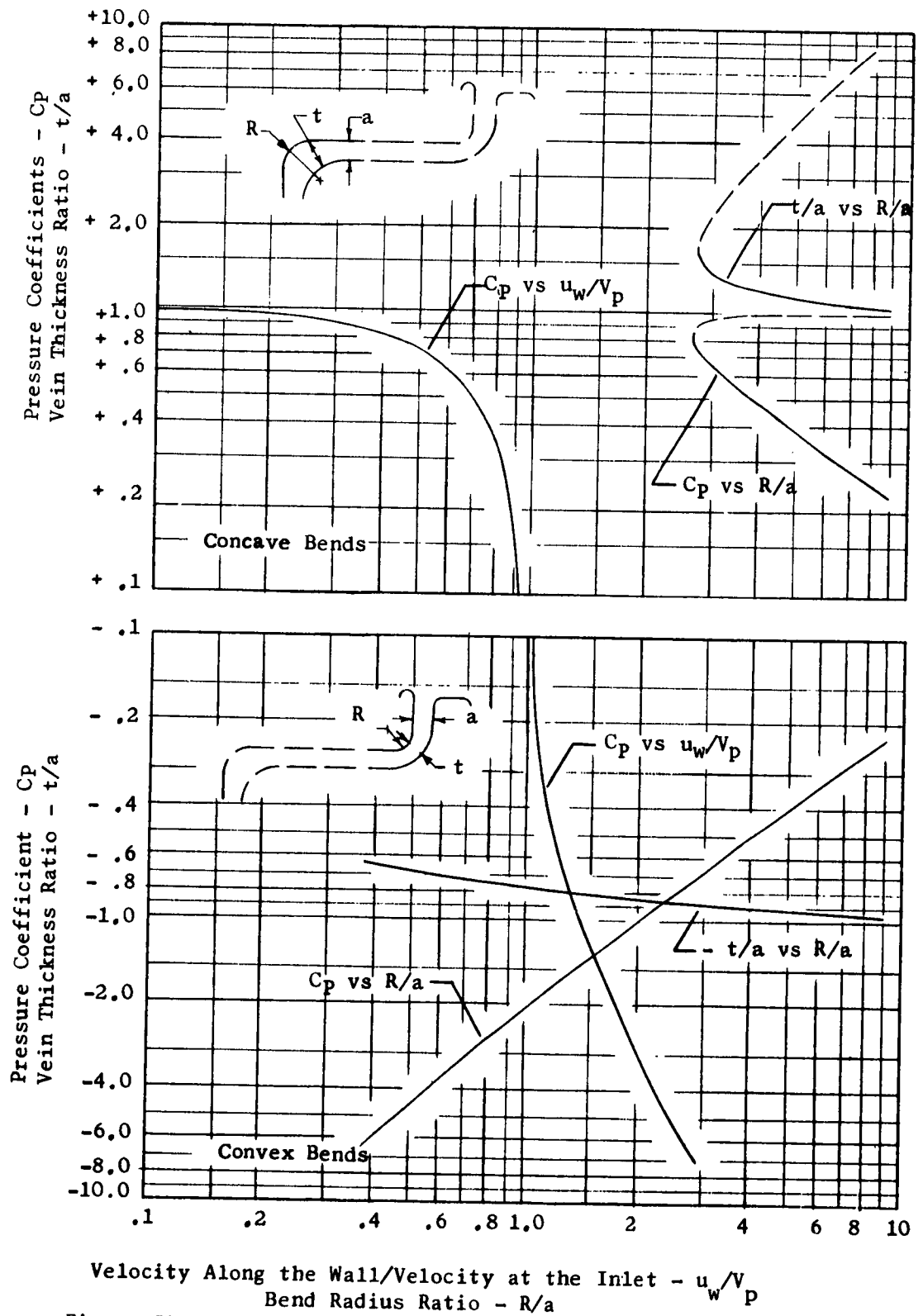


Figure 59. Potential Flow Conditions on Concave and Convex Bends

## APPENDIX II

### INVESTIGATION OF THE EFFECTS OF ARBITRARY CONTOURS ON TWO-DIMENSIONAL LAMINAR BOUNDARY LAYER SEPARATION POINTS

#### A. GENERAL

The behavior of the fluid in the boundary layer is important to controlled flow techniques for a number of reasons. The preference given to the controlled flow configuration derives partially from an anticipated better performance than that of the conventional peripheral jet because of the need for less wetted surface. In order that losses be held to a minimum, the boundary layer has to be well behaved and remain attached. A more important aspect is the effect of this layer on the stability of the whole vein. Two-dimensional models show that an early separation of the boundary layer on the Coanda bend made the entire vein separate. The separation past the Coanda bend was less critical but was sufficiently important. On the straight section downstream of the bend, separation can cause the diffusing vein to become undesirably thick. This thickening leads to a poor flow picture around the final (concave) bend.

The boundary layer can be laminar or turbulent. A turbulent boundary layer is capable of remaining attached and sustaining a more adverse pressure gradient than could a laminar one. Therefore, a turbulent layer is desirable from the point of view of vein stability if the design requires a large curvature on the Coanda bend. The friction losses are higher than those of a laminar layer but the vein stability may leave no alternative. It is possible to permit the boundary layer to build up to the point just before it would ordinarily separate, at which point a means of boundary layer control is required. If such critical points were predictable, separation could be avoided by a small but sudden change of wall curvature. This change causes the momentum of the layer to be restored and the layer emerges anew with a turbulent nature. The price of this is an increase in losses over those of a perfect condition, but in the practical case it will remain advantageous.

In order to predict the theoretical separation point for two-dimensional or axisymmetrical shapes, a solution is developed. The momentum equation for the two-dimensional laminar boundary layer is obtained by integrating the Navier Stokes equation in the direction normal to the boundary, or from the consideration of momentum influx and outflux of a control volume imagined at an arbitrary station along the boundary, including the boundary and extending normal to it to include all the layer's thickness. The resulting equation is due to Polhausen and holds for two-dimensional (or axially symmetric) incompressible steady flow of a fluid with constant viscosity.

With the assumption of a fourth order polynomial for the velocity distribution in the boundary layer, and with the substitutions due to

Holstein and Bohlen, an approximate method results which is adaptable to numerical integration. Thus, a program was written for the IBM 650.

Starting at a point of known initial conditions (e.g., stagnation point) and using the velocity distribution along the boundary calculated from potential flow equations, a step-by-step integration is carried out according to the trapezoidal rule. At each point, a value of the shape factor is assumed and another is calculated from the integral to that point. The computer iterates until the assumed and calculated values differ only by a small percentage (prescribed with the input data).

The velocity distribution, calculated for potential flow from measured pressure gradients at the wall, is presented in Figure 60. The point of separation has been taken to be that at which the shape factor has reached -12.

Two operators observed by means of an extra sensitive tuft the point of separation of the boundary layer of the profile in a two-dimensional model. The observed point of separation is shown in Figure 60. Also, the calculated point of separation is shown. Although the experimental and theoretical observations agree remarkably well, it is to be noted that:

1. The observed point was obtained by visual inspection of the reaction of a tuft and may actually be downstream of real separation;
2. The criterion of predicted separation is  $\Delta = -12$  (experimentally obtained, see Schlichting) and may vary in reality; and
3. The solution is concerned with the laminar layer, and the turbulence causes the separation to occur further downstream, other conditions remaining the same.

This theoretical approach, which permitted a better understanding of the boundary layer and the effect of the flow parameters on its behavior, makes it possible to survey analytically a number of different contour profiles prior to selecting the optimum one for design purposes.

## B. ANALYSIS

### 1. Definitions

	<u>Units</u>
$\tau_o$ = wall shear stress	lb/ft <sup>2</sup>
$\rho$ = fluid mass density	$\frac{\text{lb sec}^2}{\text{ft}^4}$
$u$ = velocity inside the boundary layer in the x-direction	ft/sec

	<u>Units</u>
$U$ = velocity outside the boundary layer in the x-direction.	ft/sec
$\delta$ = boundary layer thickness	ft
$\nu$ = kinematic viscosity of fluid	ft <sup>2</sup> /sec
$p$ = pressure	lb/ft <sup>2</sup>

## 2. Derivation

The integral form of the momentum equation of the boundary layer is found in the literature (for reference see Schlichting's Boundary Layer Theory) to be

$$\frac{\tau_o}{\rho} = \frac{d}{dx} \int_0^{\infty} u (U-u) dy + \frac{dU}{dx} \int_0^{\infty} (U-u) dy \quad . \quad (II-1)$$

The coordinates are  $x$  along the wall and  $y$  normal to the wall. The above holds for the steady incompressible flow of a fluid with constant viscosity.

With  $\delta^*$  and  $\theta$  being the displacement and the momentum thicknesses defined as

$$U \delta^* = \int_0^{\infty} (U-u) dy$$

$$U^2 \theta = \int_0^{\infty} u (U-u) dy,$$

the momentum equation can be reduced to the standard form:

$$\frac{\tau_o}{\rho} = \frac{d}{dx} (U^2 \theta) + U \delta^* \frac{dU}{dx} \quad . \quad (II-2)$$

This equation can be obtained by integrating the two-dimensional Navier Stokes in the y-direction. It can also be obtained by considering the force balance equal to the momentum net flux for a control volume imagined at a point x along the wall including a side dx of the wall and extending in the y-direction to include the whole boundary layer. Until now nothing was said about  $\tau_o$ ; thus the equation holds good for laminar and turbulent layers as well.

The following development follows the method and symbols of Schlichting and is due to Polhausen, Karman, Holstein and Bohlen. It is included here in order to make it easier for the reader to follow the method of numerical computation.

A laminar solution to this momentum equation is now sought. To this end we introduce the variable  $\eta = y/\delta(x)$  ;  $0 \leq \eta \leq 1$  and after Polhausen, introduce the assumption of a fourth-order polynomial for the velocity distribution across the boundary layer. Therefore,

$$\frac{u}{U} = f(\eta) = a \eta + b \eta^2 + c \eta^3 + d \eta^4, \text{ for } 0 \leq \eta \leq 1 \quad (II-3)$$

$$\text{and } \frac{u}{U} = 1, \text{ for } \eta \geq 1.$$

In order to evaluate the coefficients a, b, c, and d, the boundary conditions are employed:

$$\text{for } y = 0 ; u = 0 ; \nu \frac{\partial^2 u}{\partial y^2} = \frac{1}{\rho} \frac{dp}{dx} = - U \frac{dU}{dx}$$

$$\text{for } y = \delta ; u = U ; \frac{\partial u}{\partial y} = 0 ; \frac{\partial^2 u}{\partial y^2} = 0 \quad .$$

By introducing the nondimensional quantity,

$$\Lambda = \frac{\delta^2(x)}{2\nu} \frac{dU}{dx} , \quad (\text{II-4})$$

it is found that,

$$a = 2 + \frac{\Lambda}{6} ; b = -\frac{\Lambda}{2} ; c = -2 + \frac{\Lambda}{2} ; d = 1 - \frac{\Lambda}{6} .$$

Remembering the definitions of  $\delta^*$  and  $\theta$ , it is found that

$$\frac{\delta^*}{\delta} = \int_0^1 \left(1 - \frac{u}{U}\right) d\eta = \frac{3}{10} - \frac{\Lambda}{120} , \quad (\text{II-5})$$

$$\frac{\theta}{\delta} = \int_0^1 \left(1 - \frac{u}{U}\right) d\eta = \frac{37}{315} - \frac{\Lambda}{945} - \frac{\Lambda^2}{9072} . \quad (\text{II-6})$$

As for the wall shear, defined by  $\tau_o = \mu \left(\frac{\partial u}{\partial y}\right)_{y=0}$ , it is seen from equation (II-3) to equal

$$\frac{\tau_o \delta}{\mu U} = 2 + \frac{\Lambda}{6} . \quad (\text{II-7})$$

On multiplying the momentum equation (II-2) by  $\frac{\theta}{\nu}$  and expanding, it is found that

$$\frac{U\theta}{\nu} \frac{d\theta}{dx} + \left(2 + \frac{\delta^*}{\theta}\right) \frac{U\theta^2}{\nu} = \frac{\tau_o}{\mu U} . \quad (\text{II-8})$$

Now, after Holstein and Bohlen (see Schlichting), the momentum shape factor is introduced:

$$K = \frac{\theta^2(x)}{2\nu} \frac{dU}{dx} , \quad (\text{II-9}); \text{ and } Z = \frac{\theta^2}{2\nu} , \quad (\text{II-10})$$

such that

$$K = Z \frac{dU}{dx} . \quad (\text{II-11})$$

By using (II-6) and (II-4), it is found that



$$K = \left( \frac{37}{315} - \frac{\Lambda}{945} - \frac{\Lambda^2}{9072} \right)^2 \Lambda . \quad (\text{II-12})$$

Now, on noting that

$$\frac{\theta}{\mathcal{V}} \frac{d\theta}{dx} = \frac{1}{2} \frac{d}{dx} \frac{\theta^2}{\mathcal{V}} = \frac{1}{2} \frac{dZ}{dx} \quad (\text{II-13})$$

and using (II-5) and (II-6) to get

$$\frac{\delta^*}{\theta} = \frac{\frac{3}{10} - \frac{\Lambda}{120}}{\frac{37}{315} - \frac{\Lambda}{945} - \frac{\Lambda^2}{9072}} = f_1(K) , \quad (\text{II-14})$$

and (II-7) and (II-8) to get

$$\frac{\tau_{oe}}{\mu U} = \left( 2 + \frac{\Lambda}{6} \right) \left( \frac{37}{315} - \frac{\Lambda}{945} - \frac{\Lambda^2}{9072} \right) = f_2(K) , \quad (\text{II-15})$$

the momentum equation is seen to reduce to

$$\frac{1}{2} U \frac{dZ}{dx} + \left[ 2 + f_1(K) \right] K = f_2(K) . \quad (\text{II-16})$$

Let

$$F(K) = 2f_2(K) - 4K - 2K f_1(K) , \quad (\text{II-17})$$

which, written out fully in terms of  $\Lambda$ , gives

$$F(K) = 2 \left( \frac{37}{315} - \frac{\Lambda}{945} - \frac{\Lambda^2}{9072} \right) \left[ 2 - \frac{116\Lambda}{315} + \left( \frac{2}{945} + \frac{1}{120} \right) \Lambda^2 + \frac{2\Lambda^2}{9072} \right] . \quad (\text{II-18})$$

Therefore, the momentum equation now reduces to

$$\frac{dZ}{dx} = \frac{F(K)}{U}; \text{ where, by (II-11), } K = Z \frac{dU}{dx} . \quad (\text{II-19})$$

Equation (II-19) is a nonlinear differential equation of the first order for  $Z = \frac{\theta^2}{\mathcal{V}}$  as a function of the current length coordinate  $x$ . The

function  $F(K)$  is a universal one and is independent of the shape of the body and can be calculated once and for all.

### 3. Method of Solution

In order to solve the equations, it is necessary to know  $Z$  and  $(\frac{dZ}{dx})$  at  $x = 0$ . For this reason, calculation is started at a point of stagnation where  $x = 0$  and  $U = 0$ . Also,  $F(K) = 0$  at the stagnation point giving a meaningful physical situation. The zero of  $F(K)$  occurs for the vanishing of the bracket in equation (II-18). Thus  $F(K) = 0$  for  $K = K_o = .077$ , or  $\Lambda = \Lambda_o = 7.052$ . The values of  $\frac{dZ}{dx}$  and  $Z$  at the stagnation point are found from the limit to equal

$$Z_o = \frac{K_o}{U'_o} = \frac{.077}{U'_o} ; \text{ and } (\frac{dZ}{dx})_o = - .0652 \frac{U''_o}{(U'_o)^2} .$$

Thus, with  $U(x)$ ,  $U'(x)$ , and  $U''_o$  given, all the boundary layer parameters can be calculated.

The following steps are followed in the program for each  $x$ :

- (1) Assume  $\Lambda$  and find  $F(K)$  from (II-18).
- (2) Solve (II-19) for  $\frac{dZ}{dx}$  and integrate numerically to find  $Z$ .
- (3) Calculate  $K$  by (II-11) and  $\Lambda$  from (II-12).
- (4) Compare  $\Lambda$  in step (3) with that assumed in (1). If they differ by more than a prescribed percentage, then iterate until the desired accuracy is obtained.
- (5) Calculate the other parameters for the same point.

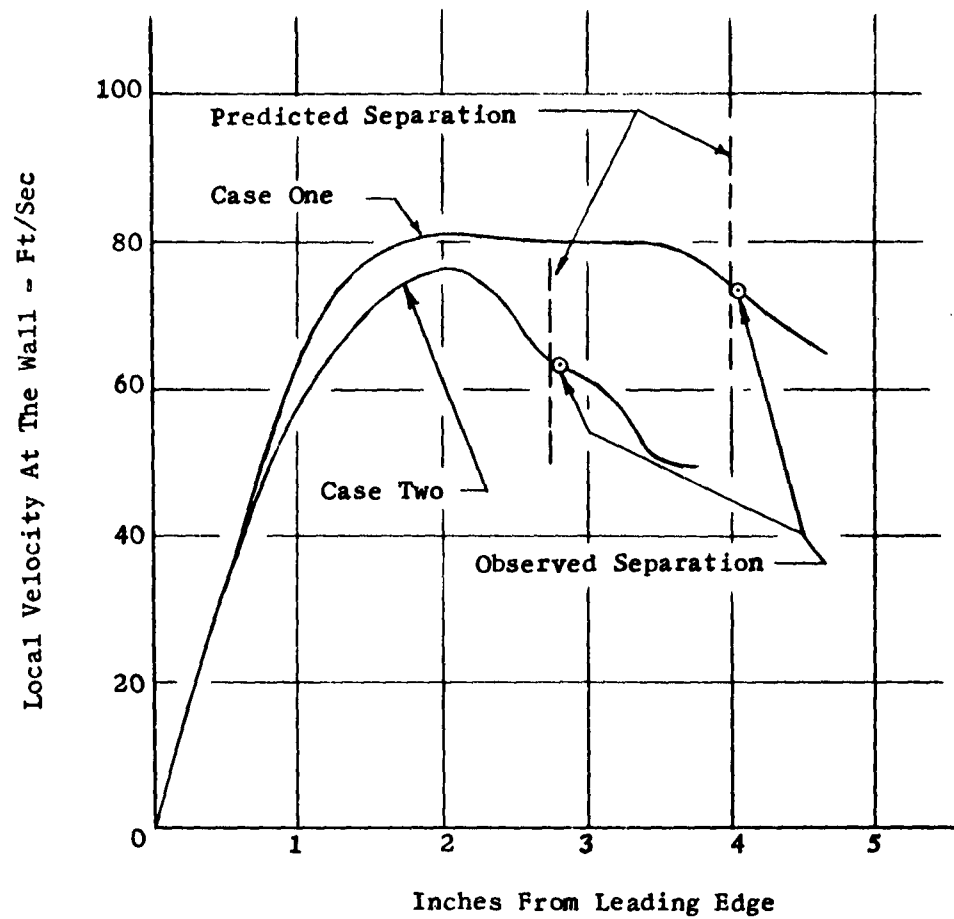


Figure 60. Coanda Bends Tested in Two-Dimensional Model; Case One, An Airfoil Curve, Case Two, A Cubic Curve

### APPENDIX III

#### DERIVATION OF THE IDEAL PERFORMANCE PARAMETER EQUATION FOR THE CONCENTRIC PERIPHERAL JET CONFIGURATION

##### A. GENERAL

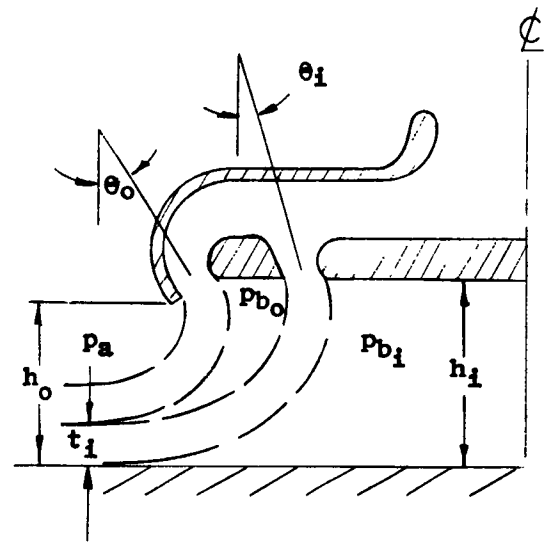
In this appendix the ideal performance parameter expression is derived for the general case of a concentric peripheral jet configuration. This derivation was undertaken since none was found in the literature reviewed. The assumptions used in this analysis are given and are similar to those of Chaplin in Reference 7. In addition, the derivation is shown to be valid for the particular case where the inner jet is deleted, in which case equation (1) in the body of the report results.

##### B. ANALYSIS

1. <u>Definitions (See Figure 61)</u>	<u>Units</u>
$c_i$ = circumference of inner jet at jet centerline	ft
$c_o$ = circumference of outer jet at jet centerline	ft
$h_i$ = height of inner jet	ft
$h_o$ = height of outer jet	ft
$p_a$ = ambient atmospheric pressure	lb/sq ft
$p_{b_i}$ = base pressure acting on inner base area	lb/sq ft
$p_{b_o}$ = base pressure acting on surface between inner and outer jets	lb/sq ft
$q_i$ = dynamic pressure of inner jet at jet exit	lb/sq ft
$q_o$ = dynamic pressure of outer jet at jet exit	lb/sq ft
$S$ = area enclosed by outer periphery of outer jet	sq ft
$S_{b_i}$ = base area enclosed by inner jet	sq ft

		<u>Units</u>
$S_{b_o}$	= base area between inner and outer jets	sq ft
$S_{j_i}$	= inner jet area at nozzle exit	sq ft
$S_{j_o}$	= outer jet area at nozzle exit	sq ft
$t_i$	= thickness of inner jet on the ground plane	ft
$\theta_i$	= inward inclination of inner jet	degrees
$\theta_o$	= inward inclination of outer jet	degrees

Figure 61. Concentric Peripheral Jet Flow Schematic



## 2. Assumptions

The following assumptions are made:

- (1) The force of the base pressure on the air curtain is equal to the net momentum change between the exit of the jet and the ground bend in the direction of that force.
- (2) The mean jet velocity at infinity equals the mean jet velocity at the nozzle.
- (3) The jet static pressure at nozzle exit varies linearly from ambient at the outer streamline to base pressure at the inner streamline.
- (4) The circulation under the base is negligible.

(5) Total head of outer jet equals total head of inner jet.

### 3. Derivation

Base pressure determination using assumption 1.

$$(p_b - p_a) hc = 2 q S_j (1 + \sin \theta) \quad (\text{III-1})$$

Solving for  $p_b$ ,

$$p_b = p_a + \frac{2qS_j(1 + \sin \theta)}{hc} \quad (\text{III-2})$$

Outer base lift equals

$$\begin{aligned} (\text{Lift})_{b_o} &= (p_{b_o} - p_a) S_{b_o} \\ &= \left[ \frac{2q_o S_{j_o} (1 + \sin \theta_o)}{(h_o - t_i) c_o} \right] S_{b_o} \end{aligned} \quad (\text{III-3})$$

But from continuity,  $t_i = \frac{S_{j_i}}{c_o}$ ; then

$$\begin{aligned} (\text{Lift})_{b_o} &= \left[ \frac{2q_o S_{j_o} (1 + \sin \theta_o)}{h_o c_o - S_{j_i}} \right] S_{b_o} \\ &= S_{j_o} q_o \left[ \frac{2S_{b_o} (1 + \sin \theta_o)}{h_o c_o - S_{j_i}} \right] \end{aligned} \quad (\text{III-4})$$

Inner base lift equals

$$\begin{aligned} (\text{Lift})_{b_i} &= (p_{b_i} - p_a) S_{b_i} \\ &= \left[ \frac{2q_i S_{j_i} (1 + \sin \theta_i)}{h_i c_i} + p_{b_o} - p_a \right] S_{b_i} \end{aligned}$$

$$(Lift)_{b_i} = \left[ \frac{2q_i S_{j_i} (1 + \sin \theta_i)}{h_i c_i} + \frac{2q_o S_{j_o} (1 + \sin \theta_o)}{h_o c_o - S_{j_i}} \right] S_{b_i} \quad (III-5)$$

Vertical lift of outer jet

From assumption 3, the mean static pressure of outer jet is  $\frac{p_{b_o} + p_a}{2}$ .

$$\begin{aligned} (Lift)_{j_o} &= \left[ 2q_o + \frac{p_{b_o} + p_a}{2} - p_a \right] S_{j_o} \cos \theta_o \\ &= \left[ 2q_o + \frac{q_o S_{j_o} (1 + \sin \theta_o)}{h_o c_o - S_{j_i}} \right] S_{j_o} \cos \theta_o \\ &= q_o S_{j_o} \left[ 2 \cos \theta_o + \frac{S_{j_o} \cos \theta_o (1 + \sin \theta_o)}{h_o c_o - S_{j_i}} \right] \quad (III-6) \end{aligned}$$

Vertical lift of inner jet

The mean static pressure of inner jet is  $\frac{p_{b_i} + p_{b_o}}{2}$ .

$$(Lift)_{j_i} = \left[ 2q_i + \frac{p_{b_i} + p_{b_o}}{2} - p_a \right] S_{j_i} \cos \theta_i$$

But

$$p_{b_o} = \frac{2q_o S_{j_o} (1 + \sin \theta_o)}{h_o c_o - S_{j_i}} + p_a$$

and

$$p_{b_i} = \frac{2q_i S_{j_i} (1 + \sin \theta_i)}{h_i c_i} + \frac{2q_o S_{j_o} (1 + \sin \theta_o)}{h_o c_o - S_{j_i}} + p_a ;$$

thus,

$$(Lift)_{j_i} = \left[ 2q_i + \frac{2q_o S_{j_o} (1 + \sin \theta_o)}{h_o c_o - S_{j_i}} + \frac{q_i S_{j_i} (1 + \sin \theta_i)}{h_i c_i} \right] S_{j_i} \cos \theta_i \quad (III-7)$$

The total lift on the vehicle is given by the summation of lifts on the inner and outer base areas and the lifts of the inner and outer jets the [summation of equations (III-4) through (III-7)]. The resulting equation for total lift can be further simplified by introducing the following substitutions based on the third assumption:

$$q_i + \frac{p_{b_i} + p_{b_o}}{2} = q_o + \frac{p_{b_o} + p_a}{2} ;$$

then

$$q_i = q_o + \frac{p_a - p_{b_i}}{2},$$

but

$$q_i = q_o - \left[ \frac{q_i S_{j_i} (1 + \sin \theta_i)}{h_i c_i} + \frac{q_o S_{j_o} (1 + \sin \theta_o)}{h_o c_o - S_{j_i}} \right] ;$$

therefore,

$$q_i = \left[ \frac{1 - \frac{S_{j_o} (1 + \sin \theta_o)}{h_o c_o - S_{j_i}}}{1 + \frac{S_{j_i} (1 + \sin \theta_i)}{h_i c_i}} \right] q_o . \quad (\text{III-8})$$

The resulting equation for total lift becomes

$$\begin{aligned} (\text{Lift})_{\text{tot.}} = & 2q_o \left\{ S_{j_o} \cos \theta_o \left[ 1 + \frac{\left( \frac{S_{j_o}}{2} + \frac{S_{b_o}}{\cos \theta_o} \right) (1 + \sin \theta_o)}{h_o c_o - S_{j_i}} \right] + \right. \\ & S_{j_i} \cos \theta_i \left[ \frac{1 - \frac{S_{j_o} (1 + \sin \theta_o)}{h_o c_o - S_{j_i}}}{1 + \frac{S_{j_i} (1 + \sin \theta_i)}{h_i c_i}} \right] \left( 1 + \frac{S_{j_i} (1 + \sin \theta_i)}{h_i c_i} \right) + \end{aligned}$$



$$\left( \frac{S_{j_o} (1 + \sin \theta_o)}{h_o c_o - S_{j_i}} \right) \left[ + S_{b_i} \left[ \left( \frac{1 - \frac{S_{j_o} (1 + \sin \theta_o)}{h_o c_o - S_{j_i}}}{1 + \frac{S_{j_i} (1 + \sin \theta_i)}{h_i c_i}} \right) \left( \frac{S_{j_i} (1 + \sin \theta_i)}{h_i c_i} \right) + \left( \frac{S_{j_o} (1 + \sin \theta_o)}{h_o c_o - S_{j_i}} \right) \right] \right] \quad (III-9)$$

The expression for the ideal power requirement is derived next.

$P =$  air power of outer jet + air power of inner jet

$$= \left[ S_{j_o} \left( q_o + \frac{p_{b_o} + p_a}{2} \right) \sqrt{q_o} + S_{j_i} \left( q_i + \frac{p_{b_i} + p_{b_o}}{2} - p_a \right) \sqrt{q_i} \right] \sqrt{\frac{2}{\rho}}$$

Now, substituting the expressions for  $p_{b_o}$  and  $p_{b_i}$  in terms of  $q_o$  and  $q_i$  given before equation (III-7), and further substituting equation (III-8) for  $q_i$ , the final expression for ideal total power becomes

$$P = q_o^{3/2} \sqrt{\frac{2}{\rho}} \left\{ \left[ 1 + \frac{S_{j_o} (1 + \sin \theta_o)}{h_o c_o - S_{j_i}} \right] \left[ S_{j_o} + S_{j_i} \left( \frac{1 - \frac{S_{j_o} (1 + \sin \theta_o)}{h_o c_o - S_{j_i}}}{1 + \frac{S_{j_i} (1 + \sin \theta_i)}{h_i c_i}} \right)^{\frac{1}{2}} \right] \right\} \quad (III-10)$$

To arrive at the final expression for the performance parameter for the concentric jet, equation (III-9) is raised to the 1.5 power and divided by equation (III-10). Further, the horse power conversion factor, 550, is included and the jet area, base area and jet circumference terms are divided by S to form geometric ratios. In addition, the substitution  $\rho = \rho_o \sigma'$  is made. The final equation for the concentric jet performance parameter is

$$\frac{L^{3/2}}{HP \sqrt{\sigma' S}} = 1100 \sqrt{\rho_o} \left\{ \left( \frac{S_{jo}}{S} \right) \cos \theta_o \left[ 1 + \frac{\left[ \frac{1}{2} \left( \frac{S_{jo}}{S} \right) + \left( \frac{S_{bo}}{S} \right) \frac{1}{\cos \theta_o} \right] [1 + \sin \theta_o]}{h_o \left( \frac{c_o}{S} \right) - \left( \frac{S_{ji}}{S} \right)} \right] + \left( \frac{S_{ji}}{S} \right) \cos \theta_i \left[ \frac{1 - \left( \frac{S_{jo}}{S} \right) \left[ \frac{1 + \sin \theta_o}{h_o \left( \frac{c_o}{S} \right) - \left( \frac{S_{ji}}{S} \right)} \right]}{1 + \left( \frac{S_{ji}}{S} \right) \left[ \frac{1 + \sin \theta_i}{h_i \left( \frac{c_i}{S} \right)} \right]} \right] \right. \\ \left. \left( 1 + \frac{\left( \frac{1}{2} \right) \left( \frac{S_{ji}}{S} \right) [1 + \sin \theta_i]}{h_i \left( \frac{c_i}{S} \right)} \right) + \left( \frac{S_{jo}}{S} \right) \left[ \frac{1 + \sin \theta_o}{h_o \left( \frac{c_o}{S} \right) - \left( \frac{S_{ji}}{S} \right)} \right] + \left( \frac{S_{bi}}{S} \right) \left[ \frac{1 - \left( \frac{S_{jo}}{S} \right) \left[ \frac{1 + \sin \theta_o}{h_o \left( \frac{c_o}{S} \right) - \left( \frac{S_{ji}}{S} \right)} \right]}{1 + \left( \frac{S_{ji}}{S} \right) \left[ \frac{1 + \sin \theta_i}{h_i \left( \frac{c_i}{S} \right)} \right]} \right] \left( \frac{S_{ji}}{S} \right) [1 + \sin \theta_i] + \right. \\ \left. \left( \frac{S_{jo}}{S} \right) \left[ \frac{1 + \sin \theta_o}{h_o \left( \frac{c_o}{S} \right) - \left( \frac{S_{ji}}{S} \right)} \right] \right]^{3/2} \left\{ \left[ 1 + \frac{\left( \frac{S_{jo}}{S} \right) [1 + \sin \theta_o]}{h_o \left( \frac{c_o}{S} \right) - \left( \frac{S_{ji}}{S} \right)} \right] \left[ \left( \frac{S_{jo}}{S} \right) + \left( \frac{S_{ji}}{S} \right) \frac{1 - \left( \frac{S_{jo}}{S} \right) \left[ \frac{1 + \sin \theta_o}{h_o \left( \frac{c_o}{S} \right) - \left( \frac{S_{ji}}{S} \right)} \right]}{1 + \left( \frac{S_{ji}}{S} \right) \left[ \frac{1 + \sin \theta_i}{h_i \left( \frac{c_i}{S} \right)} \right]} \right]^{1/2} \right\}^{-1} \quad (III-11)$$

To obtain the equation for the special case of the single peripheral jet, the inner jet area,  $S_{ji}$ , and the inner base area,  $S_{bi}$ , are set equal to zero. In addition, the jet area,  $S_j$ , is assumed equal to the fan area,  $S_f$ . After a rearrangement of terms and using the identity

$$(\sin \theta_o) (\cos \theta_o) = \frac{\sin 2 \theta_o}{2},$$

the final equation for the single peripheral jet performance parameter is shown to be

$$(M_{pi}) = \frac{L^{3/2}}{HP \sqrt{\sigma' S}} = 1100 \sqrt{\rho_o} \left[ \cos \theta + \frac{1}{2} \left( \frac{S}{hc} \right) \left( \frac{S_f}{S} \right) \left( \cos \theta + \frac{\sin 2 \theta}{2} \right) + \left( \frac{S}{hc} \right) \left( \frac{S_b}{S} \right) (1 + \sin \theta) \right]^{3/2} \left[ \frac{\sqrt{S_f/S}}{1 + \left( \frac{S}{hc} \right) \left( \frac{S_f}{S} \right) (1 + \sin \theta)} \right] \quad (III-12)$$

The total lift on the vehicle is given by the summation of lifts on the inner and outer base areas and the lifts of the inner and outer jets the [summation of equations (III-4) through (III-7)]. The resulting equation for total lift can be further simplified by introducing the following substitutions based on the third assumption:

$$q_i + \frac{p_{b_i} + p_{b_o}}{2} = q_o + \frac{p_{b_o} + p_a}{2};$$

then

$$q_i = q_o + \frac{p_a - p_{b_1}}{2},$$

but

$$q_i = q_o - \left[ \frac{q_i S_{j_i} (1 + \sin \theta_i)}{h_i c_i} + \frac{q_o S_{j_o} (1 + \sin \theta_o)}{h_o c_o - S_{j_i}} \right];$$

therefore,

$$q_i = \left[ \frac{1 - \frac{S_{j_o} (1 + \sin \theta_o)}{h_o c_o - S_{j_i}}}{1 + \frac{S_{j_i} (1 + \sin \theta_i)}{h_i c_i}} \right] q_o. \quad (\text{III-8})$$

The resulting equation for total lift becomes

$$\begin{aligned} (\text{Lift})_{\text{tot.}} = & 2q_o \left\{ S_{j_o} \cos \theta_o \left[ 1 + \frac{\left( \frac{S_{j_o}}{2} + \frac{S_{b_o}}{\cos \theta_o} \right) (1 + \sin \theta_o)}{h_o c_o - S_{j_i}} \right] + \right. \\ & \left. S_{j_i} \cos \theta_i \left[ \frac{1 - \frac{S_{j_o} (1 + \sin \theta_o)}{h_o c_o - S_{j_i}}}{1 + \frac{S_{j_i} (1 + \sin \theta_i)}{h_i c_i}} \right] \left( 1 + \frac{S_{j_i} (1 + \sin \theta_i)}{h_i c_i} \right) + \right. \end{aligned}$$

$$\left( \frac{S_{j_o} (1 + \sin \theta_o)}{h_o c_o - S_{j_i}} \right) \left[ + S_{b_i} \left[ \left( \frac{1 - \frac{S_{j_o} (1 + \sin \theta_o)}{h_o c_o - S_{j_i}}}{1 + \frac{S_{j_i} (1 + \sin \theta_i)}{h_i c_i}} \right) \left( \frac{S_{j_i} (1 + \sin \theta_i)}{h_i c_i} \right) + \left( \frac{S_{j_o} (1 + \sin \theta_o)}{h_o c_o - S_{j_i}} \right) \right] \right] \quad (III-9)$$

The expression for the ideal power requirement is derived next.

$P =$  air power of outer jet + air power of inner jet

$$= \left[ S_{j_o} \left( q_o + \frac{p_{b_o} + p_a}{2} - p_a \right) \sqrt{q_o} + S_{j_i} \left( q_i + \frac{p_{b_i} + p_{b_o}}{2} - p_a \right) \sqrt{q_i} \right] \sqrt{\frac{2}{\rho}}$$

Now, substituting the expressions for  $p_{b_o}$  and  $p_{b_i}$  in terms of  $q_o$  and  $q_i$  given before equation (III-7), and further substituting equation (III-8) for  $q_i$ , the final expression for ideal total power becomes

$$P = q_o^{3/2} \sqrt{\frac{2}{\rho}} \left\{ \left[ 1 + \frac{S_{j_o} (1 + \sin \theta_o)}{h_o c_o - S_{j_i}} \right] \left[ S_{j_o} + S_{j_i} \left( \frac{1 - \frac{S_{j_o} (1 + \sin \theta_o)}{h_o c_o - S_{j_i}}}{1 + \frac{S_{j_i} (1 + \sin \theta_i)}{h_i c_i}} \right)^{\frac{1}{2}} \right] \right\} \quad (III-10)$$

To arrive at the final expression for the performance parameter for the concentric jet, equation (III-9) is raised to the 1.5 power and divided by equation (III-10). Further, the horse power conversion factor, 550, is included and the jet area, base area and jet circumference terms are divided by S to form geometric ratios. In addition, the substitution  $\rho = \rho_o \sigma$  is made. The final equation for the concentric jet performance parameter is

$$\begin{aligned} \frac{L^{3/2}}{HP \sqrt{\sigma' S}} &= 1100 \sqrt{\rho_o} \left\{ \left( \frac{S_{jo}}{S} \right) \cos \theta_o \left[ 1 + \frac{\left[ \frac{1}{2} \left( \frac{S_{jo}}{S} \right) + \left( \frac{S_{bo}}{S} \right) \frac{1}{\cos \theta_o} \right] [1 + \sin \theta_o]}{h_o \left( \frac{c_o}{S} \right) - \left( \frac{S_{ji}}{S} \right)} \right] + \left( \frac{S_{ji}}{S} \right) \cos \theta_i \left[ \frac{1 - \left( \frac{S_{jo}}{S} \right) \left[ \frac{1 + \sin \theta_o}{h_o \left( \frac{c_o}{S} \right) - \left( \frac{S_{ji}}{S} \right)} \right]}{1 + \left( \frac{S_{ji}}{S} \right) \left[ \frac{1 + \sin \theta_i}{h_i \left( \frac{c_i}{S} \right)} \right]} \right] \right. \\ &\quad \left. \left( 1 + \frac{\left( \frac{1}{2} \right) \left( \frac{S_{ji}}{S} \right) (1 + \sin \theta_i)}{h_i \left( \frac{c_i}{S} \right)} \right) + \left( \frac{S_{jo}}{S} \right) \left( \frac{1 + \sin \theta_o}{h_o \left( \frac{c_o}{S} \right) - \left( \frac{S_{ji}}{S} \right)} \right) + \left( \frac{S_{bi}}{S} \right) \left[ \frac{1 - \left( \frac{S_{jo}}{S} \right) \left[ \frac{1 + \sin \theta_o}{h_o \left( \frac{c_o}{S} \right) - \left( \frac{S_{ji}}{S} \right)} \right]}{1 + \left( \frac{S_{ji}}{S} \right) \left[ \frac{1 + \sin \theta_i}{h_i \left( \frac{c_i}{S} \right)} \right]} \right] \left( \frac{S_{ji}}{S} \right) (1 + \sin \theta_i) + \right. \\ &\quad \left. \left( \frac{S_{jo}}{S} \right) \left( \frac{1 + \sin \theta_o}{h_o \left( \frac{c_o}{S} \right) - \left( \frac{S_{ji}}{S} \right)} \right) \right]^{3/2} \left[ 1 + \frac{\left( \frac{S_{jo}}{S} \right) (1 + \sin \theta_o)}{h_o \left( \frac{c_o}{S} \right) - \left( \frac{S_{ji}}{S} \right)} \right] \left[ \left( \frac{S_{jo}}{S} \right) + \left( \frac{S_{ji}}{S} \right) \frac{1 - \left( \frac{S_{jo}}{S} \right) \left[ \frac{1 + \sin \theta_o}{h_o \left( \frac{c_o}{S} \right) - \left( \frac{S_{ji}}{S} \right)} \right]}{1 + \left( \frac{S_{ji}}{S} \right) \left[ \frac{1 + \sin \theta_i}{h_i \left( \frac{c_i}{S} \right)} \right]} \right]^{1/2} \right]^{-1} \end{aligned} \quad (III-11)$$

To obtain the equation for the special case of the single peripheral jet, the inner jet area,  $S_{ji}$ , and the inner base area,  $S_{bi}$ , are set equal to zero. In addition, the jet area,  $S_j$ , is assumed equal to the fan area,  $S_f$ . After a rearrangement of terms and using the identity

$$(\sin \theta_o) (\cos \theta_o) = \frac{\sin 2 \theta_o}{2},$$

the final equation for the single peripheral jet performance parameter is shown to be

$$\left( \frac{M_{P1}}{P1} \right) = \frac{L^{3/2}}{HP \sqrt{\sigma' S}} = 1100 \sqrt{\rho_o} \left[ \cos \theta + \frac{1}{2} \left( \frac{S}{hc} \right) \left( \frac{S_f}{S} \right) \left( \cos \theta + \frac{\sin 2 \theta}{2} \right) + \left( \frac{S}{hc} \right) \left( \frac{S_b}{S} \right) (1 + \sin \theta) \right]^{3/2} \left[ \frac{\sqrt{(S_f/S)}}{1 + \left( \frac{S}{hc} \right) \left( \frac{S_f}{S} \right) (1 + \sin \theta)} \right]. \quad (III-12)$$

## DISTRIBUTION LIST

USAWC	(1)
Rs ch Ana1 Corp	(1)
ARO, Durham	(2)
ARO, OCRD	(1)
USAAVNS, CDO	(1)
USAERDL	(2)
USAOTAC, Center Line	(2)
QMRECOMD	(1)
USATCDA	(1)
USATB	(1)
USATMC	(18)
USATSCH	(1)
USATRECOM	(74)
TCLO, USAABELCTBD	(1)
USAEWES	(1)
TCLO, USAAVNS	(1)
AFSC (SCS-3)	(1)
CNO	(3)
CNR	(3)
BUWEPS, DN	(6)
ACRD(OW), DN	(1)
USNSRDF	(1)
USNPGSCH	(1)

# DISTRIBUTION LIST - Continued

BUSHP, DN	(1)
Dav Tay Mod Bas	(2)
MCLFDC	(3)
MCEC	(3)
Langley Rsch Cen, NASA	(3)
Geo C. Marshall Sp Flt Cen, NASA	(4)
NASA, Wash., D. C.	(6)
Ames Rsch Cen, NASA	(1)
Lewis Rsch Cen, NASA	(1)
USGPO	(1)
ASTIA	(10)
MOCOM	(3)
USAMC	(5)
USMA	(1)
Bell Helicopter Company	(10)

Bell Helicopter Company

Fort Worth, Texas  
INVESTIGATION OF CONTROLLED FLOW PHENOMENA  
FOR AIR CUSHION VEHICLES - J. DeTore and  
R. Wernicke

Report No. 532-099-001, November 1962, 128 pp,  
61 illus, 9 tables (Contract DA 44-177-TC-744)  
Task 9R 99-01-005-05, TCREC Technical Report  
62-46.

Unclassified Report

This report presents the results of an analytical and experimental model investigation of controlled flow configured air cushion vehicles. Controlled flow is defined as the flow pattern which exists when a peripheral jet is established without the use of internal ducting or a base plate.

(over)

1. Fluid Dynamics
2. Internal Flow -  
Ground Effect  
Machines

3. Stability, Control  
and Propulsion -  
Ground Effect  
Machines

4. Contract  
DA 44-177-TC-744

Bell Helicopter Company

Fort Worth, Texas  
INVESTIGATION OF CONTROLLED FLOW PHENOMENA  
FOR AIR CUSHION VEHICLES - J. DeTore and  
R. Wernicke

Report No. 532-099-001, November 1962, 128 pp,  
61 illus, 9 tables (Contract DA 44-177-TC-744)  
Task 9R 99-01-005-05, TCREC Technical Report  
62-46.

Unclassified Report

This report presents the results of an analytical and experimental model investigation of controlled flow configured air cushion vehicles. Controlled flow is defined as the flow pattern which exists when a peripheral jet is established without the use of internal ducting or a base plate.

(over)

1. Fluid Dynamics
2. Internal Flow -  
Ground Effect  
Machines

3. Stability, Control  
and Propulsion -  
Ground Effect  
Machines

4. Contract  
DA 44-177-TC-744

Bell Helicopter Company

Fort Worth, Texas  
INVESTIGATION OF CONTROLLED FLOW PHENOMENA  
FOR AIR CUSHION VEHICLES - J. DeTore and  
R. Wernicke

Report No. 532-099-001, November 1962, 128 pp,  
61 illus, 9 tables (Contract DA 44-177-TC-744)  
Task 9R 99-01-005-05, TCREC Technical Report  
62-46.

Unclassified Report

This report presents the results of an analytical and experimental model investigation of controlled flow configured air cushion vehicles. Controlled flow is defined as the flow pattern which exists when a peripheral jet is established without the use of internal ducting or a base plate.

(over)

1. Fluid Dynamics
2. Internal Flow -  
Ground Effect  
Machines

3. Stability, Control  
and Propulsion -  
Ground Effect  
Machines

4. Contract  
DA 44-177-TC-744

Bell Helicopter Company

Fort Worth, Texas  
INVESTIGATION OF CONTROLLED FLOW PHENOMENA  
FOR AIR CUSHION VEHICLES - J. DeTore and  
R. Wernicke

Report No. 532-099-001, November 1962, 128 pp,  
61 illus, 9 tables (Contract DA 44-177-TC-744)  
Task 9R 99-01-005-05, TCREC Technical Report  
62-46.

Unclassified Report

This report presents the results of an analytical and experimental model investigation of controlled flow configured air cushion vehicles. Controlled flow is defined as the flow pattern which exists when a peripheral jet is established without the use of internal ducting or a base plate.

(over)

1. Fluid Dynamics
2. Internal Flow -  
Ground Effect  
Machines

3. Stability, Control  
and Propulsion -  
Ground Effect  
Machines

4. Contract  
DA 44-177-TC-744



Main objectives of the investigation included achieving a practical approximation to ideal controlled flow which depends heavily on the Coanda phenomenon, then comparing the characteristics of controlled flow versions with conventional forms of the plenum and peripheral jet. Criteria for evaluating the relative merits of controlled flow include considerations of stability, controllability and integrated propulsion system characteristics as well as performance in hovering flight. Thirty variations in planform and internal arrangements are discussed. The findings indicate that on a performance basis controlled flow configurations outperform base plate peripheral jet configurations. In addition, improvements in stability characteristics over the base plate peripheral jet configuration were also achieved and potential for further optimization was indicated. Controlled flow techniques applied to external flow air cushion vehicles were briefly explored.

Main objectives of the investigation included achieving a practical approximation to ideal controlled flow which depends heavily on the Coanda phenomenon, then comparing the characteristics of controlled flow versions with conventional forms of the plenum and peripheral jet. Criteria for evaluating the relative merits of controlled flow include considerations of stability, controllability and integrated propulsion system characteristics as well as performance in hovering flight. Thirty variations in planform and internal arrangements are discussed. The findings indicate that on a performance basis controlled flow configurations outperform base plate peripheral jet configurations. In addition, improvements in stability characteristics over the base plate peripheral jet configuration were also achieved and potential for further optimization was indicated. Controlled flow techniques applied to external flow air cushion vehicles were briefly explored.

Main objectives of the investigation included achieving a practical approximation to ideal controlled flow which depends heavily on the Coanda phenomenon, then comparing the characteristics of controlled flow versions with conventional forms of the plenum and peripheral jet. Criteria for evaluating the relative merits of controlled flow include considerations of stability, controllability and integrated propulsion system characteristics as well as performance in hovering flight. Thirty variations in planform and internal arrangements are discussed. The findings indicate that on a performance basis controlled flow configurations outperform base plate peripheral jet configurations. In addition, improvements in stability characteristics over the base plate peripheral jet configuration were also achieved and potential for further optimization was indicated. Controlled flow techniques applied to external flow air cushion vehicles were briefly explored.

Main objectives of the investigation included achieving a practical approximation to ideal controlled flow which depends heavily on the Coanda phenomenon, then comparing the characteristics of controlled flow versions with conventional forms of the plenum and peripheral jet. Criteria for evaluating the relative merits of controlled flow include considerations of stability, controllability and integrated propulsion system characteristics as well as performance in hovering flight. Thirty variations in planform and internal arrangements are discussed. The findings indicate that on a performance basis controlled flow configurations outperform base plate peripheral jet configurations. In addition, improvements in stability characteristics over the base plate peripheral jet configuration were also achieved and potential for further optimization was indicated. Controlled flow techniques applied to external flow air cushion vehicles were briefly explored.